THE HONG KONG
POLYTECHNIC UNIVERSITY
香港理工大學
Pao Yue-kong Library
包玉剛圖書館

Copyright Undertaking

This thesis is protected by copyright, with all rights reserved.

By reading and using the thesis, the reader understands and agrees to the following terms:

1. The reader will abide by the rules and legal ordinances governing copyright regarding the use of the thesis.
2. The reader will use the thesis for the purpose of research or private study only and not for distribution or further reproduction or any other purpose.
3. The reader agrees to indemnify and hold the University harmless from and against any loss, damage, cost, liability or expenses arising from copyright infringement or unauthorized usage.

If you have reasons to believe that any materials in this thesis are deemed not suitable to be distributed in this form, or a copyright owner having difficulty with the material being included in our database, please contact lbsys@polyu.edu.hk providing details. The Library will look into your claim and consider taking remedial action upon receipt of the written requests.

Pao Yue-kong Library, The Hong Kong Polytechnic University, Hung Hom, Kowloon, Hong Kong

http://www.lib.polyu.edu.hk

Simulation of Vibrational Structure of Photoelectron and Electronic Spectra of Selected Triatomic Molecules Using Anharmonic Potential Functions

by

Wang Dechao

DOCTOR OF PHILOSOPHY

in

CHEMISTRY

at

The Hong Kong Polytechnic University

2001

Pao Yue-Kong Library
PolyU • Hong Kong

Simulation of Vibrational Structure of Photoelectron and Electronic Spectra of Selected Triatomic Molecules Using Anharmonic Potential Functions

ABSTRACT

Author: Wang Dechao

Supervisor: Professor Foo-tim Chau

Submitted for the degree of Doctor of Philosophy in Chemistry

at the Hong Kong Polytechnic University in 2001.

Photoelectron (PE) spectroscopy and electronic spectroscopy, notably absorption, emission and fluorescence spectroscopy, are some primary experimental tools used in studying the electronic structure of molecules and radicals in the gas phase. From the observed spectra, information on the geometries, vibrational frequencies, bonding properties and thermochemical values of the species involved in the corresponding electronic transitions can be either obtained directly, or extracted with the aid of appropriate analyses of the spectra. When vibrational structure is observed in an electronic band, one of the techniques useful for spectral analysis is the Franck-Condon (FC) analysis method with the consideration of the associated vibrational intensity distribution. The aim of this project is to apply the technique together with the iterative Franck-Condon analysis (IFCA) procedure to study the vibrational structures of

photoelectron (PE) and electronic spectra of selected triatomic molecules of $SiCl_2$, BrO_2, AlCN, Cl_2O, ClO_2 and F_2O using harmonic and/or anharmonic potential energy functions (PEFs). A multidimensional FC method (Chen, 1994) with the combination of ab initio molecular orbital calculations has been employed in these studies with the inclusion of Duschinsky effect.

The Chen's FC model (Chen, 1994) was adopted in this work for spectral simulation. In this model, the Cartesian coordinates instead of internal coordinates for both the neutral molecules and ions and/or excited molecules were used in the FC analysis procedure for the photoionization process and electronic transition. The Duschinsky effect, which arises from the rotation of the normal modes of the two electronic states involved in these processes, was also formulated in Cartesian coordinates. The major advantage of this approach is that it describes accurately the vibrational intensities even for electronic transition and photoionization process with large geometric changes but still assumes a harmonic force field. In the present work, we have extended the generating function method of Sharp and Rosenstock (Sharp and Rosenstock, 1964) to evaluate FC integrals for up to eight and four vibrational modes for transitions arising from the 'vibrationless' states and 'hot' bands, respectively. The software package CART-FCF for the multidimensional harmonic Franck-Condon factor (FCF) calculation was coded in the MATLAB (Bangert *et al.*, 1993) environment.

The commonly used harmonic oscillator model, might be inadequate in cases, where anharmonicity effects are important, such as for vibronic transitions involving vibrational levels of high quantum numbers and also species containing H atom. This work has also developed a multi-dimensional anharmonic FCF method for non-linear polyatomics. It is based on the Watson's Hamiltonian (Watson, 1968) and includes the Duschinsky effect, through employing multi-dimensional anharmonic potential energy

functions (PEFs). The anharmonic vibrational wavefunctions are expressed as linear combinations of the products of harmonic oscillator functions (Botschwina, 1989, 1997). A software package AN-FCF in the FORTRAN environment (Microsoft, 1993) has been coded based on this anharmonic FCF method.

The IFCA procedure which involves a systematic adjustment of the ionic or excited molecular geometry based on a computed ab initio geometry was also developed in the present works, in order to obtain the best experimentally fitted geometry for the ionic or excited molecular state involved. In the IFCA treatment, the experimental structural parameters of the neutral molecules available in the literature were utilized and fixed while those of the excited molecules or ions were varied systematically to give the best match between the computed and observed vibrational intensity distributions of the photoelectron, emission or absorption spectrum under study. The simulated spectra were produced by employing a Gaussian shape function for each vibrational component with its relative intensity given by the computed Franck-Condon factors, with an appropriate full-width-at-half-maximum (FWHM) as estimated from the corresponding experimental.

The above proposed harmonic IFCA method with the combination of ab initio calculations and multidimensional Franck-Condon (FC) analysis has been applied to investigate the emission or the single vibrational level (SVL) dispersed fluorescence spectra of $SiCl_2$ and AlCN and the He I PE spectra of Cl_2O and BrO_2, respectively. Comparison between the simulated and the observed spectra gave, for the first time, the experimentally derived geometries of the molecular excited states and the cationic states involved. The adiabatic ionization energy (AIE) position and the vibrational assignments of the Cl_2O^+ $A^2B_2 \leftarrow Cl_2O$ X^1A_1 band as reported in the literature were revised, based on spectral simulations, which included "hot" bands.

There are different theoretical and practical advantages and disadvantages associated with the above proposed harmonic and anharmonic FCF methods. The method chosen for simulation depends on the problem under consideration, the quality of the experimental information in PE and electronic spectrum, and the available computational resources. The He I PE spectra of ClO_2 and F_2O, which are of the importance in atmospheric chemistry, have been selected as a testing case for spectral simulation, employing both the above developed harmonic FCF code CART-FCF and anharmonic FCF code AN-FCF. The highly accurate CASSCF/MRCI PEFs of the neutral ground state and low-lying cationic states of ClO_2 available in literatures and the CCSD(T) anharmonic PEFs of the neutral ground state and cationic states of F_2O obtained in this work have been used for anharmonic FCF spectral simulations. For the first PE band of ClO_2 and F_2O, the harmonic FCF model was shown to be inadequate and the anharmonic FCF simulation gave a much-improved agreement with the observed spectrum. The experimentally derived geometries of the ground cationic states of ClO_2 and F_2O were obtained, for the first time, via the anharmonic IFCA procedure. The spectral simulations reported here led also to re-assignments of the observed overlapping second PE band of ClO_2 and the experimental overlapping second and third PE bands of F_2O. The adiabatic ionization energy position of the F_2O^+ $A^2B_2 \leftarrow F_2O$ X^1A_1 in the observed He I PE spectrum (Brundle et al., 1972) was also revised.

In investigations of different molecular systems using the FCF methods, ab initio calculations of the states involved in the electronic transitions of the selected molecules at the different levels of theory were performed to provide a reliable input of harmonic force constants, vibrational frequencies and minimum-energy geometries for the subsequent FCF simulation. Also, the ab initio single point energies of F_2O at the levels of the CCSD(T)/aug-cc-pVQZ for the neutral ground state and cationic ground

state and of the CCSD(T)/aug-cc-pVTZ for the lowest three cationic excited states were computed for the fittings of their anharmonic potential energy functions.

DECLARATION

This is to declare that this work has been done by the author in the Department of Applied Biology and Chemical Technology of The Hong Kong Polytechnic University, Hong Kong and this thesis has not been submitted to this or other institution for any academic qualification.

Wang Dechao

ACKNOWLEDGMENT

I am grateful to the Research Grant Council (RGC) of the Hong Kong Special Administrative Region (Project Nos. POLYU 5156/98P) for the kind support of the studentship for my Ph.D. study. I also wish to express my gratitude to all those have helped in various ways during the course of this work.

I would like to thank Prof. F.T. Chau, my supervisor, for his critical advice and supervision of this project as well as his comments on the final draft of this thesis and the other publications. He also gave me a lot of freedom in my research works and let me to participate in the development of other related projects.

I would like to thank Prof. J.M. Dyke and Dr. E.P.F. Lee of the Department of Chemistry, Southampton University, UK, and Dr. D.K.W. Mok, a research fellow of the Department of Applied Biology and Chemical Technology of PolyU, for their valuable discussions and comments on ab initio calculations and spectral simulations.

Finally, I am indebted to my wife and my son in the Mainland for their constant encouragement during the course of this work especially in the hard times.

TABLE OF CONTENTS

LIST OF TABLES

LIST OF FIGURES

LIST OF ABBREVIATIONS AND SYMBOLS

Abbreviations

AIE	Adiabatic ionization energy
AIP	Adiabatic ionization potential
ANO	Atomic natural orbital
FC	Franck-Condon
FCF	Franck-Condon factor
FWHM	Full-width-at-half-maximum (i.e. the spectral resolution)
IE	Ionization energy
IFCA	Iterative Franck-Condon analysis
LIF	Laser induced fluorescence
NCA	Normal coordinate analysis
PE	Photoelectron
PEFs	Potential energy functions
PES	Photoelectron spectrum
PIMS	Photoionization mass spectrometer
QCPE	Quantum chemistry program exchange
SVL	Single vibrational level
UV	Ultraviolet spectroscopy
VIE	Vertical ionization energy
VIP	Vertical ionization potential
~~amu~~	~~Atomic mass unit~~

Symbols

Note:	The quantities appeared in this thesis, which with double primed and single primed superscript signs are corresponding to the neutral molecules or radicals and the ions or excited molecules involved in photoionization process and electronic transition, respectively.
$^+$	Indicates the transpose of matrix
N	Atom number in a molecule
n	Normal mode number for a molecule, n=3N-5 for a linear molecule and n=3N-6 for a non-linear molecule
Γ'	A diagonal matrix (n×n), which the diagonal elements are the normal mode frequencies in the ions or excited molecules, scaled to 0.029660ν (cm^{-1})
Γ''	A diagonal matrix (n×n), which the diagonal elements are the normal mode frequencies in the neutal radicals or molecules, scaled to 0.029660ν' (cm^{-1})
A	A matrix (n×n), analogous to C matrix, which are a measure of the change in frequencies of a photoionization process or electronic transition
adm	Cartesian atom displacement matrix (3N×n) expressing the n normal mode displacements Q as 3N Cartesian displacements X, with $X=(adm)Q$ and $adm=M^{-1}(L^{-1}B)^{+}$
B′	1) A transformation matrix (n×3N) from Cartesian displacements to internal coordinate displacements in the ions or excited molecules; 2)

analogous to the D vector (n×1) below and is used in Franck-Condon simulations with hot bands

B″ A transformation matrix (n×3N) from Cartesian displacements to internal coordinate displacements in the neutral radicals or molecules

C A matrix (n×n), which the elements go directly into evaluating the Franck-Condon factors. They are a measure of the change in frequencies of a photoionization process or electronic transition

D A vector (n×1), which the elements are the major contribution to the Franck-Condon factors

E A matrix (n×n), which is a measure of the change in frequencies for evaluating the hot band FCFs

G Atomic mass matrix (n×n) in a molecule, $G = BM^{-1}B^{+}$, identities used in calculating the molecular kinetic energy

g98′ A matrix (3N×n) from the GAUSSIAN 98 output, which is the square root of the reduced masses weighted atom displacement matrix in the ions or excited molecules, i.e. $g98 = (adm)V'^{\frac{1}{2}}$

g98″ A matrix (3N×n) from the GAUSSIAN 98 output, which is the square root of the reduced masses weighted atom displacement matrix in the neutral radicals or molecules, i.e. $g98' = (adm')V''^{\frac{1}{2}}$

J A matrix (n×n) to rotate a set of Q′ into a set of Q″: $J = (L''^{-1}B'')ZM^{-1}(L'^{-1}B')^{+}$

K A vector (n×1) to give the offset of the origins of Q′ and Q″: $K = (L''^{-1}B'')R$

L′	A transformation matrix (n×n) from normal mode displacements to internal mode displacements in the ions or excited molecules, $L' = B'(g98')V'^{-1/2}$
L″	A transformation matrix (n×n) from normal mode displacements to internal mode displacements in the neutral radicals or molecules, $L'' = B''(g98'')V''^{-1/2}$
M^{-1}	A diagonal matrix (3N×3N), elements m_i^{-1}, once for each Cartesian direction
Q′	Normal coordinate displacement vector (n×1) containing the displacement of the n normal modes of the ions or excited molecules in electronic transitions
Q″	Normal coordinate displacement vector (n×1) containing the displacement of the n normal modes of the neutral radicals or molecules in electronic transitions
R	A vector (3N×1) to be the difference in equilibrium geometries of a photoionization process or electronic transition in the Cartesian coordinate system of the neutral centered on the molecular center of mass, $R = R_{eq}' - R_{eq}''$
R_{eq}'	Equilibrium geometry vector (3N×1) of the ions or excited molecules in the Cartesian coordinate of the ions or excited molecules
R_{eq}''	Equilibrium geometry vector (3N×1) of the neutral in the Cartesian coordinate of the neutral
V′	A diagonal matrix (n×n), which elements are the reduced masses in the ions or excited molecules

V''	A diagonal matrix (n×n), which elements are the reduced masses in the neutral
X'	Cartesian displacement vector (3N×1) of the cation in the ion's or excited molecule's coordinate system
X''	Cartesian displacement vector (3N×1) of the neutral in the neutral's coordinate system, $X''=ZX'+R$
Z	A rotation matrix (3N×3N) rotating the full atom displacement matrix from the ion's coordinate system into the neutral's coordinate system, which is a unit matrix for most molecules of C_{2v} or higher symmetry

CHAPTER 1

Introduction

Excited molecules and ions involve in many chemical reactions in atmospheric chemistry, chemical vapour deposition, combustion, microcircuit etching and industrial chemical processing. In recent years, molecular information about geometry, molecular, electronic and thermochemical properties, as well as potential energy surfaces of these transient species have been subjects of intensive investigations for a better understanding of the related mechanisms and control of the chemical processes. Up to now, data of this kind is still rare.

There has been a rapid development in spectroscopic techniques in recent years such that absorption, emission, fluorescence and photoionization spectroscopies are used almost routinely to investigate small molecules, reactive species and clusters. Spectra obtained from these experimental methods yield valuable information about the geometries, bonding properties and thermochemical values of molecules in the electronic states investigated. However, these spectroscopic techniques still suffer from limitations. For instance, it is difficult to interpret electronic spectra with complicated overlapping vibrational structure or to determine the adiabatic ionization potential from a poorly resolved or unresolved photoelectron (PE) spectrum or a photoelectron spectrum containing two or more overlapping bands.

Ab initio *molecular orbital* calculation at different levels of theory has been applied extensively to study electronic or photoelectron spectra. This is mainly due to the high level at which the theoretical values can be derived. This kind of calculation can provide optimized geometries, force constants, heats of formation and other quantities for a molecule in various electronic states. Hence, transition energy for a particular electronic transition under study can be generated to compare with the

experimental value. To further confirm the assignment, simulation of the associated vibrational fine structure is desirable (Chau *et al.*, 1997; Cederbaum & Domcke, 1977; Chen, 1994; Mebel, 1996; Takeshita, 1994). In addition, the theoretical spectrum can be utilized to optimize the geometries of the molecule in the electronic states involved by comparison with the experimental spectrum (Chau *et al.*, 1997; Chen, 1994), to study the anharmonicity of the potential energy surface (Baltzer *et al.*, 1996; Botschwina *et al.*, 1989, 1995, 1996 & 1997; Ho *et al.*, 1990), and to study the vibronic coupling mechanisms between electronic states (Bunker & Sears, 1985; Mayer *et al.*, 1994; Peric *et al.*, 1995; Peyerimhoff, 1980; Takeshita, 1987; Takeshita & Shida, 1996; Zigerski *et al.*, 1995).

The Franck-Condon (FC) principle has been applied quantitatively to study vibrational intensities accompanying electronic transitions to deduce geometries as well as other molecular information of molecules in the ground, excited and ionic states. With the advancement in microelectronics, there is a growing trend to carry out vibrational intensity calculations coupled with ab initio calculations to simulate electronic and photoionization spectra of molecules to deduce molecular and thermochemical properties.

In the literature, FC analysis has been widely used for determining geometric changes in a transition and hence the geometries of excited molecules or ions as mentioned above (Chau & McDowell, 1990; Göthe *et al.*, 1990). It has also been used in the simulation of experimental spectra to assist or confirm assignment and study of the processes involved in the electronic transition or photoionization process (Chau *et al.*, 1996 & 1997; Bunter & Sears, 1985; Stock & Domcke, 1993). A few groups of workers have been involved in this kind of research work. Yamaguchi et al. (1990) have developed a computer program for Franck-Condon factor (FCF) calculation which

use Kupka and Cribb's (1986) generating function method for spectral simulation. This program has been used by Miller et al. (1997) to identify an absorption spectrum of OBrO to be arisen from the $C^2A_2 \leftarrow X^2B_1$ electronic transition and to assign the reported photoelectron spectrum of phenyl cation (Butcher *et al.*, 1987) by Hrusak *et al.* (1997).

In the harmonic oscillator approximation, the FCF within a band for an electronic transition of a diatomic molecule can be computed through the use of the recursion formulae similar to those given by Ansbacher (1959) and Manneback (1951). For more accurate results, the Morse potential function can be utilized (Morse, 1929; Chau, 1985). However, the evaluation of FCF is not that simple for polyatomic molecules owing to the change in geometry, force constants and/or symmetry in the process. Therefore, the normal coordinates of the two electronic states involved are not identical and mode mixing or Duschinsky effect (Duschinsky, 1937) between different vibrational modes needs to be considered in the computation. In the literature, there are mainly three different ways to deal with the Duschinsky effect. The crudest model, known as the parallel mode approximation was proposed by Coon *et al.* (1962). A better model was proposed by Sharp and Rosenstock (1964). They assumed that the same internal coordinates can be adopted for molecule in the two electronic states involved. This approach gives reasonable results for systems with small geometric changes. Yet, the most accurate way to handle the Duchinsky effect is to use Cartesian coordinates for both electronic states involved (Warshel & Karplus, 1972, 1974; Warshel, 1975; Chen 1994).

Chen *et al.* (Chen, 1994) developed a FC analysis procedure for the photoionization process using Cartesian coordinates instead of internal coordinates for both the neutral molecules and cations and the generating function method (Sharp and

Rosenstock, 1964). The major advantage of this approach is that it describes accurately the vibrational intensities even for electronic transition and photoionization process with large geometric changes but still assumes a harmonic force field. The all input data used to calculate the FCF in this approach can be obtained from the output of ab initio calculations. Chen has given an algorithm to perform FCF calculations with two- and three-dimensional normal modes for electronic transition of a vibrationally cold molecule (no hot band included) by using the combination process of FCF calculations and ab initio calculations in the generating function method. In the present work, the procedure was modified with the inclusion of the anharmonic force field and the transition energy factor to account for vibrational intensity distributions of photoelectron, absorption and emission spectra. The generating function method of Sharp and Rosenstock has been extended to evaluate FC integrals for up to eight and four vibrational modes for transitions arising from the 'vibrationless' states and 'hot' bands, respectively, within Chen's model. Both the optimized geometries and the harmonic vibrational frequencies adopted in spectral simulation were obtained from ab initio calculations. Also, the ab initio single energies at various levels of theory were used in the fitting of anharmonic potential energy functions (PEFs). The spectral simulation programs for harmonic model and anharmonic model as developed in this work for FC analysis were coded in the MATLAB and FORTRAN environments respectively and were applied to the selected molecular systems.

An iterative FC analysis (IFCA) procedure which involves a systematic adjustment of the ionic or excited molecular geometry based on a computed ab initio geometry was also included in this work. The method was used to obtain the best experimentally fitted geometry for the ionic or excited molecular state involved. This was achieved by matching the computed and observed vibrational intensity distributions

of the photoelectron, emission or absorption spectrum under study by varing the geometry of the ions systematically. The experimental structural parameters of the neutral molecules available in the literature were utilized and fixed in the IFCA procedure. The theory and methodology of the FC analysis procedures will be described in Chapter 2. The emphasis will be directed towards the combination of ab initio calculations and multidimensional Franck-Condon (FC) analysis with the use of the harmonic oscillator model and anharmonic model to simulate electronic and photoelectron spectra. Chapter 3 through Chapter 5 will cover applications of the proposed IFCA method to investigate the emission or the single vibrational level (SVL) dispersed fluorescence spectra of $SiCl_2$ and AlCN and the PE spectra of BrO_2 and Cl_2O, respectively, in the harmonic oscillator model. In Chapter 6 and Chapter 7, the He I PE spectra of ClO_2 and F_2O, which are of the importance of atmospheric chemistry, have been chosen as a testing case for spectral simulations, employing both the developed harmonic and anharmonic IFCA procedures.

CHAPTER 2

Theory and Methods of Franck-Condon Analysis

In this Chapter, the theory and methodology involved in this work for FC analysis will be described in details. These involve the ab initio calculations for preparing input data for the subsequent multi-dimensional FCF calculations with the Chen's (1994) generating method; the FC analysis techniques using the harmonic and anharmonic models; and the IFCA method for generating reliable experimentally derived geometries of transient species involved in the study. The starting point involved in this work is to perform geometry optimization, frequency calculation and single point energy calculation to supply the necessary input data for the subsequent FC analysis and the fitting of anharmonic potential energy function, respectively, within the Chen's model. Therefore, a simple description of ab initio calculation will first be given. The FC analysis techniques with harmonic and anharmonic potential energy functions and the IFCA method developed in this work will be introduced starting from the Section 2.2 of this Chapter in details.

2.1. Ab initio molecular orbital calculation

2.1.1. Background

Molecular orbital calculations may be broadly divided between ab initio and semi-empirical calculations. The later one involves the use of experimental data for parametrization of some quantities such as two electron integrals to reduce the computational time. As for the former one, no experimental data are used and all calculations are carried out starting from the first principle. Applications of these two types of molecular orbital calculations are largely governed by the size of the molecular system to be studied. With advancement in computer technology, the computationally

more demanding ab initio calculations become possible for larger molecular systems than before. It is therefore anticipated that ab initio calculations would gradually take over semi-empirical calculations in the studies of larger systems in the future. From a theoretical point of view, the various degrees of sophistication in the level of ab initio calculation are traceable, while the reliability of a semi-empirical method depends heavily on the appropriateness of its parameterization. Hence, we will only focus on discussing ab initio methods in this sub-section.

Recently, a newcomer, the density functional theory (DFT) method, has been getting popular among computational chemists. It is largely considered as an ab initio method though some may prefer to call it semi-ab initio. Similar to semi-empirical methods, the main advantage of DFT is its economy. In addition, theoretically, it accounts for electron correlation and is found to work particularly well for systems containing transition metals. However, it possesses an empirical element that certain functionals work well only for certain classes of molecules, and there is little work one can do in the case when a certain functional does not work. One can only to try another functional. Researchers in this field are still searching for new functionals, which may have a universal application. Although many ab initio software packages can also perform DFT calculations, we would not further discuss DFT in the following. Some popular ab initio software packages with relevant information have been listed in Table 2.1 for references.

Table 2.1. Some popular ab initio software packages with relevant information (Chau, 2001)

Package	Major authors/owners	Further Information	Comments/ specialities
GAUSSIAN 98	Gaussian,Inc.	Www.gaussian.com	Most popular all-rounder
MOLPRO 98	Werner, H.-J. and Knowles, P. J.	Www.tc.bham.ac.uk/molpro/molpro.html	CASSCF, Internally-contracted MRCI, RCCSD(T): the best CI program for energy calculation
ACES2	Bartlett, R. J.	Aces2@qtp.ufl.edu	ROHF/MP2, CCSD(TQ), CCSDT, EOM-CCSD, ROHF-CCSD(T) analytic gradients; the most advanced CC program
GAMESS	Schmidt, M. W.	Www.msg.ameslab.gov/GAMESS/GAMESS.html, Gamess-users-request@glue.umd.edu	General, spin-orbit coupled wavefunction; free of charge
GAMESS-UK6	Guest, M.	www.dl.ac.uk/CFS	General, SERHF, MRDCI, RPA, OVGF, 2ph-TDA
CADPAC6	Amos, R.	Cadpac@theor.ch.cam.ac.uk	General, analytic derivatives, ROHF/MP2 gradients
MOLCAS	Roos, B. O.	Department of Chemistry, Chemical Centre, P.O. Box 124, S-22100 Lund, Sweden.	CASPT2, relativistic contribution and solvent effect
QCHEM	Johnson, B.G.	Q-Chem, Inc., Pittsburgh, PA	MP2, DFT, excited states (CIS, RPA, XCIS); fast integration and DFT

2.1.2. Theory of ab initio calculation and its applications

The basis of ab initio theory is the Hartree-Fock (HF) method, which is non-relativistic and within the Born-Oppenheimer approximation which assumes that electrons move much faster than nuclei because of the mass difference. In a HF calculation, the electronic wavefunction and its energy are obtained by the self-consistent-field (SCF) method, where the total electronic energy of the system is minimized by varying the coefficients of a set of basis functions (the one-particle basis). The linear combinations of these basis functions form the molecular orbitals of the electronic wavefunction of the system. Within the HF model, instantaneous electron interaction, which is called dynamic electron correlation, is neglected. In addition, a SCF calculation usually employs a single configurational wavefunction of restricted-spin RHF or unrestricted-spin UHF wavefunction, where the pairs of α-spin and β-spin electrons have different spatial orbitals. Yet, this approach cannot describe correctly any degenerate electronic states such as the $^1\Delta$ and $^1\Sigma$ states arising from a π^2 configuration, or the $^2\Pi$ state from a π^1 configuration. Also it is inadequate in the region of the energy surface, where there are states of near-degeneracy such as those near an avoided crossing. This inadequacy is called non-dynamic or structural electron correlation. Moreover, another weakness in practical ab initio calculation, which also relates to electron correlation, is the unavoidable employment of a finite basis set.

In order to account for non-dynamic electron correlation, one way to tackle the problem is to take a multi-configurational approach, such as the multi-configuration SCF, MCSCF, method, where a number of important configurations are included in the SCF procedure. Also both the coefficients of these configurations and the basis

function coefficients are varied. The most popular and balanced way to choose the configurations to be included is the complete-active-space SCF, CASSCF, method. It considers all configurations formed by all possible permutations of electron arrangement (full configuration interaction, FCI) within a chosen set of molecular orbitals or active space. Nevertheless, the choice of the active space is not trivial. It requires a good understanding of the problem in hand and some experiences with the technique.

For handling dynamic electron correlation, there are mainly two types of correlation methods being used. They are configuration interaction (CI) and perturbative methods. The former one approximates the true wavefunction as a linear combination of a very large number of configurations, formed by single, double, triple, ... excitations from a reference configuration. This reference configuration is usually a RHF configuration obtained from a SCF calculation. The ultimate limit is a FCI calculation involving all possible configurations with all molecular orbitals to account for all electron correlation for the system with the basis set used. However, FCI is only possible for small molecules with a small basis set, as the size of the configuration space would easily become unmanageable for a larger system. The most commonly used CI method is CI with single and double excitations, CISD. The CI wavefunction and energy are obtained variationally with a fixed set of molecular orbitals (the many-particle basis) obtained previously in some ways from such as a SCF or CASSCF calculation or the natural orbitals obtained from a CI calculation. The major advantages of the CI method are, firstly, restricted-spin orbitals are usually employed and thus there is no spin-contamination problem as in the UHF calculation. Secondly, non-dynamic electron correlation can be readily considered via the CASSCF and the subsequent multi-reference CI (MRCI) method. Thirdly, it is a variational method, which gives the

energy as a higher limit to the true one. Finally, excited states can be considered via higher roots of the CI problem. However, it is not a black-box type method, which requires experiences in choosing, for example, the appropriate many-particle basis and/or reference configurations for a problem.

As for perturbative methods, electron correlation is assumed to be a perturbation to a reference configuration wavefunction which is usually UHF for open-shell species, in spite of the ROHF/MP2 method being available in some suite of programs (see Table 2.1). Among these methods, the Moller-Plesset method to the n^{th} order (MPn) is the most popular one. The main advantages of the MPn method, particularly the MP2 method are that, firstly, analytic energy derivatives (especially the first and second derivative) with respect to geometric displacements can be derived. This facilitates geometry optimization and harmonic vibrational frequency calculation for characterizing the nature of the stationary point obtained in a geometry optimization. Secondly, the MPn method is computationally less demanding than the CI method, for a similar degree of accuracy. Yet, the method has its own disadvantages. In general, it is good only when the single-reference zeroth-order wavefunction is dominant and appropriate. Possible large spin-contamination in an UHF wavefunction could lead to serious errors. The MPn series may oscillate, particularly in off-equilibrium geometry and/or when spin-contamination is large. It is not variational and hence its predicted energy could be too low or too high.

There is another method which is called the couple-cluster (CC) method which is usually considered as a kind of perturbative methods. The CC wavefunction is related to the reference wavefunction by exp(T), where T is an operator for single, double, triple .... excitations. The CC method is iterative, but non-variational, and can be used to account for higher-order correlation. It is recognized to be the best single-reference

correlation method and has been shown to work well even when the reference wavefunction employed is not a good one or when spin-contamination is large. Although, it is computational much more demanding than the MPn method, the couple-cluster single and double excitations plus perturbative triples, CCSD(T), has become very popular, because of its high accuracy. With a large basis set, CCSD(T) results have been shown to be even more reliable than available experimental results!

There is another type of method that links CI type (CASSCF) and perturbative type calculations together. The CASPT2 method of Roos (see table 2.1) has been developed to account for both non-dynamic (CASSCF) and dynamic correlation (PT2 or MP2) on an even footing. The CASPT2 method has been shown to be particularly useful for transition-metal compounds (such as Cr_2), where both dynamic and non-dynamic correlations are important. Although this type of method is not a black-box type method, it has been shown to do well for excited states and for medium-size systems. In addition, solvent effect and relativistic effect (mass-velocity and spin-orbit) could be included with the use of the MOLCAS software package (see table 2.1).

A major concern in the ab initio calculation is the choice of basis set, which determines the quality of the results to be obtained. There are many standard basis sets available in literatures which have been designed for different purposes. One latest and most popular type for high-quality calculation is the various correlation-consistent basis sets of Dunning (1989) of cc-pVXZ, aug-cc-pVXZ, cc-pCVXZ, aug-cc-pCVXZ, etc, where X = D, T, Q, 5, ... The advantages of this type of basis sets are that, they are designed for correlation calculation, to be compact and balanced in every way, and for basis size extrapolation. For the latter, a series of calculation employing successively larger basis sets enables the extrapolation of the computed quantities to the basis set limit. To achieve this process, there are different techniques available in the literature,

such as the Valence Focal-point Analysis of Allen and Schaefer (Schaefer *et al.*, 1992) and the CBS (complete-basis-set) method of Peterson (Peterson *et al.*, 1991).

Ab initio calculations have been found to contribute significantly to the understanding of the thermodynamics and kinetics of chemical reactions including photo-initiated reactions, and to the interpretation of spectroscopic observations. Combining with standard statistical mechanical methods, for instance, the rigid-rotor-harmonic-oscillator-model, ab initio calculations are capable of yielding thermodynamic quantities, such as enthalpy, entropy and Gibbs free energy, to the chemical accuracy of 1 kcal/mole. There are composite methods, which are designed specifically for this purpose, for examples, the G1, G2 and G3 methods by Pople and Curtiss (Pople *et al.*, 1989; Curtiss et al., 1991, 1998) and their variants (Curtiss et al., 1993, 1996), and the CBS type methods of Peterson (Peterson *et al.*, 1991).

High-level ab initio energy hyper-surfaces are very valuable in many areas, such as reaction dynamics, trajectory calculations, scattering processes and reaction kinetics. The theoretic energy surfaces are particularly useful in regions, where experimental investigation is either difficult in the laboratory or impossible. With the availability of analytic energy derivatives, important stationary points, such as the transition state structure and reaction intermediate, as well as the minimum energy path (MEP) of a reaction can be located by ab initio transition state search, geometry optimization, or intrinsic reaction coordinate (IRC) calculation. Combining the variational transition state theory (VTST) with the MEP obtained from reliable ab initio calculations, reaction rate can be evaluated by standard programs, such as, POLYRATE by Truhlar (Truhlar *et al.*, 2000). Ab initio energy surface is the base for many varied theoretic investigations.

In the present work, the main aim of the ab initio calculations was to obtain the reliable minimum-energy geometries, the harmonic vibrational frequencies and the potential energy surfaces for the neutral and excited molecules or their ions involved, so as to carry out the subsequent FCF calculations and spectral simulations. The ab initio package of GAUSSIAN 98 (Frisch et al.) or MOLPRO 98 (Werner et al.) has been used in this procedure.

2.2. Franck-Condon factor calculations with the harmonic oscillator model

A Franck-Condon factor calculation of the electronic transition requires the wave functions of the initial and final state. These functions are usually expressed as the products of the electronic and vibration wave functions in the Born-Oppenheimer approximation (Born & Oppenheimer, 1927). In this approach, the theoretical vibrational intensity of the transition is proportional to the square of the product of the electronic transition moment and the vibrational overlap integral (or FC integral). Generally, the electronic transition moment or photoionization cross section is assumed to be constant over the band envelope (Chau, 1984; Chen, 1994). With this approximation, the relative transition probability of a vibrational component, I_{mn}, between the mth and nth vibrational levels of the final and initial electronic state, respectively, for a given vibrational mode in the transition process may be written as (Herzberg, 1966)

$$I_{mn} = AE_{mn}^{p} b_{mn}^{2} \qquad (2.1)$$

where A is a constant, E_{mn} is the transition energy, b_{mn} is the vibrational overlap integral (Franck-Condon integral) and b_{mn}^2 is the FCF. The positive integer p has values of 0, 1 and 3 for photoionization, absorption and emission or fluorescence processes respectively. As the transition energy is directly proportional to the frequency of the peak observed in a spectrum, E_{mn}^p is called frequency factor.

2.2.1. The Duschinsky effect

The theoretical vibrational intensities within a band for an electronic transition of the diatomic molecule can be obtained through equation (2.1). In the harmonic oscillator approximation, the vibrational overlap integrals can be computed through the use of the recursion formulae similar to those given by Ansbacher (1959) and Manneback (1951). For more accurate results, the Morse potential function can be utilized (Morse, 1929; Chau, 1985). However, the evaluation of FCFs is not that simple for polyatomic molecules owing to the change in geometry, force constants and/or symmetry in the process. Therefore, the normal coordinates of the two electronic states involved are not identical and mode mixing or Duschinsky effect (Duschinsky, 1937) between different vibrational modes needs to be considered in the computation. In the literature, there are mainly three different ways to deal with the Duschinsky effect. The crudest model, known as the parallel mode approximation was proposed by Coon *et al.* (1962). This simply ignores the differences between the normal coordinates of the two related electronic states. Latter, Sharp and Rosenstock (1964) proposed a better model for this kind of calculation. They assumed that the same internal coordinates can be adopted for molecule in the two electronic states involved. This approach gives reasonable results for systems with small geometric

changes. The most accurate way to handle the Duchinsky effect is to use Cartesian coordinates with which a set common to both the two combining electronic states can always be found (Warshel & Karplus, 1972, 1974; Warshel, 1975; Chen 1994).

In adopting the parallel mode method to calculate the theoretical vibrational intensities, each normal mode plays its own role in contributing to the vibrational intensities. The recursion formulae by Smith and Warshop (1968) can be used to evaluate the FC integrals within this model. FCF calculation with the use of Coon *et al.*'s method has been widely employed for confirmation of spectral assignment, determination of geometry of excited molecules or ions (Chau, 1983; Hollas & Sotherley, 1971; Heilbonner, 1971; Aoki *et al.*, 1996; Xu *et al.* 1998). A procedure in utilizing this method to find out the geometry of an ion through FC analysis of a vibrationally resolved photoelectron spectrum is provided here to illustrate how the method works (Chau, 1983). The experimental vibrational frequencies of the molecule and ion are used to evaluate the vibrational intensities for a given change in the normal coordinate $\Delta \boldsymbol{Q}$. If the computed relative intensities do not fit the observed ones, then $\Delta \boldsymbol{Q}$ is varied to give the best fit between the two. The normal coordinates $\boldsymbol{Q}'$ thus obtained for the ion (or the final state) is then transformed to the corresponding internal symmetry coordinates $\boldsymbol{S}'$ and, hence, the internal coordinates $\boldsymbol{R}_{int}'$ which represent the bond length or bond angle. The transformation matrix $\mathbf{L}_s'$ ($\mathbf{S}' = \mathbf{L}_s'\mathbf{Q}'$) required in this calculation is obtained by carrying out normal coordinate analysis (NCA) on the related ionic state (Wilson *et al.*, 1955). NCA programs of QCMP012, BMAT and UMAT (McIntosh *et al.*, 1977, 1992) are available from QCPE for this purpose.

The parallel mode approximation does not give satisfactory results even for small geometric changes upon electronic transition. With the use of internal

coordinates, Sharp and Rosenstock (1964) have derived an expression which relates the normal coordinates in the final state (Q′) to those in the initial state (Q″)

$$\mathbf{Q''} = \mathbf{JQ'} + \mathbf{K} \tag{2.2}$$

where J and K are, respectively, the Duschinsky rotation matrix and the shift between the two sets of normal coordinates. The J matrix is equal to $(L_s'')^{-1}\mathbf{L}_s'$. Sharp and Rosenstock also introduced the use of the multidimensional generating function method to calculate the FC integrals. Chen (1994) has proposed to adopt the Cartesian coordinates X (Warshel and Kauplus, 1972, 1974; Warshel, 1975) for handling the Duschinsky effect with

$$\mathbf{X''} = \mathbf{ZX'} + \mathbf{R} \tag{2.3}$$

where X' and X'' are distortions expressed as Cartesian displacements from the equilibrium geometries of the molecules in the final and the initial electronic states respectively. $\mathbf{R}(= Z\mathbf{R}''_{eq})$ is the change in equilibrium geometry between the molecules in the final and initial states in Cartesian coordinates on the molecular center of mass and Z is a rotation matrix (Özkan, 1990), which is a unit matrix for most molecules of C_{2v} or higher symmetry. In a conventional normal mode analysis, the Cartesian displacements, X, are transformed to internal coordinates, R_{int}, and then to normal coordinates, Q, and *vice versa*, by the B and L matrices (Wilson *et al.*, 1955):

$$R_{\text{int}} = BX \tag{2.4}$$

$$R_{\text{int}} = LQ \tag{2.5}$$

Q can be related to X by the Cartesian atom displacement matrix, $\text{adm}[= M^{-1}(L^{-1}B)^{+}]$ by:

$$X = (adm)Q \tag{2.6}$$

where M is a diagonal matrix with the atomic masses on the diagonal, one for each Cartesian direction, to give the proper mass weighting for the adm. The atom displacement matrix can then be used after mathematical manipulation to relate Q′ to Q″ by:

$$Q''=(L''^{-1}B'')[ZM^{-1}(L'^{-1}B')^{+}Q'+R] \quad (2.7)$$

where the superscript + indicates the transpose of the matrix. Substitution of equation (2.7), into equation (2.2) gives the expressions for J and K as:

$$J=(L''^{-1}B'')ZM^{-1}(L'^{-1}B')^{+} \quad (2.8)$$

$$K=(L''^{-1}B'')R \quad (2.9)$$

The Gaussian package (Frisch *et al.*, 1998) of ab initio electronic structure programs provides, as part of its output, a reduced-mass-weighted atom displacement matrix representation of the normal modes of the molecule under study. For a non-linear molecule with N atoms, there are 3N-6 normal modes (or 3N-5 normal modes for linear molecule). If we define a (3N×3N-6) matrix, g98, containing the normal mode output, and a (3N-6×3N-6) diagonal matrix, V, containing the reduced masses for each mode on the diagonal in atomic mass units, then

$$adm=(g98)V^{-1/2} \quad (2.10)$$

removes the reduced-mass weighting. Substituting equation (2.10) into equation (2.8) and (2.9), and using the definition of adm produce the final working equations for J and K in terms of the Gaussian outputs of g98, V and R.

$$J=[M(g98'')V''^{-1/2}]^{+}Z(g98')V'^{-1/2} \quad (2.11)$$

$$K=[M(g98'')V''^{-1/2}]^{+}R \quad (2.12)$$

Having computed J and K from the output of ab initio calculations for the two transition states, the Sharp and Rosenstock's method can then be used for calculating

FCFs with the algebraic expressions as given in the next section. The advantage of this approach is that the results obtained are still applicable to the case with large geometric changes upon an electronic transition and can be used to handle an arbitrary number quanta for the two molecular electronic states involved in a transition.

2.2.2. Evaluation of the Franck-Condon integral

2.2.2.1. Background

Once the method used for handling the Duschinsky effect is selected, different procedures can be used to evaluate the FC integral. If the parallel mode approximation is adopted, the method as described previously can be employed to compute FCFs. For multi-mode FCF calculations with the use of internal coordinates or Cartesian coordinates, different methods have been proposed to do so. Sharp and Rosenstock (1964) derived an analytical expression for FCF for an arbitrary number of quanta of excitation for a single mode. However, for combination and hot bands, only expressions up to four modes with vibrational quantum numbers less than five were given. Later, Kupka and Cribb (1986) based on Sharp and Rosenstock's work derived sophisticated analytical formulae to evaluate multidimensional FCFs.

Doktorov *et al.* (1975) applied the coherent-state method to deduce recurrence relations for two-dimensional FC integrals. In addition, these authors generalized the Herzberg-Teller formula for fractional intensity of the 0-0 band to two-dimensional vibrations which has been used by Zgierski *et al.* (1991, 1994, 1995, 1997) to interpret vibronic structures of electronic spectra of medium-size polyatomic molecules. Later,

Faulkner and Richardson (1979) and Subbi (1988) utilized a coordinate transformation to remove any Duschinsky mixing to render the multidimensional FC integral to be expressed simply as a sum of integrals with each of which being a product of one-dimensional harmonic oscillator overlap integrals. Yet the method is confined to cases where one of the vibrational wave functions in the FC integral is required to be in the vibrationless state. Chen and Pei (1990) proposed another method to compute the two-dimensional FC integrals with the aids of addition theorems of harmonic oscillator wave functions. Mebel *et al.* (1996) proposed analytical expressions for evaluation of FCFs up to four vibrational modes using outputs of Gaussian 94 calculations. However, the formulae are good only for the transitions originating from the vibrationless state.

In recent years, Neumark and co-workers have taken a different approach of using the wave packet technique for simulating spectra from ZEKE (Zero-electron-kinetic-energy) and photodetachment spectroscopic techniques [Neumark *et al.*, 1991, 1993 and 1995]. The reactive scattering method for reaction dynamics was adopted by these authors to calculate FCFs. Transitions originating from the vibrationless state were considered for spectral simulations. Details of the wave packet method can be found in Neumark *et al.*'s publications and are not repeated here. In the next section, the FCF methods as developed in this work will be described.

2.2.2.2. The generating function method for computation of Franck-Condon integral

To account for the vibrational structures of electronic and photoelectron spectra of polyatomics more accurately, the generating function method (Sharp and Rosenstock, 1964; Chen *et al.*, 1994) with the inclusion of ab initio calculation and the use of

Cartesian Coordinates has been adopted in the present work. The advantages of this approach or known as Chen's method have been described previously. We have generalized Sharp and Rosenstock's formulae for up to eight modes or higher like Chen did (1994). All these FCF procedures were implemented in this work in a software package CART-FCF.

Following Sharp and Rosenstock (1964), the arrays A through E are defined in terms of the Duschinsky rotation arrays, J and K, and the harmonic frequencies (in appropriate units), a diagonal matrix Γ with the harmonic frequencies as diagonal elements. If the mass has unit in amu and distances in Angstroms, then the Γ matrix elements are the frequencies, in cm^{-1}, multiplied by a factor of 0.029660:

$$A = 2\Gamma''^{1/2} J[J^{+}\Gamma'' J + \Gamma']^{-1} J^{+}\Gamma''^{1/2} - 1 \qquad (2.13)$$

$$B = -2\Gamma''^{1/2}[J(J^{+}\Gamma'' J + \Gamma')^{-1} J^{+}\Gamma'' - 1]K \qquad (2.14)$$

$$C = 2\Gamma'^{1/2}[J^{+}\Gamma'' J + \Gamma']^{-1}\Gamma'^{1/2} - 1 \qquad (2.15)$$

$$D = -2\Gamma'^{1/2}[J^{+}\Gamma'' J + \Gamma']^{-1} J^{+}\Gamma'' K \qquad (2.16)$$

$$E = 4\Gamma''^{1/2}[J^{+}\Gamma'' J + \Gamma']^{-1} J^{+}\Gamma''^{1/2} \qquad (2.17)$$

If one were computing Franck-Condon factors for a vibrationally hot molecule, i.e. hot bands, then all the above A, B, C, D and E arrays are necessary. By using the above arrays and the Chen's method (1994), for example, we came up with an expression for the multidimensional Franck-Condon factors for transitions from an initial molecular state with three vibrational modes of r, s and t, to a final molecular state with three vibrational modes of v, w and x as:

$$FCF(r,s,t,v,w,x)=\frac{r!s!t!v!w!x!}{2^{(v+w+x)}}\{\sum_{q2=0}^{\binom{v}{r}}\sum_{p2=0}^{\binom{v-q2}{s}}\sum_{q1=0}^{\binom{v-q2-p2}{t}}\sum_{p1=0}^{\binom{w}{r-q2}}\sum_{q=0}^{\binom{w-p1}{s-p2}}\sum_{p=0}^{\binom{w-q-p1}{t-q1}}$$

$$\sum_{o=0}^{\binom{x}{r-p1-q2}}\sum_{n=0}^{\binom{x-o}{s-q-p2}}\sum_{m=0}^{\binom{x-n-o}{t-p-q1}}\sum_{l=0}^{\binom{v-q1-q2-p2}{w-p-q-p1}}\sum_{k=0}^{\binom{v-l-q1-q2-p2}{x-m-n-o}}\sum_{j=0}^{\binom{w-l-p-q-p1}{x-k-m-n-o}}$$

$$[\frac{v-k-l-q1-q2-p2}{\sum_{i}^{2}}][\frac{w-j-l-p-q-p1}{\sum_{h}^{2}}][\frac{x-j-k-m-n-o}{\sum_{g}^{2}}]\sum_{f=0}^{\binom{r-o-p1-q2}{s-n-q-p2}}\sum_{e=0}^{\binom{r-f-o-p1-q2}{t-m-p-q1}}$$

$$\sum_{d=0}^{\binom{s-f-n-q-p2}{t-e-m-p-q1}}[\frac{r-e-f-o-p1-q2}{\sum_{c}^{2}}][\frac{s-d-f-n-q-p2}{\sum_{b}^{2}}][\frac{t-d-e-m-p-q1}{\sum_{a}^{2}}]$$

$$[2^{(d+e+f+j+k+l)}A_{11}^{c}A_{22}^{b}A_{33}^{a}A_{12}^{f}A_{13}^{e}A_{23}^{d}C_{11}^{i}C_{22}^{h}C_{33}^{g}C_{12}^{l}C_{13}^{k}C_{23}^{j}$$

$$E_{11}^{q2}E_{12}^{p2}E_{13}^{q1}E_{21}^{p1}E_{22}^{q}E_{23}^{p}E_{31}^{o}E_{32}^{n}E_{33}^{m}$$

$$B_1^{r-2c-e-f-o-p1-q2}B_2^{s-2b-d-f-n-q-p2}B_3^{t-2a-d-e-m-p-q1}$$

$$D_1^{v-2i-k-l-q1-q2-p2}D_2^{w-2h-j-l-p-q-p1}D_3^{x-2g-j-k-m-n-o}]/[\prod_{\lambda=a}^{q2}\lambda!$$

$$(r-2c-e-f-o-p1-q2)!(s-2b-d-f-n-q-p2)!$$

$$(t-2a-d-e-m-p-q1)!(v-2i-k-l-q1-q2-p2)!$$

$$(w-2h-j-l-p-q-p1)!(x-2g-j-k-m-n-o)!]\}^2 \qquad (2.18)$$

where the symbol ( ) means to take the smaller value of the two numbers, and the symbol [ ] means to take the integer value less than or equal to that obtained from the bracketed expression. The above expression for FCF calculation has been used in the spectral simulations of the selected triatomic molecules involved in this work.

2.3. IFCA method with the harmonic oscillator model

2.3.1. Principle

The ab initio geometries of radicals and ions or excited molecules may not be very accurate owing to finite basis sets used in computation, incomplete accounting for electron correlation, etc. Using the molecular geometries and the harmonic vibrational frequencies obtained from ab initio calculations for molecules and its ions or excited molecules, the simulated Franck-Condon vibrational band structure of the corresponding PE or electronic spectrum can be obtained. However, the agreement between the theoretical and experimental vibrational band profiles may not be good. Since the force field is not too sensitive to a small change in the molecular geometry, the ab initio force field, which is defined only at the computed minimum energy structure, could be translated or transferred to another, similar, structure (Chen, 1994). Based on this argument, the geometries of the ions or the excited molecules can be optimized using the experimental vibrational structure of PE or electronic spectrum with the neutral molecule fixed at the experimental geometry, by adopting the following iterative scheme. Firstly, the geometric parameters of the final state in photoionization process or electronic transition were varied systematically (with changes in the parameters initially being given by the results of the ab initio calculations). Then the calculated spectrum is compared with the observed spectrum. The variations in the geometrical parameters are being carried out iteratively until satisfactory agreement with the observed spectrum is achieved. The degree of certainty that one claims for the fit depends on the number of significant geometric parameters, the extent of FC activity in the spectrum and spectral resolution. The detail of iterative Franck-Condon analysis procedure will be described in next section briefly.

2.3.2. IFCA procedure

The iterative FC analysis procedure employed in this work is similar to that suggested by Chen (1994). The procedure is listed out in detail as follows:

A. The first cycle

A1. Starting with the ab initio geometries of the final state (single primed) and initial neutral state (double primed) in $R'_{eq,calc}$ and $R''_{eq,calc}$, respectively, from a combined geometry optimization and frequency job in GAUSSIAN 98 (Frisch *et al.*, 1998), the B'_{calc}, B''_{calc}, G'_{calc} and G''_{calc} matrices can be obtained according to the Wilson (Wilson *et al.*, 1955) GF formalism using the NCA program (McIntosh *et al.*,1977, 1992). The subscript 'calc' denotes an ab initio calculated value as distinct from the subscript 'trial' for the slightly modified geometry. Note that the B matrices, for a given choice of internal coordinates, depend only on the geometry. The G matrices require only the additional input of atomic masses ($G = BM^{-1}B^{+}$).

A2. Using the normal modes from GAUSSIAN 98 frequency job output, compute the L matrices by

$$L''_{calc} = (B''_{calc})(g98'')V''^{-1/2} \text{ (the initial state)}$$

$$\text{and} \quad L'_{calc} = (B'_{calc})(g98')V'^{-1/2} \text{ (the final state)} \qquad (2.19)$$

A3. Determine the force constant matrix, defined for the chosen internal coordinates, using the harmonic frequencies ν_i and the L matrices. Following the GF formalism, define a square diagonal matrix λ or Λ for the radical (double primed) and the ion or excited molecule (single primed)

$$\lambda''_{ii} = (\nu''_i / 1302.83)^2$$

and $$\lambda'_{ii} = (\nu'_i / 1302.83)^2 \qquad (2.20)$$

with ν''_i and ν'_i in cm^{-1}. The force constant matrix F in internal coordinates is then

$$F'' = (L''^{+}_{calc})^{-1} \lambda'' (L''_{calc})^{-1}$$

and $$F' = (L'^{+}_{calc})^{-1} \lambda' (L'_{calc})^{-1} \qquad (2.21)$$

where the units are mdyn/Å and the superscript + indicates the transpose of the matrix. The two matrices, F″ and F′, are the ab initio force fields that will be used (not be changed) in the simulations at other geometry.

B. The second cycle

B1. Set the bond lengths and angles of the initial state (neutral state in this case) to the experimental values. These values will not be changed in the IFCA treatment. Then, set the geometry of the final state to a trial set, slightly displaced from the ab initio values and hence, evaluate $R''_{eq,trial}$ and $R'_{eq,trial}$. Then compute B''_{trial}, B'_{trial}, G''_{trial} and G'_{trial} using the NCA program. No input of the force field is needed yet because the B and G matrices depend only on geometries and masses.

B2. Set up and diagonalize (G'_{trial} F′) and (G''_{trial} F″). The eigenvalues are the harmonic frequencies for the ab initio force field at the slightly displaced geometries. The eigenvectors are normalized to form the new L matrices for the displaced geometries, L'_{trial} and L''_{trial}. The following is the concise procedure to normalize the L matrices obtained from the diagonization of GF matrices.

The eigenvector matrix L, obtained by diagonalizing the GF matrix, is not normalized properly. What is formed is a matrix, £, in which only the relative values within a given column are meaningful, but which, nonetheless, diagonalizes the GF. We know that a properly normalized L matrix should exhibit the property:

$$LL^{\dagger} = G \tag{2.22}$$

To correctly weight the columns of £ obtained by diagonalizing the GF matrix, a weighting factor W in the form of a diagonal matrix is applied as:

$$L = £W \tag{2.23}$$

where $W_{ij} = 0$ if $i \neq j$. Therefore, it can be written as

$$LL^{\dagger} = (£W)(£W)^{\dagger} = £W\ W^{\dagger}£^{\dagger} = G \tag{2.24}$$

with

$$C = WW^{\dagger} \tag{2.25}$$

$$C_{ii} = \sum_k W_{ik} W_{ki}^{\ +} = W_{ii} W_{ii}^{\ +} = W_{ii}^2$$

$$C_{ij} = \sum_k W_{ik} W_{kj}^{\ +} = 0 \text{ for i } \neq \text{ j since } W_{ik} = 0 \text{ unless k=i.}$$

Now the problem to be solved is

$$£C£^{\dagger} = G \tag{2.26}$$

Therefore

$$C = £^{-1} G (£^{\dagger})^{-1} = £^{-1} G (£^{-1})^{+} \tag{2.27}$$

The column weights, W_{ii}, can be easily calculated by taking the positive square root of the diagonal elements of the C matrix. After performing the matrix multiplication of equation (2.23) we will have our proper eigenvector L. In this way, direct applications of the following equations

$$J = (L''^{-1} B'')ZM^{-1}(L'^{-1} B')^{+} \qquad (2.28)$$

and $$K = (L''^{-1} B'')R \qquad (2.29)$$

yield the Duschinsky matrices J and K, i.e. J_{trial} and K_{trial} for the new geometries. The FCFs are then calculated using the generating function method as described in the above Section 2.2 and compare with the observed intensities available in literatures. If the agreement is good, the adjusted geometry of the final state (ion or excited molecule) is accepted and no more iterative computation is needed. If not, steps B1 and B2 are repeated until good agreement is obtained. The procedure as proposed by Chen (1994) and adopted routinely in this work can give more accurate geometries of the cations and/or the excited molecules.

2.4. Franck-Condon factor calculations with the consideration of the anharmonic effect

2.4.1. Background

For vibrational transitions involving floppy molecules, vibrational levels of high quantum numbers or spectra with long progressions of a single or combined vibrational mode, especially those molecules containing a hydrogen atom, anharmonic effect becomes significant and the harmonic oscillator model cannot give satisfactory results (Chau *et al.*, 1998). FCF calculations with the consideration of the anharmonic effect are necessary in such circumstances. The inclusion of anharmonicity into a one-dimensional model (i.e. single vibrational mode) of FCF calculations is relatively

straightforward and has been reviewed (Chau *et al.*, 1998). However, the applicability of a one-dimensional anharmonic FCF model is rather limited.

An anharmonic FCF calculation involves three steps, namely the determination of the multi-dimensional potential energy surfaces (PEFs) of the two electronic states involved in the electronic transition, the determination of the vibrational wavefunctions of both electronic states, and the evaluation of the vibrational overlap integrals (or the FCFs). Each of these steps requires in-depth considerations and could be a subject on its own. The aim of the following discussion is to provide a concise background picture on various aspects of the advantages and limitations of different methods available, which are relevant to the methodology employed in this work. Since the multi-dimensional anharmonic PEFs can be obtained by fitting the ab initio single energies at some level of theory, in the following discussion, we will focus only on the determination of vibrational wavefunction by variational calculation and FCF evaluation.

Variational methods have been widely used in determining ro-vibrational energies of polyatomic molecules. Readers can refer to the two excellent reviews by Carter and Handy (1986) and Searles and von Nagy-Felsobuki (1991) for details. Based on the Born-Oppenheimer approximation, the ro-vibrational Hamiltonian is a sum of the ro-vibrational kinetic operator and a potential term representing the averaged electrostatic energy. The matrix elements of the Hamiltonian are evaluated with the use of certain basis functions. Commonly used basis functions are the harmonic oscillator functions, the Morse oscillator functions, the Legendre polynomials, and numerical solution of the one dimensional Schrödinger equation. The Hamiltonian matrix obtained is then diagonalized to give the ro-vibrational wavefunctions and energies.

The commonly used Hamiltonian for the nuclear motions has been expressed in many different coordinate systems. The Watson's Hamiltonian (Watson, 1968, 1970)

was the first one known to be quantum mechanically correct. This Hamiltonian was widely employed in ro-vibrational calculations in the seventies (Carney et al., 1976; Whitehead et al., 1976). It is expressed in the normal coordinate system, and the main drawback is that the Hamiltonian has different forms for linear and non-linear geometrical configurations. This is particularly problematic for floppy molecules as the linear configuration or near-linear configurations may both be involved to give a proper description of the molecular vibrations. Hence, other forms of the ro-vibrational Hamiltonian have been proposed, for instance, the internal coordinate one proposed by Carter and Handy (1986), the MORBID Hamiltonian of Jensen (1988, 1989), and the scattering coordinate Hamiltonian of Tennyson and Sutcliffe(1982, 1983). All these Hamiltonians have the same form for the linear and non-linear configurations.

The Vibrational Self-Consistent Field (VSCF) method developed by Bowman (1986) tries to solve the ro-vibrational problem in a different approach. Bowman reduced the multi-modal vibrational problem into a set of coupled single mode equations in normal coordinates. The coupling of vibrational modes is approximated in an average way. This approach is similar to that in the Hartree-Fock theory in the case of electronic structure calculation. The coupled equations are then solved iteratively until self-consistence is achieved. Despite the approximation made, the VSCF is a promising method for application to large molecules. A vibrational calculation of a protein containing 58 amino acids has been reported (Roitberg et al., 1995).

A simple way to include anharmonicity in an FCF calculation is to express the anharmonic vibrational wavefunctions as linear combinations of the products of harmonic oscillator functions. In this way, the anharmonic vibrational FCF can be reduced to a sum of harmonic overlap integrals, which can be evaluated readily with the analytical formulae available. Botschwina and coworkers are one of the few research

groups performing anharmonic FCF calculations in this way (Botschwina et al., 1989, 1995, 1997). In their approach, the PEF of an electronic state is expressed as a polynomial of internal coordinates and the molecular force constants are obtained by fitting to a set of ab initio energies. Both the wavefunctions of the neutral molecule and the ion or excited neutral state are expressed as linear combinations of the same basis of orthogonal harmonic oscillator product functions using compromise exponents of the Gaussian functions in the basis set in order to speed up convergence of the CI expansion. The analytical anharmonic PEFs for the two corresponding states which have been obtained through fitting the single point energies of ab intio computations are inserted into the following Hamiltonian for nuclear motion:

$$H_{vib} = -\tfrac{1}{2}\hbar^2 \sum_{k=1}^{3N-6} \frac{\partial^2}{\partial Q_k^{\,2}} + V(Q_1, Q_2, \ldots, Q_{3N-6}) = \tfrac{1}{2}\sum_k P_k^{\,2} + V(Q_1, Q_2, \ldots, Q_{3N-6}) \qquad (2.30)$$

The eigenvalues E_k and eigenfunctions Ψ_k of the approximate vibrational hamiltonian H_{vib} are obtained by variationally expanding the vibrational wavefunctions using a sufficiently large basis of harmonic oscillator product functions with optimized exponents. Matrix elements are calculated by a numerical integration of Gauss-Hermite which requires a local transformation of the potential from curvilinear symmetry coordinates to rectilinear normal coordinates at the integration points. However, the Duschinsky effect was not included in their method. This is probably because most of the studies by the Botschwina and his co-workers were on infrared spectra, which consist of purely vibrational transitions within an electronic state. Thus, there is no change of equilibrium geometrical configuration during the process.

Recently, there are a few other types of anharmonic FCF methods published, such as the works of Takeshita *et al.* (1987, 1996), Malmqvist *et al.* (1998) and Xie and Guo (1999). These authors preferred the use of internal coordinate system (or symmetry

adapted internal coordinates). Takeshita *et al.* employed the basis set expansion method of Shida *et al.* (1989) to solve the nuclear Schrödinger equation and the FCFs were obtained through numerical integration. Malmqvist and Forsberg (1998) developed a simple formula for the vibrational overlap integrals, which they called the LU formula and applied it in their anharmonic FCF study. The LU formula is supposed to be more readily extendable to higher dimensional problems. Both Takeshita *et al.* and Malmqvist et al. assume a common internal coordinate for the electronic states involved in the transition (the same approach of Sharp and Rosenstock (1964)) to handle the Duschinsky effect. As for the anharmonic FCF method of Xie and Guo, it is unclear whether they have used the same approach to handle the Duschinsky effect; the details of their method have not been published. Lastly, a novel lie algebraic formalism has been reported very recently for the evaluation of multi-dimensional FCFs (Muller et al., 1999). In this work, the $\tilde{C}\,^1A' \leftarrow \tilde{X}\,^1A'$ emission spectrum of S_2O was successfully simulated, only with the explicit incorporation of off-diagonal anharmonicities for the $\tilde{C}\,^1A'$ state.

2.4.2. Anharmonic FCF calculation

The anharmonic FCF method developed in this investigation is based on that of Botschwina *et al.* (1989, 1995, 1997). One main reason for choosing the approach of Botschwina *et al.* is that, it can be readily incorporated into our developed harmonic FCF model (see later text). In this way, the Duschinsky effect, which is lacking in the method of Botschwina *et al.*, as mentioned above, is included in the present anharmonic FCF method. At the same time, with the use of ab initio PEFs and the Cartesian coordinate approach (Warshel and Karplus, 1972, 1974, 1975) (which is good for an

electronic transition even with a large geometrical change), many advantageous features of our previous harmonic FCF method are retained (Chau, 1998). Thus, with relatively straightforward modifications on our existing harmonic FCF code, anharmonicity can be incorporated into a multi-dimensional FCF calculation, which handles also the Duschinsky effect. It is therefore expected that the improved FCF method, which includes anharmonicity, should give more reliable results than the harmonic FCF method. In the following, the anharmonic FCF method encoded in this work is described in details.

The anharmonic FCF method discussed below is based on a non-linear three-dimensional system (*i.e.* considering the three normal modes of a non-linear triatomic molecule) for the sake of simplicity, though the method can be readily extended to systems of higher dimensions. Firstly, the anharmonic vibrational wavefunction of the **m**-th vibrational state is expressed as follows,

$$|\mathbf{m}\rangle = \sum c_{\mathbf{m},\mathbf{v}} \phi(v_1)\phi(v_2)\phi(v_3) \qquad (2.31)$$

where $c_{\mathbf{m},\mathbf{v}}$'s are the expansion coefficients, the subscript **v** denotes (v_1, v_2, v_3) and $\phi(v_i)$ are the v-th order harmonic oscillator functions of the normal mode *i*. The expansion coefficients, $c_{\mathbf{m},\mathbf{v}}$, are obtained by diagonalizing the Watson's Hamiltonian (Watson, 1968, 1970). The ro-vibrational Hamiltonian of a non-linear molecule given by Watson has the form,

$$H = \tfrac{1}{2}\sum_{\alpha\beta}(\Pi_\alpha - \pi_\alpha)\mu_{\alpha\beta}(\Pi_\beta - \pi_\beta) + \tfrac{1}{2}\sum_k P_k^2 - \tfrac{1}{8}\hbar^2\sum_\alpha \mu_{\alpha\alpha}^2 + V \qquad (2.32)$$

with α, β = x, y, z; and k = 1, 2, ..., 3N-6. In the above expression, Π is the total angular momentum with respect to the axes of the normal coordinates (labeled by the Greek subscripts, α, β, ...), π is the internal angular momentum arising from coupling of vibration modes, P_k is momentum conjugate to the *k*-th normal coordinate, μ is the

effective reciprocal inertia tensor and V is the electronic PEF. The anharmonicities of the vibrational motions are included in the present formalism via an anharmonic PEF, V, and the anharmonic vibrational wavefunctions defined in equation (2.31). Hamiltonian (2.32) is widely employed in ro-vibrational calculation of a molecule. The difference between the Hamiltonians used by Watson and Botschwina is that the Watson's ro-vibrational Hamiltonian (Watson, 1968) contains two additional terms of the rotational energy $-\frac{1}{8}\hbar^2\sum_{\alpha}\mu_{\alpha\alpha}$ and the vibration-rotational interaction $\frac{1}{2}\sum_{\alpha\beta}(\Pi_\alpha-\pi_\alpha)\mu_{\alpha\beta}(\Pi_\beta-\pi_\beta)$. The Π operators are not considered in our FC calculations because it operates only on the Euler angles. The Hamiltonian matrix elements, $<\mathbf{n}\mid H\mid\mathbf{m}>$, are evaluated using the Gauss-Hermite quadrature along each normal mode. Generally speaking, an ab initio PEF is usually not in normal coordinate. Thus, each quadrature grid point is transformed to the coordinate system of the PEF to obtain the corresponding value. Both the vibrational wavefunctions of the initial and final electronic states are determined in this way. Hence, the anharmonic FCF can be expressed as,

$$\mathrm{FCF}(\mathbf{m},\mathbf{n}) = <\mathbf{m}\mid\mathbf{n}>^2 = \Big(\sum_{v',v''} c_{\mathbf{m},v'}\,c_{\mathbf{n},v''}<v_1',v_2',v_3'\mid v_1'',v_2'',v_3''>\Big)^2 \qquad (2.33)$$

where the single primed and double primed quantities correspond to those of the final state and the initial state respectively. The expansion coefficients $c_{m,v'}$ and $c_{n,v''}$ are determined in the variational calculation, and $<v_1',v_2',v_3'\mid v_1'',v_2'',v_3''>$ are the overlap integral of the corresponding harmonic functions. Since the anharmonic wavefunctions are expressed as linear combination of harmonic functions in normal coordinates, the overlap integral can be evaluated readily using Chen's method (Chen,

1994). Since the Duschinsky rotation matrix is included in this method, the anharmonic FCF obtained in this way has incorporated the effect of anharmonicity and Duschinsky rotation.

2.4.3. IFCA with the anharmonic FCF method

FCFs are known to be very sensitive to the relative geometries of the electronic states involved in the electronic transition. Thus, if the equilibrium geometry of one of the two electronic states (usually the ground state of the neutral molecule, in the case of a PE spectrum) is available experimentally, the geometry of the other state can be obtained by adjusting its geometrical parameters systematically, until the simulated spectrum matches the experimental spectrum. This Iterative Franck-Condon Analysis (IFCA) procedure has been applied successfully employing the harmonic FCF method in our previous studies (Chau et al., 1997, 1998), with its details given in Section 2.2. A similar IFCA procedure can be carried out employing the anharmonic FCF method. In this case, during the IFCA procedure, the shape/form of the ab initio PEF's of the two electronic states are kept unchanged. The equilibrium position of one of two states is fixed to the available experimental geometry, while the geometrical parameters of the other state are varied systematically (initially according to the computed geometry change from ab initio calculations), until the best match between the simulated and observed spectra is achieved. More technical details of the IFCA procedure are given below.

In general, the changes in the geometrical parameters in the IFCA procedure is very small; thus, the expansion coefficients $c_{m,v'}$ and $c_{n,v''}$ obtained at the equilibrium geometry of the PEF can be kept unchanged in the IFCA procedure. However, the

harmonic overlap integrals are very sensitive to the changes in the geometrical parameters. Thus, in the case of anharmonic FCF calculation, when the geometrical parameters of one state (the cationic state in the case of a PE spectrum) are varied, a new set of harmonic overlap integrals would be evaluated, which then give a new set of anharmonic FCFs according to equation (2.33). The simulated spectrum based on this new set of anharmonic FCF is then compared to the observed spectrum until the best match is obtained.

CHAPTER 3

The X^1A_1, a^3B_1 and A^1B_1 States of $SiCl_2$: Ab initio Calculation and Simulation of Emission Spectra

3.1. Background

The dichlorosilylene molecule, $SiCl_2$, has been studied a number of times by various spectroscopic techniques (Suzuki et al., 1986 & Karolczak et al., 1993), partly because of its importance in the semiconductor industry, notably in the plasma-chemical etching processes (Suzuki et al., 1986; Sameith et al., 1986). The geometry of the X^1A_1 state of $SiCl_2$ has been derived from the experimental studies of electron diffraction (Hargittai et al., 1983), microwave (Tanimoto et al., 1989) and laser-induced fluorescence (LIF) (Meijier et al., 1989) spectroscopic studies. Among these experimentally derived geometries for the ground state of $SiCl_2$, the microwave values of r(SiCl) = 2.0700 ± 0.0012 Å and θ(ClSiCl) = 101.25 ± 0.10 ° are the most reliable, with the smallest quoted experimental uncertainties.

As for the low-lying A^1B_1 and a^3B_1 states of $SiCl_2$, it seems that no reliable geometrical parameters are available. Suzuki *et al.* (1986) attempted to extract geometric information of the upper state from their jet-cooled LIF (excitation) and single-vibrational-level (SVL) dispersed (emission) fluorescence spectrum of the A^1B_1-X^1A_1 transition by matching the computed Franck-Condon (FC) intensity patterns with the experimental ones. Employing the method of Coon et al. (1962) (the parallel mode approximation) in the FCF calculations, four sets of geometrical parameters were possible for the A^1B_1 state to fit the experimental envelopes. Among them, two sets were selected, based on deductions made from Walsh's rule (r = 2.03 ± 0.17 Å, θ = 120.8 ± 0.9° and r= 2.14 ± 0.17 Å, θ = 116.9 ± 0.9°). Clearly, the uncertainties in these derived parameters are large and the authors of this work resorted to results of available ab initio calculations (see later text) for comparison, but no conclusion could be made regarding the preferred choice of parameters.

It should be pointed out that the intensity pattern of the photolytic jet-cooled excitation fluorescence (absorption) spectrum of Suzuki et al. (1986) differs significantly from the pyrolytic jet-cooled LIF excitation (absorption) spectrum of Karolczak and Clouthier (1993). In the spectrum of Suzuki et al., which shows maximum intensity at 321.7nm, the relative intensities of the higher energy vibrational components are much weaker than those in the spectrum of Karolczak and Clouthier. The strongest observed vibrational component in the spectrum of Suzuki et al. was assigned to the A(0,7,0)←X(0,0,0) transition, while in the spectrum of Karolczak and Clouthier, the strongest peak was observed at a considerably higher energy and was probably associated with the A(0,10,0)←X(0,0,0) or A(0,11,0)←X(0,0,0) transition. The reasons for the differences in the two LIF excitation spectra are not clear. However, the gas-phase UV absorption spectrum of $SiCl_2$ (Ruzsicska et al., 1985) shows lower resolution than either of these studies peaks at 317.4nm in agreement with the LIF spectrum of Karolczak et al., and shows a very similar envelope to that of Karolczak et al. Hence this indicates that the LIF excitation spectrum of Karolczak et al. is a more reliable representation of the absorption spectrum than the LIF spectrum of Suzuki et al. Hence the vibrationally resolved LIF spectrum of Karolczak et al. for the $A^1B_1 \leftarrow X^1A_1$ transition will be used in our Franck-Condon simulations to estimate the A^1B_1 geometry. In addition, it should be noted that the geometry given by Karolczak et al. for the A^1B_1 state of $SiCl_2$ was obtained from the analysis of the rotationally resolved LIF spectrum of the $A^1B_1(0,6,0)$-$X^1A_1(0,0,0)$ transition of $SiCl_2$ as provided by Meijer et al. (1989), employing the rotational constants of the $A^1B_1(0,6,0)$ level. Therefore, the parameters derived are those for the (0,6,0) vibrational level and not those of the (0,0,0) level or the equilibrium geometry. Also, to our knowledge no experimentally derived geometric parameters have been published for the first excited state of $SiCl_2$, the a^3B_1

state. Among the reported a^3B_1-X^1A_1 emission spectra of $SiCl_2$, those by Du et al. (1991) and Sekiya et al. (1991) appear to be of the highest resolution and they look very similar to each other. The assignments of the vibrational components in the observed main $a^3B_1(0,0,0)$-$X^1A_1(0,v_2'',0)$ progression given in these two studies differ by one vibrational quantum number in v_2'' in these two studies. In addition, it seems that the assignments of the next most intense progression are also different, with Du *et al.* (1991) assigning it to the $a^3B_1(0,0,0)$-$X^1A_1(1,v_2'',0)$ progression, while Sekiya *et al.* assigning it to the $a^3B_1(0,3,0)$-$X^1A_1(0,v_2'',0)$ progression. Reliable spectral simulation would almost certainly help in resolving the above uncertainties. Moreover, the geometry thus derived for the a^3B_1 should be useful because to our knowledge, no experimental geometry was reported in the Literature. A number of ab initio molecular orbital studies have been reported on the X^1A_1, a^3B_1 and A^1B_1 states of $SiCl_2$ (Ha et al., 1986; Gosavi et al., 1996 & Kudo et al., 1986). However, these calculations, particularly those which calculated minimum-energy geometries and harmonic vibrational frequencies, were performed at relatively low levels of theory (HF/MP2) with a small basis set (6-31G* or DZP). MRCI calculations of the A^1B_1 state, which gave a geometrical parameters of $r = 2.096$ Å and $\theta = 119.3°$, were mentioned in the work of Suzuki et al. (1986), but the details of the calculation and the basis set used seem not to have been published (Kudo et al. 1986). In the present study, we propose to perform a thorough ab initio study on the X^1A_1, a^3B_1 and A^1B_1 states of $SiCl_2$, employing various types of computational methods and basis sets with the aim of deriving the geometrical parameters of the a^3B_1 and A^1B_1 states of $SiCl_2$ by simulating their emission spectra, utilizing the experimentally established equilibrium geometry of the X^1A_1 state and the computed changes in geometry on excitation to the a^3B_1 and A^1B_1 states.

3.2. Computational Details

3.2.1. Ab initio Calculations

A variety of computational methods of CIS, CASSCF, MP2, B3LYP, CISD, CCSD(T), MR-CISD, G1 and G2 at different levels of theory were applied to investigate the closed-shell singlet (X^1A_1), open-shell singlet (A^1B_1) and triplet (a^3B_1) states of $SiCl_2$, so as to access the suitability/reliability of these methods in obtaining different computed quantities. These include the minimum-energy geometries, harmonic vibrational frequencies and/or the electronic transition energies between these states. For the MP2, B3LYP, CCSD(T), G1 and G2 methods, unrestricted-spin wavefunctions were employed for the open-shell states (A^1B_1 and a^3B_1) in the geometry optimization and frequencies calculations. The ab initio calculations on the $SiCl_2$ molecule were carried out with the GAUSSIAN suite of program (Frisch et al. 1998).

3.2.2. Spectral Simulation

The FC analysis on the emission spectra of $SiCl_2$ were based on the harmonic oscillator model with the consideration of the Duschinsky effect (Duschinsky, 1937) and the method involved has been described in Chapter 2. We have chosen the two A^1B_1-X^1A_1 SVL emission spectra of Suzuki et al. (1986) (dispersed fluorescence after excitation of the 2_0^5 and 2_1^3 bands) and the a^3B_1-X^1A_1 emission spectrum of Du *et al.* (1991) as references against which our simulations will be compared. The geometry of the X^1A_1 state was fixed at the microwave experimental geometry of Tanimoto *et al.* (1989) in the IFCA procedure, where the geometric parameters of the upper states were

varied systematically (with changes in the parameters initially being given by the results of ab initio calculations), until the best match between the simulated and observed spectra was achieved. In this IFCA procedure, a Gaussian line shape was used for each vibronic component in the simulations with a full-width-at-half-maximum (FWHM) which was significantly smaller than that in the corresponding observed spectrum. This was necessary in order to assess the changes in the simulated spectral patterns with the upper state geometry changes (see next section). The final simulated spectra have, however, employed the appropriate experimental FWHM values.

3.3. Results and Discussion

The ab initio results obtained in this work are summarized in Tables 3.1-3.4 and compared with available experimental values (the experimental errors, which were quoted in the original papers, are given in parentheses in these tables). The simulated spectra which match best with the experimental spectra are given in Figures 3.1–3.6.

3.3.1. Ab initio Calculations

Considering the optimized minimum-energy geometries of the three electronic states studied, it can be seen that the variation in the computed bond angle (θ) with the levels of theory and the basis sets used is small (within 2°; see Tables 3.1, 3.2 and 3.3) for all the states of $SiCl_2$ (except for the a^3B_1 state at the CIS level, a level of theory which does not account for electron correlation; see Table 3.3). The consistency in the computed values of bond angle suggests that they should be reasonably reliable.

Comparing the computed values for the X^1A_1 state with the experimentally derived values for this state shows good agreement, supporting this conclusion.

However, the magnitudes of the computed bond lengths, r, at the levels of calculation as shown in Tables 3.1 to 3.3, have a rather large spread of ca 0.04 Å. The calculations using the lanl2-valence-augmented basis sets, lanl2(5s5p3d) and lanl2(5s5p3d1f), gave significantly shorter bond lengths (by ca 0.02 Å) compared with those from calculations with the all electron basis sets. Comparing the computed bond lengths with the available experimentally derived values for the X^1A_1 state of $SiCl_2$, the B3LYP value is too large, while the MP2 values seem to be the most reasonable one (despite the differences between the available experimental values; see Table 3.1). The basis set effect at the MP2 level on the optimized geometry is very small for the X^1A_1 state, though this is not so for the A^1B_1 and a^3B_1 states. Lastly, it should be noted that for the A^1B_1 state, although the MRCI bond angle of 119.3° given by Kudo et al. (1986), agrees well with our computed values, the MRCI bond length of 2.096 Å by these authors is considerably larger than all the computed bond lengths obtained in this work. Since the details of the MRCI calculations by Kudo et al. are unavailable to us. We are unable to trace the source of this difference.

Table 3.1. The computed and experimental geometries (r(SiCl) (Å) and θ(ClSiCl) (deg)) and vibrational frequencies (in cm^{-1}) of the X^1A_1 state of $SiCl_2$

Method	r	θ	ν_1	ν_2	ν_3
CASSCF/6-31+G*	2.0828	102.0	532.6	216.1	528.6
MP2/6-31G*	2.0751	101.7	540.8	207.4	539.8
MP2/6-311+G(2df)	2.0767	101.4	530.3	203.7	526.4
B3LYP/6-311+G(3df)	2.0943	101.9	497.9	192.3	488.2
MP2/lanl2(5s5p3d)	2.0599	101.4	521.1	207.0	514.5
CCSD(T)/lanl2(5s5p3d1f)	2.0538	101.7	530.5	206.7	529.1
microwave[a]	2.0700(12)	101.25(10)			
eD/mass[b]	2.083	102.8			
LIF[c]	2.067	101.5		198(3)	
emission[d]				200(2)	
emission[e]			529.2(3.0)	201.2(1.1)	
emission[f]			511(4)	200(2)	
emission[g]				198.5(3.7)	
LIF[h]			521.6(1)	200.6(1)	
IR[i]			512.5	202.2	501.4
IR[j]			513(3)	202(1)	502(3)

[a] Tanimoto et al., 1993. [b] Electron diffraction/mass-spectrometry; Mass et al., 1972. [c] Harmonic values; Suzuki et al., 1986. [d] Sekiya et al., 1991. [e] Harmonic values; Suzuki et al., 1986. [f] Harmonic values, the average of the two values obtained from two progressions; Du et al., 1991. [g] Sameith et al., 1986. [h] Harmonic values; Karolczak et al., 1993. [i] Mass et al., 1972. [j] Milligan et al., 1968.

Table 3.2. The computed and experimental geometries (r(SiCl) (Å) and θ(ClSiCl) (deg)) and vibrational frequencies (in cm^{-1}) of the A^1B_1 state of $SiCl_2$

Method	r	θ	ν_1	ν_2	ν_3
CIS/6-311+G(2df)	2.0613	117.9	474.0	170.4	595.3
CASSCF/6-31+G*	2.0628	119.1	480.5	168.0	611.7
MP2/6-31G*	2.0585	118.6	490.3	164.0	617.0
MP2/6-311+G(2df)	2.0482	118.5	495.0	162.9	626.5
MP2/lanl2(5s5p3d)	2.0297	119.1	492.9	171.5	619.4
CCSD(T)/lanl2(5s5p3d1f)	2.0232	117.4	515.1	162.6	631.2
emission[a]				148.9(3.4)	
emission[b]				149.9(5)	
LIF[c]			428.9(1)	149.75(6)	
IFCA	2.055(8)	119.4(4)			

[a] Sameith et al., 1986. [b] Harmonic values; Suzuki et al., 1986. [c] Harmonic values; Karolczak et al., 1993.

Table 3.3. The computed and experimental geometries (r(SiCl) (Å) and θ(ClSiCl) (deg)) and vibrational frequencies (in cm^{-1}) of the a^3B_1 state of $SiCl_2$

Method	r	θ	ν_1	ν_2	ν_3
CIS/6-311+G(2df)	2.0474	115.7	524.7	179.6	622.2
CASSCF/6-31+G*	2.0526	117.0	524.2	176.2	633.2
MP2/6-31G*	2.0514	118.2	511.0	168.1	629.7
MP2/6-311+G(2df)	2.0468	117.3	508.8	165.2	622.6
B3LYP/6-311+G(3df)	2.0618	119.2	463.5	153.0	577.3
MP2/lanl2(5s5p3d)	2.0293	117.6	507.0	173.8	616.5
CCSD(T)/lanl2(5s5p3d1f)	2.0265	118.2	504.9	169.7	623.1
emission[a]				159(2)	
emission[b]				164(2)	
IFCA[c]	2.041(3)	115.4(3)			

[a] Harmonic value; Du et al., 1991. [b] Sekiya et al., 1991. [c] see text.

Considering the computed vibrational frequencies obtained at different levels of theory, they are quite consistent for the three states studied. The only exceptions are the B3LYP values for the a^3B_1 and X^1A_1 states which are significantly smaller than the others for all the three vibrational modes (Tables 3.1 and 3.3). On comparing the computed vibrational frequencies with the experimental values, it should be noted that the computed values given in Tables 3.1-3.3 are harmonic frequencies. Harmonic experimental values are also given in these tables where available, and this is stated in the footnote of each table; otherwise, the experimental values given are the fundamentals. For the X^1A_1 state, where experimental harmonic constants are available for all the three modes, the agreement between theory and experiment is quite good, particularly for the ν_2 mode. As for the a^3B_1 state, experimental values are available only for the ν_2 mode; however, the agreement between theory and experiment is also very good for this mode, particularly for the MP2/6-311+G(2df) computed frequency. For the A^1B_1 state, the discrepancies between the computed and observed values are larger than those for the other two states. Specifically, the computed values are consistently too large, particularly for the ν_1 mode, though only one experimental harmonic value is available for comparison. Both the CIS and CASSCF values were not in better agreement with experimental values than computed values from other methods, suggesting that the discrepancies are probably not due to the problem of spin-contamination associated with the UHF-based correlation methods. In view of the relatively improved agreement with the experiment value (within ca 14 cm^{-1}) for the ν_2 frequency at the MP2/6-311+G(2df) and CCSD(T)/lanl2(5s5p3d1f) levels of calculation for the A^1B_1 state, it may be concluded that a higher level of theory with better treatment of electron correlation and /or a better quality basis set than what has been

used would be required to describe the energy surfaces of this open-shell singlet state accurately. However, this kind of calculation would be computationally very demanding. For the purpose of carrying out FCF simulations, the MP2/6-311+G(2df) geometries and force constants, which have showed overall good agreement with experiment were employed in this study.

Table 3.4. Computed and observed transition energies (eV) of $SiCl_2$

Method	a^3B_1-X^1A_1	A^1B_1-X^1A_1
RHF/6-311G(2df)	1.55	3.70
CIS/6-311+G(2df)[a]	1.46	3.83
CASSCF/6-31+G*	2.05	4.30
CASSCF/MP2/6-31+G*[b]	1.91	4.84
MP2/6-31G*	2.07	3.64
MP2/6-311+G(2df)	2.18	3.54
B3LYP/6-311+G(3df)	2.29	-
MP2/lanl2(5s5p3d)	1.97	3.50
CCSD(T)/lanl2(5s5p3d1f)	2.12	2.46
G1	2.47	2.74
G2	2.42	2.71
CISD/6-311G(2df)[c]	1.99	3.76
CISD+Q/6-311G(2df)[c]	2.15	3.75
MR-CISD/6-311G(2df)[c]	2.18	3.82
MR-CISD+Q/6-311G(2df)[c]	2.31	3.78
Experimental[d] (Sekiya et al., 1991)	2.32	
Experimental (Du et al., 1991)	2.36	
Experimental (Sameith et al., 1986)		3.76
Experimental (Suzuki et al., 1986)		3.72

[a] Vertical transition at the CIS optimized geometry of the corresponding upper states; the rest of the computed values are for the adiabatic transitions at the respective optimized geometries, unless otherwise stated. [b] At the corresponding CASSCF optimized geometries. [c] At the corresponding MP2/6-311+G(2df) optimized geometries. [d] All the experimental values are T_0, while all computed values are T_e, except the G1 and G2 values, which are the enthalphy changes at 298 K.

Table 3.4 lists the computed T_e transition energies (adiabatic electronic transition energy, unless otherwise stated in the footnote) and the experimental T_0 values. It is obvious that those calculations with a larger basis set and at a higher level of correlation give results closer to those from experiment. The best computed transition energy for the a^3B_1-X^1A_1 transition is that at the MR-CISD+Q/6-311G(2df)//MP2/6-311+G(2df) level. The agreement of within 0.05 eV is, indeed, very pleasing.

3.3.2. Spectral Simulations

For the SVL A^1B_1-X^1A_1 emissions, the simulated spectra, which match best with the SVL emission spectra of Suzuki et al., are shown in Figure 3.1 and 3.2 with the FWHM having value of 0.3 nm and 0.6nm respectively for the energy range under study. The IFCA geometry obtained for the A^1B_1 state, using the procedure described earlier in the Computational Details section, is r(SiCl) = 2.055 ± 0.008 Å and θ(ClSiCl) = 119.4 ± 0.4°. The rather large uncertainty associated with the IFCA bond length is due to the weak intensities of the vibrational components arising from the A(0,3,0)-X(1,v_2'',0) and A(0,5,0)-X(1,v_2'',0) progressions in the experimental spectra. The IFCA geometry given above is one that gives the best match for both the dispersed fluorescence spectra of $SiCl_2$ excited at 325.02 nm and 330.45 nm (the A(0,5,0)←X(0,0,0) excitation and A(0,3,0)←X(0,1,0) excitations, respectively; Suzuki et al., 1986). It should be noted that the observed intensities of the emission peaks at the excitation energies (*i.e.*, the A(0,5,0)→X(0,0,0) and {A(0,3,0)→X(0,1,0) emissions) were enhanced due to contributions from the respective excitation lines. In making the comparison between the simulated and the experimental spectra, these peaks have been ignored. It was found that apart from these peaks, the agreement between the

experimental SVL spectra and the simulated spectra employing the IFCA geometry for the upper state given above is very good. As noted previously (Chau et al., 1998), with the harmonic oscillator model adopted in the FC simulation, it is expected that the agreement between simulation and observation would gradually deteriorate for transitions involving high vibrational quantum numbers where the effect of anharmonicity becomes larger. This was found to be the case in Figures 3.1 and 3.2 where the agreement for the first 10 resolved components close to the excitation line was good, but the agreement with the features to higher wavelength, which were a lot weaker and not so well resolved, was not so good. The relative intensity of the 10 resolved components close to the excitation line was the structure from which the IFCA upper state geometry was derived.

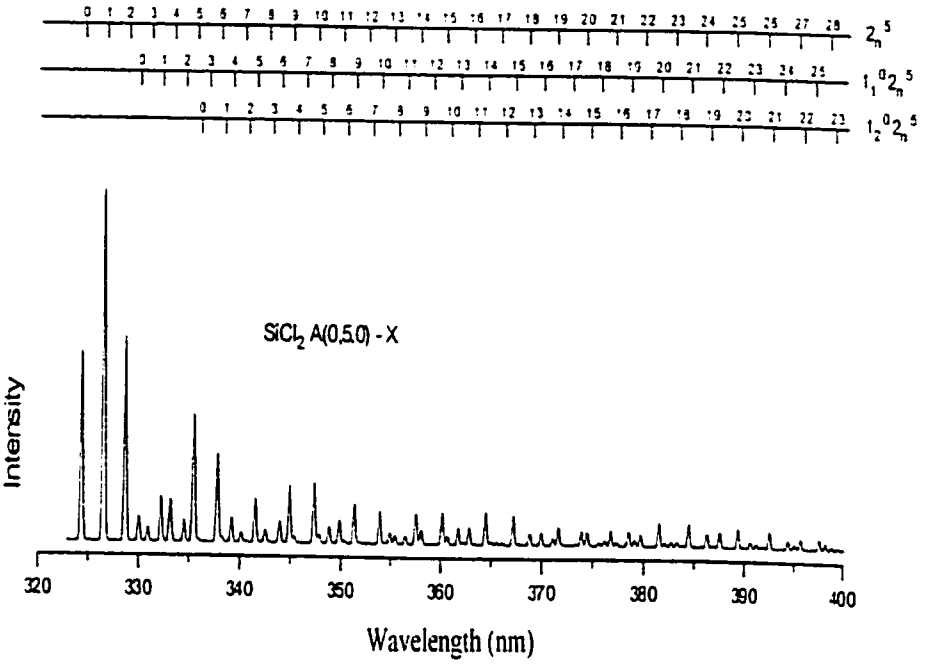

Figure 3.1. Simulation of the SVL emission spectrum of $SiCl_2$ excited at 325.02 nm (the A(0,5,0) ← X(0,0,0) excitation). The Gaussian bands used for this simulation have a fwhm of 0.3 nm. This spectrum shows good agreement with the experimental spectrum reported by Suzuki et al. (1986). (Reproduced in Figure 3.7a).

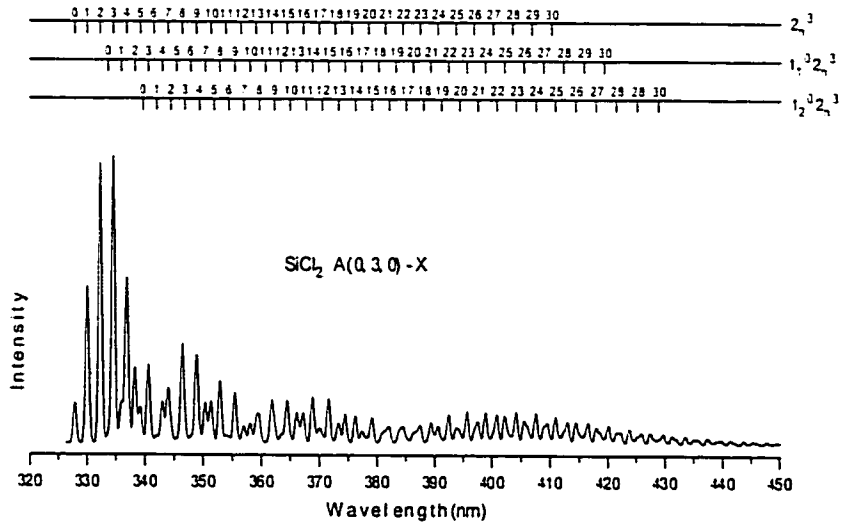

Figure 3.2. Simulation of the SVL emission spectrum of $SiCl_2$ excited at 330.45 nm (the A(0,3,0) ← X(0,1,0) excitation). The Gaussian bands used for this simulation have a fwhm of 0.6 nm. This spectrum shows good agreement with the experimental spectrum reported by Suzuki et al. (1986). (Reproduced in Figure 3.7b).

With A^1B_1 IFCA geometry of r(SiCl)=2.055 ± 0.008 Å and θ(ClSiCl) = 119.4 ± 0.4°, the A-X absorption spectrum has also been simulated and this is shown in Figure 3.3. (The simulation was performed using a Gaussian line shape with FWHM of 0.02 nm and at a temperature of 150 K, assuming a Boltzmann distribution of the vibrational levels of the ground state). Although a direct comparison with the LIF excitation spectrum of Karolczk and Clouthier is not possible because of the complex rotational structures and contributions from different isotopes, the simulated intensity distribution agrees reasonably well with the observed envelope. It is clear that the agreement with the LIF spectrum of Karolczk and Clouthier (1993) is much better than with that of Suzuki et al. (1986). Given this evidence and the fact that the spectrum of Karolczk and

Clouthier shows a similar envelope and maximizes at the same wavelength as the UV absoption spectrum of $SiCl_2$ (obtained at lower resolution, Ruzsicska et al., 1985), unlike the LIF excitation spectrum of Suzuki et al. (1986), we conclude that the LIF fluorescence spectrum of Kolczak and Clouthier is more representative of the absorption spectrum than of Suzuki et al. (1986). In addition, the fact that employing the same IFCA geometry in simulating different spectra gave good agreement between theory and experiment in all cases adds weight to the reliability of the method used in extracting geometrical parameters in this way and also to the IFCA A^1B_1 geometry thus obtained. It should also be noted that if the geometry of the $A^1B_1(0,6,0)$ $SiCl_2$ state, as determined by the LIF spectroscopy (Mejier et al., 1989), is used in the simulation, very different simulated spectra are obtained for Figures 3.1, 3.2 and 3.3 which are in poor agreement with the corresponding experimental spectra (Suzuki et al., 1986; Karolczak and Clouthier, 1993).

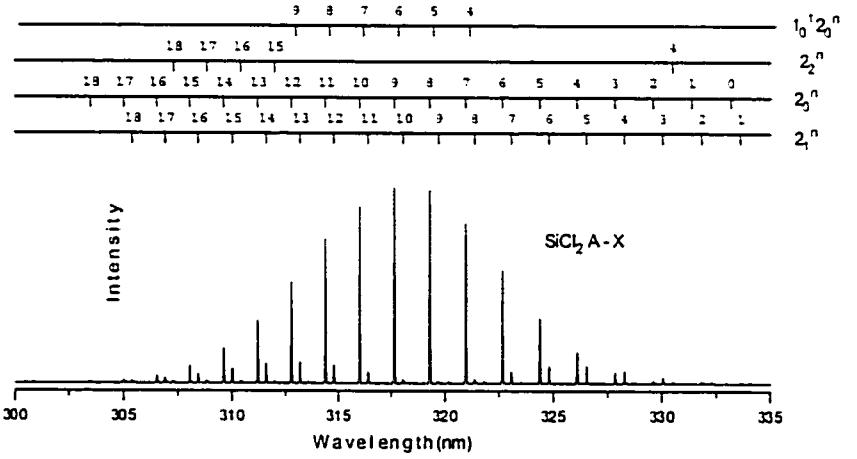

Figure 3.3. Simulation of the A-X absorption spectrum of $SiCl_2$ using the IFCA derived geometry from Figures 3.1 and 3.2 of the A^1B_1 state of r(SiCl)=2.055 ± 0.008 Å and θ(ClSiCl) = 119.4 ± 0.4°. (Reproduced in Figure 3.7c). This spectrum was simulated using a Boltzmann distribution of the vibrational levels in the X^1A_1 state at a temperature of 150 K. The Gaussian bands in this simulation have a fwhm of 0.02nm. Good agreement was obtained with the LIF excitation spectrum by Karolczak et al. (1993).

For the a^3B_1-X^1A_1 emission, the simulated spectrum which matches best with the emission spectrum reported by Du et al. (1991) is shown in Figure 3.4. A temperature of 300 K was used in this simulation and a Boltzmann distribution was assumed for the relative populations of the various low-lying vibrational levels of the upper state. Variations in the temperature and the IFCA geometry were carried out in our investigation. It can be seen that a temperature of 300 K is adequate to give a simulated intensity distribution which accounts for all the observed transitions arising from the excited vibrational levels of the upper state. In addition, the assumption of a Boltzmann distribution also seems adequate. However, our simulations could not

produce the underlining unresolved background observed in the spectrum of Du et al. (1991) (which also appeared in the observed spectrum of Sekiya et al. (1991)). Lowering the resolution in the simulations even to an extent that some of the observed structures become blurred still could not reproduce the substantial background of the observed spectrum. Consequently, the matching between the simulations and the observed spectrum was based on the resolved vibrational structure above the background. The IFCA geometry employed for the a^3B_1 state to produce Figure 3.4 is r(SiCl) = 2.041 ± 0.003 Å, and θ(ClSiCl) = 115.4±0.3°.

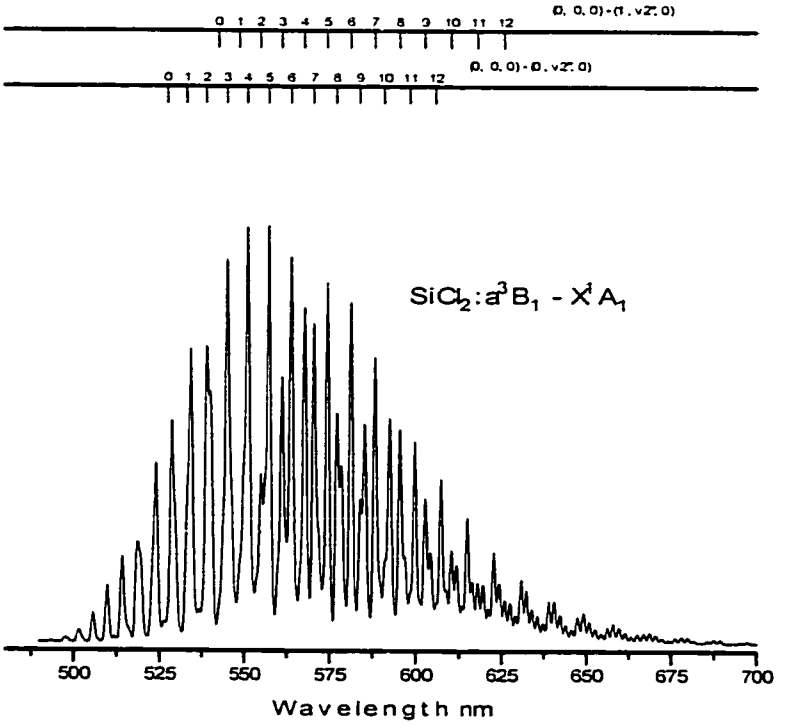

Figure 3.4. Simulation of the a^3B_1-X^1A_1 $SiCl_2$ emission spectrum. This spectrum shows good agreement with that shown in the work of Du et al. (1991). The IFCA geometry employed for the a^3B_1 state to produce this figure is r(SiCl) = 2.041 ± 0.003 Å, θ(ClSiCl) = 115.4 ± 0.3°. An initial 300 K Boltzmann vibrational distribution in the a^3B_1 state was assumed in the simulation.

It should be noted that in the IFCA procedure, the intensity pattern was found to be very sensitive to the upper state geometry variation and this is reflected in the small uncertainties given above for the IFCA geometrical parameters. The absolute uncertainties would be smaller if it were not for the relatively poor resolution of the

observed spectrum, and the possibility of an alternative vibrational assignement (see later).

The a-X emission of $SiCl_2$ consists of a large numbers of vibrational series. Figure 3.5 shows the computed relative intensities of the eight strongest vibrational progressions. Based on the vibrational analysis, it is quite certain that the observed second most intense vibrational series is due to the $a^3B_1(0,0,0)$-$X^1A_1(1,v_2'',0)$ transitions as assigned by Du et al. (1991) rather than the $a^3B_1(0,3,0)$-$X^1A_1(0,v_2'',0)$ transitions as assigned by Sekiya et al. (1991). Attempts were also made to simulate the a-X emission spectrum according to the assignments of Sekiya et al.(1991) for the main series {the $a^3B_1(0,0,0)$-$X^1A_1(0, v_2'', 0)$ transitions}, so as to determine the position of T_0 as mentioned in the Background. The best match is shown in Figure 3.6. In obtaining this simulated spectrum, the IFCA bond angle used was 114.0°, 1.4° smaller than that of the assignment of Du *et al.* (1991), but the bond length was almost the same as that given above. It can be seen that with a slightly different upper state IFCA geometry, a simulated spectrum similar to that which matches the assignment of Du *et al.* (1991) can be obtained. Comparing the simulated spectra in Figure 3.4 and 3.6 with the experimental spectrum of Du *et al.* (1991) in detail, Figure 3.4 was considered to be a marginally better match, particularly at the low wavelength region, than Figure 3.6.

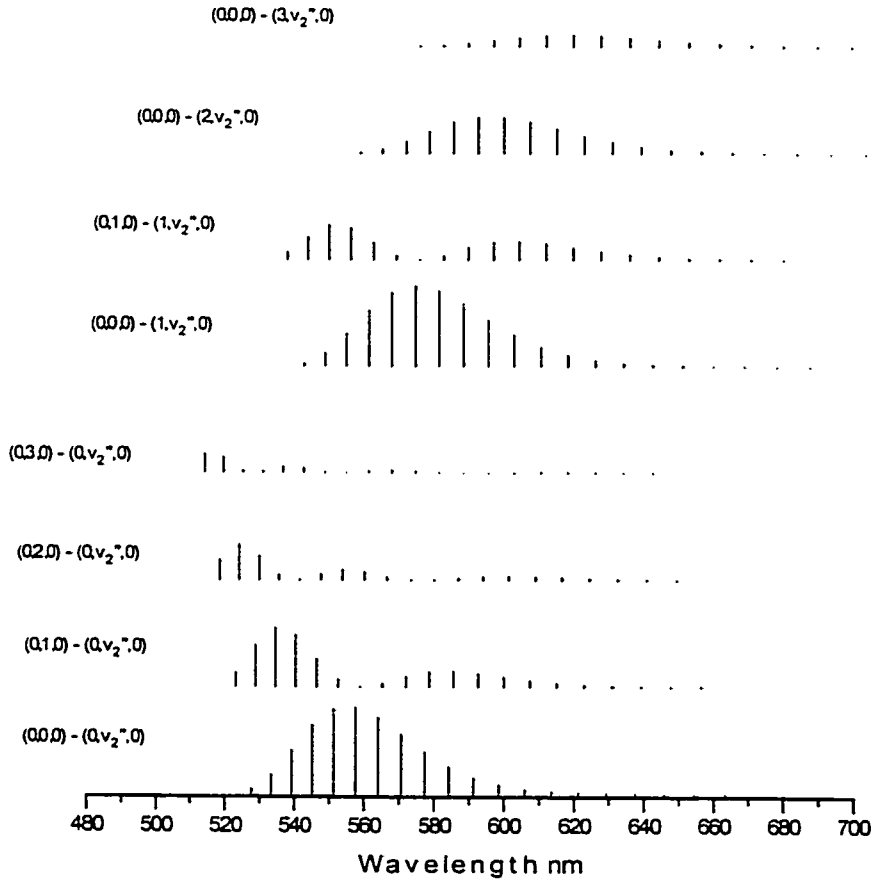

Figure 3.5. A diagram showing the computed relative intensities of the 8 strongest vibrational progressions in the a^3B_1-X^1A_1 emission spectrum. Based on this simulation, it is clear that the observed second most intense vibrational series arises from the $a^3B_1(0,0,0)$-$X^1A_1(1,v_2'',0)$ transition as assigned by Du et al. (1991) rather than the $a^3B_1(0,3,0)$-$X^1A_1(0,v_2'',0)$ transitions assigned by Sekiya et al. (1991).

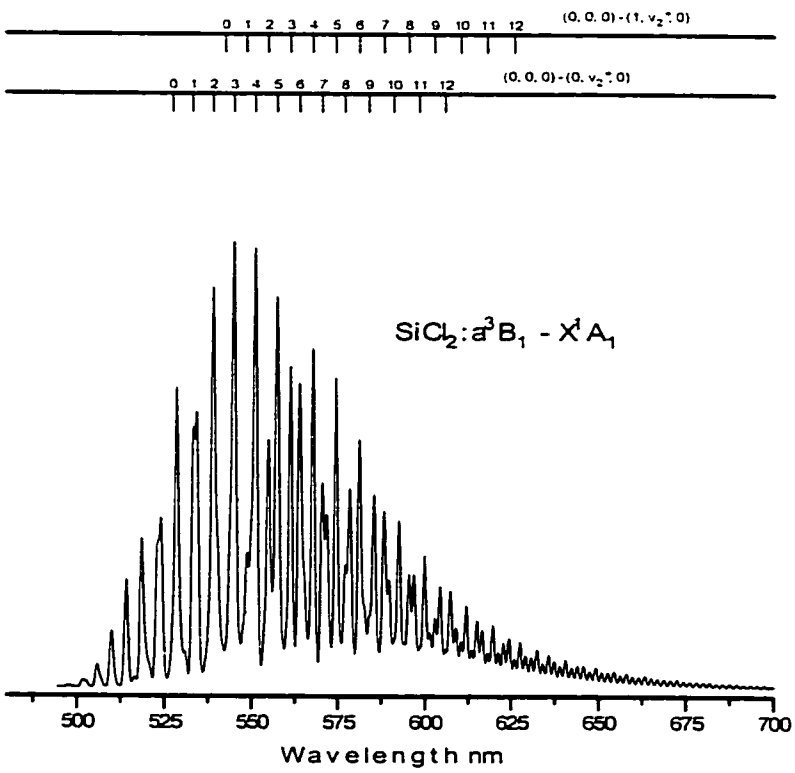

Figure 3.6. Simulation of the a^3B_1-X^1A_1 emission spectrum which fits the experimental spectrum with the assignments of Sekiya et al. for the main series (the $a^3B_1(0,0,0)$-$X^1A_1(0,v_2'',0)$ series). The best match that was obtained, with the assignment of Sekiya et al., was with an a^3B_1 geometry of r(SiCl) = 2.041 ± 0.003 Å, θ(ClSiCl) = 114.0 ± 0.3° (see text).

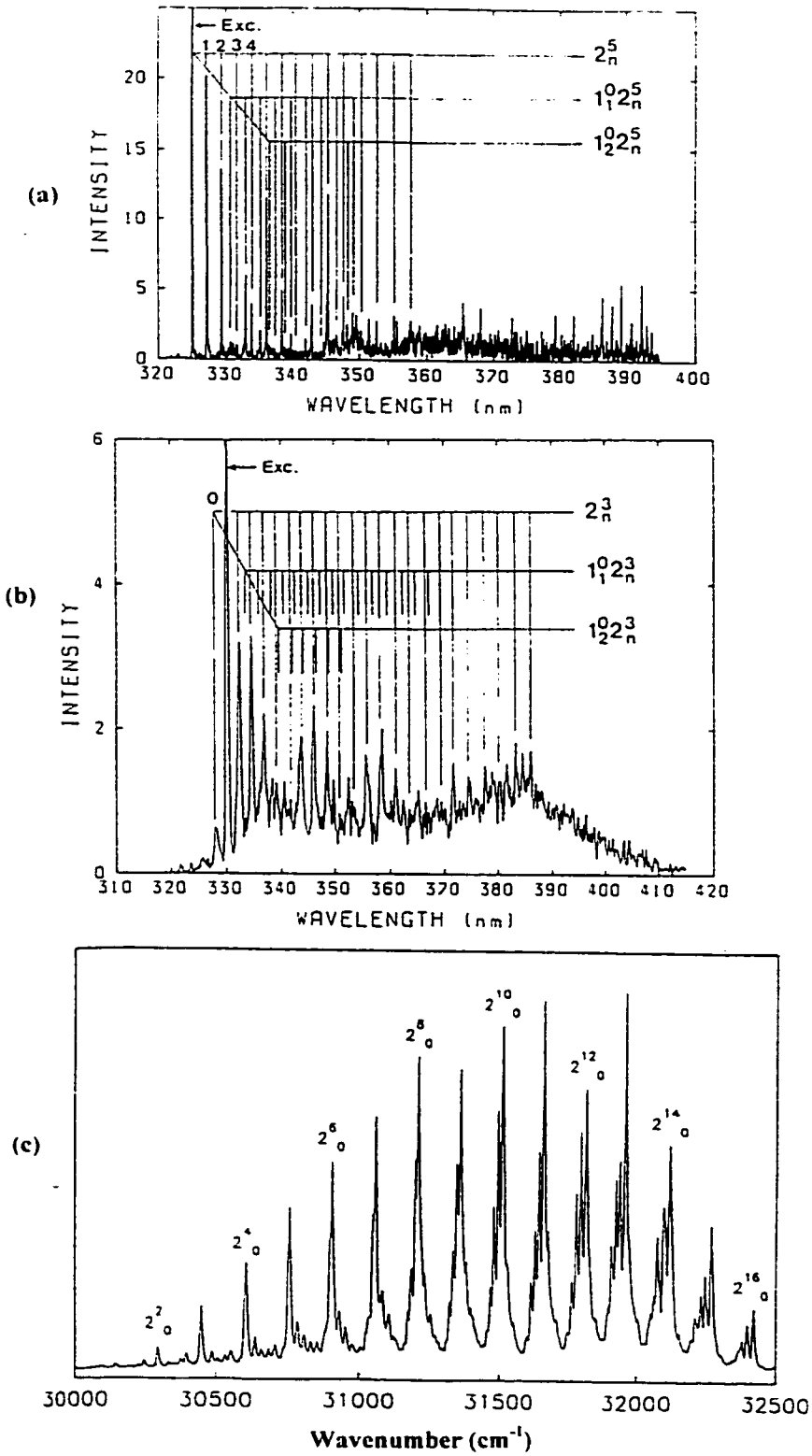

Figure 3.7. Experimental spectra of $SiCl_2$: (a) Dispersed fluorescence spectrum of jet-cooled $SiCl_2$ recorded on the 2_0^5 excitation by Suzuki et al.(1986). This spectrum can be compared with Figure 3.1 if the excitation line (marked "Exc") is removed. (b) Dispersed fluorescence spectrum of $SiCl_2$ recorded on 2_0^3 excitation in an effusive flow source by Suzuki et al. (1986). This spectrum can be compared with Figure 3.2 if the excitation line (marked "Exc") is removed. (c) Experimental A-X absorption spectrum of $SiCl_2$ presented by Karolczak et al. (1993). This spectrum was obtained under jet-cooled conditions.

3.4. Concluding Remarks

In this work, attempts were made to extract the equilibrium geometries of the a^3B_1 and A^1B_1 states of $SiCl_2$ from the a-X and A-X emission spectra by spectral simulation using geometries derived from ab initio calculations. It is shown that accurate calculations of the geometries of the low-lying electronic states of $SiCl_2$ (particularly the bond length) are at present beyond the reach of practical ab initio calculations at reasonably high levels of theory. However, combining such ab initio calculations with FC analysis and spectral simulation, reasonably reliable geometries were obtained and they are probably the most reliable ones currently available for the a^3B_1 and A^1B_1 states of $SiCl_2$.

Attempts were also made to clarify some disagreements in the assignments of the a-X emission spectra available in the literature. With the spectral simulations provided in this study, the assignment of the observed second main vibrational series should be unambiguous and it is assigned to the A(0,0,0)-X(1,v_2",0) series. Regarding the a-X T_0 position, it is clear that for such a system such as $SiCl_2$, practical ab initio calculations are still some way from being able to reach an accuracy which could decide between assignments differing by one vibrational spacing. Although our spectral simulations could not distinguish unambiguously between the two proposed assignments from two previous experimental studies, it seems that the assignment of Du et al. (1991) is favored. This places T_0 at 2.36 eV for the $a^3B_1 - X^1A_1$ transition.

For the A-X emission, attempts were made to rationalize the difference in the spectral pattern between two experimental LIF excitation spectra reported previously and it was concluded that the excitation spectrum of Karolczak and Clouthier (1993) should be more representative of the absorption spectrum. The above conclusions show

the advantage of combining ab initio calculations with FC simulations in relation to information extractable from the relative intensities observed in emission spectra.

In conclusion, ab initio molecular orbital calculations combined with Franck-Condon simulations have proved very useful in simulating the absorption and emission spectra of $SiCl_2$ and in deriving excited-state geometrical parameters.

CHAPTER 4

Simulations of the He I Photoelectron Spectrum of BrO_2 and the Single Vibrational Level Dispersed Fluorescence Spectrum of AlCN

4.1. Background

In last chapter, we have successfully applied the IFCA technique, which combines ab initio molecular orbital calculations with Franck-Condon calculations, to the emission spectra of $SiCl_2$, and obtained for the first time, experimentally derived geometrical parameters of the upper states involved in the electronic transitions. However, sometimes, when a complex reaction scheme is involved in producing the species of interest, and/or when a spectrum with complicated vibrational structure is observed, the interpretation of the observed spectrum may not be straightforward. In some cases, even the identity of the molecular carrier of the spectrum may not be certain from the observed spectra, and hence a careful and in-depth theoretical investigation is required to assist spectral interpretation. In this chapter, we demonstrate the usefulness of a combined application of ab initio calculations and Franck-Condon (FC) analysis to study some photoelectron and electronic spectra, where there were uncertainties in their assignments. The spectra chosen are the He I photoelectron spectrum of BrO_2 and the single vibrational level (SVL) dispersed fluorescence spectra of AlCN. With suitable ab initio calculations and subsequent spectral simulations, assignments of these spectra can now be made. In addition, the iterative Franck-Condon analysis (IFCA) procedure was also applied to the first PE band of BrO_2 in order to derive the cationic state geometry.

Dunlavey *et al.* (1978) reported the He I photoelectron spectrum recorded for the reaction products of the gas phase reaction, $O + Br_2$. A photoelectron band, associated with a short-lived intermediate, showing at least two vibrational components, separated by 830 cm^{-1}, was observed at 10.29 ± 0.01 eV; it was assigned to the BrO^+ ($\tilde{X}\,^3\Sigma^-$) ← BrO ($\tilde{X}\,^2\Pi_{3/2}$) ionization (see Figure 4.1a). A more recent photoionization mass spectrometric (PIMS) study of BrO, produced also from the $O + Br_2$ reaction, obtained a

value of 10.46 ± 0.02 eV (Monks et al., 1993) for the first adiabatic ionization energy (AIE) of BrO. In addition, the AIE value of BrO, as measured in the PIMS study, is supported by the most reliable, calculated value of 10.455 ± 0.035 eV reported recently by Francisco *et al.* (1998). This theoretical AIE was obtained through CCSD(T) calculations with large atomic natural orbital (ANO) basis sets, and extrapolation to the one-particle basis set limit. Clearly, the discrepancies between the He I experimental AIE value and those from the PIMS and CCSD(T) studies are beyond the quoted uncertainties. In view of the results obtained from the later experimental and theoretical studies on BrO, the assignment of the 10.29 eV band in the O + Br_2 He I photoelectron spectrum to BrO seems questionable. One aim of this work is to re-examine the assignment of the 10.29 eV band in the He I photoelectron spectrum of Dunlavey *et al.* (1978), by performing high-level ab initio calculations, FC analyses and spectral simulations on a number of possible alternative molecular candidates.

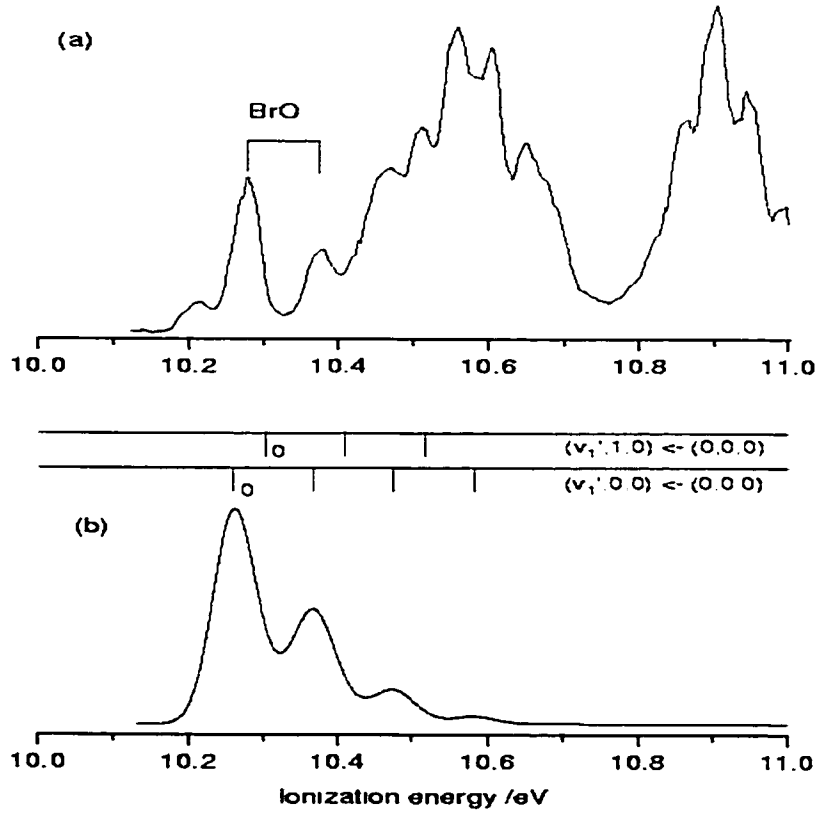

Figure 4.1. (a) The experimental spectrum of Dunlavey *et al.* (1978); (b) The simulated photoelectron spectra of BrO_2 (C_{2v}) with the IFCA geometry (see text). The estimated experimental FWHM of 65 meV were used to generate the spectrum.

Very recently two laser induced fluorescence (LIF) studies on AlNC/AlCN were reported, where investigations were made in supersonic free jet expansions (Fukushima, 1998; Gerasimov et al., 1999). Excitation LIF spectra and single vibrational level (SVL) dispersed fluorescence spectra were recorded in both studies. In the first study, Fukushima (1998) observed an electronic band system at 28754 cm^{-1}, which was attributed to the $^1A' \leftarrow \tilde{X}\,^1\Sigma^+$ transition of AlNC based on ab initio computed relative

energies and vibrational frequencies. In the second study, Gerasimov *et al.* observed a band system at 36398 cm^{-1}, which was assigned to the $\tilde{A}^1\Pi - \tilde{X}^1\Sigma^+$ transition of AlNC, based on changes of derived rotational constants on isotopic substitution and the analysis of the observed rotational structure. In order to clarify the assignment of the 28754 cm^{-1} band system reported by Fukushima, Gerasimov *et al.* also examined the 28754 cm^{-1} region of their LIF spectrum and observed the same band system of Fukushima. It was found that the vibrational energy spacings in the ground electronic state $\tilde{X}^1\Sigma^+$ observed in the dispersed fluorescence spectra of the 28754 cm^{-1} band, were different from those measured for the $\tilde{A}^1\Pi - \tilde{X}^1\Sigma^+$ AlNC band at 36398 cm^{-1}. In addition, the rotational constant of the lower state of the band at 28754 cm^{-1} derived from the observed rotational structure was essentially the same as the ab initio computed value of the ground state of AlCN (Ma et al., 1995). Hence, the 28754 cm^{-1} band system was re-assigned to an electronic transition of the isomer, AlCN, rather than to a transition of AlNC as in the first study (Fukushima, 1998). Fukushima (1998) also performed ab initio calculations on the lowest-lying $^3\Pi$ and $^1A'$ states of both AlCN and AlNC in order to assist interpretation of the observed LIF and dispersed fluorescence spectra, which showed rather complicated vibrational structure. Unfortunately, no $^1\Pi$ states were considered in these calculations. In the present study, ab initio and FCF calculations were carried out on the lowest-lying $X^1\Sigma^+$ and $A^1\Pi$ states of AlCN with the aim of confirming the assignments of the 28754 cm^{-1} band system observed in the work of Fukushima (1998) and Gerasimov *et al.* (1999).

4.2. Theoretical method and Computational Details

The GAUSSIAN98 suites of programs (Frisch et al., 1998) was employed for geometry optimization and vibrational frequency calculations at the CIS, MP2, QCISD and CCSD(T) levels. Single energy calculations at the CASSCF/MRCI level were performed with MOLPRO98 (Werner et al., 1998). The composite G2 method was also employed to calculate the AIEs of Br_2O, using GAUSSIAN98. The CASSCF/MRCI method is most suitable for open-shell species. However, the CASSCF/MRCI method is in general computationally much more demanding than the perturbative and couple cluster methods. The latter methods were therefore employed for geometry optimization and frequency calculations. Nevertheless, single geometry CASSCF/MRCI calculations were performed to check the reliability of the perturbative and couple cluster computed results. It was found that the latter results are reasonably reliable.

The method of the combination of FC analysis and ab initio calculations followed in this work has been described in Chapter 2. The harmonic oscillator model with the consideration of Duschinsky effect and the IFCA procedure have been used in this investigation.

For the investigation of the He I photoelectron spectrum reported by Dunlavey *et al.* (1978), the BrOBr (C_{2v}) and BrBrO (C_s) were first studied, as they are the most obvious candidates for the possible products from the reaction

$$O(^3P) + Br_2(^1\Sigma_g^+) \rightarrow \text{products} \qquad (4.1)$$

Then BrO_2 was investigated. The He I photoelectron spectrum of the valence iso-electronic molecule ClO_2 has been published (Flesch et al., 1993) and the first band of

ClO_2 exhibits a vibrational envelope, which differs significantly from that of the 10.29 eV band in the experimental He I spectrum by Dunlavey *et al.* (1978). However, in a very recent study of experimental laboratory methods to produce OBrO, reaction (4.1) was found to produce a substantial amount of OBrO, as a secondary product, via the self-reaction of vibrationally excited BrO (Li, 1999).

4.3. Results and Discussions

4.3.1. Br_2O : the C_{2V} (BrOBr) and C_S (BrBrO) structures

Since the BrOBr structure is more stable Br_2O structure, it may be expected that BrOBr would be observed, when Br_2O is produced. However, BrBrO has a computed harmonic vibrational frequency of 793 cm^{-1} for the BrO stretch (Lee, 1995), which is close to the observed vibrational spacing of 830 cm^{-1} observed in the He I photoelectron spectrum of Dunlavey *et al.* (1978). In relation to the assignment of the 10.29 eV band, we are particularly interested in the computed vibrational frequencies of the ground cationic states of the two structures, for which no experimental values are available. Summarizing the ab initio results obtained (Tables 4.1-4.2), the highest harmonic vibrational frequencies of the symmetric stretching mode were computed to be ca. 540 (740) cm^{-1} for of $BrOBr^+$ $\tilde{X}\,^2B_1$ ($BrBrO^+$ $\tilde{X}\,^2A'$), while the G2 AIEs were 10.37 (9.93) eV respectively. The simulated first photoelectron band of both $BrOBr^+$ $\tilde{X}\,^2B_1$ and $BrBrO^+$ $\tilde{X}\,^2A'$, employing QCISD computed force constants (Tables 4.1-4.2), show a much more complicated vibrational envelope (Figures 4.2-4.3) than that of the 10.29 eV band as shown in Figure 4.1(a). Based on the computed vibrational frequencies (Tables

4.1-4.2), AIEs and spectral simulations (Figures 4.2-4.3), the 10.29 eV band observed by Dunlavey *et al.* (1978) cannot be assigned to ionization of BrOBr or BrBrO.

Table 4.1. Optimized geometries and harmonic vibrational frequencies (cm^{-1}) of the X^1A_1 state of $BrOBr(C_{2v})$ and the X^2B_1 state of $BrOBr^-(C_{2v})$ at the QCISD level of theory.

Method / State	BrO/Å	θ / °	$\nu_1(a_1)$	$\nu_2(a_1)$	$\nu_3(b_2)$
$BrOBr(X^1A_1)$:					
QCISD/lanl2dz+2d	1.869	113.3	535	181	664
Microwave[a]	1.838	112.2			
IR Ar[b]			525.3		622.2
$BrOBr^-(X^2B_1)$:					
QCISD/6-311G(2d)	1.812	119.6	535	194	542

[a] Muller et al., 1997
[b] Kolm et al., 1998.

Table 4.2. Calculated optimized geometries and harmonic vibrational frequencies (cm^{-1}) of the X^1A state of BrBrO (C_s) and the X^2A' state of $BrBrO^+$ (C_s) at the QCISD/6-311G(2d) level.

Method / State	BrO/ Å	BrBr/ Å	θ / °	ν_1(BrO)	ν_2(BrBr)	ν_3(bend)
$BrBrO(X^1A)$:						
QCISD/6-311G(2d)	1.693	2.470	111.6	737	247	165
IR (Ar)[a]				804	235.8	
IR (Ar)[d]				804.6		
$BrBrO^+(X^2A')$:						
QCISD/6-311G(2d)	1.677	2.342	108.6	738	286	194

[a] Tevault et al., 1978; [b] Kolm et al., 1998

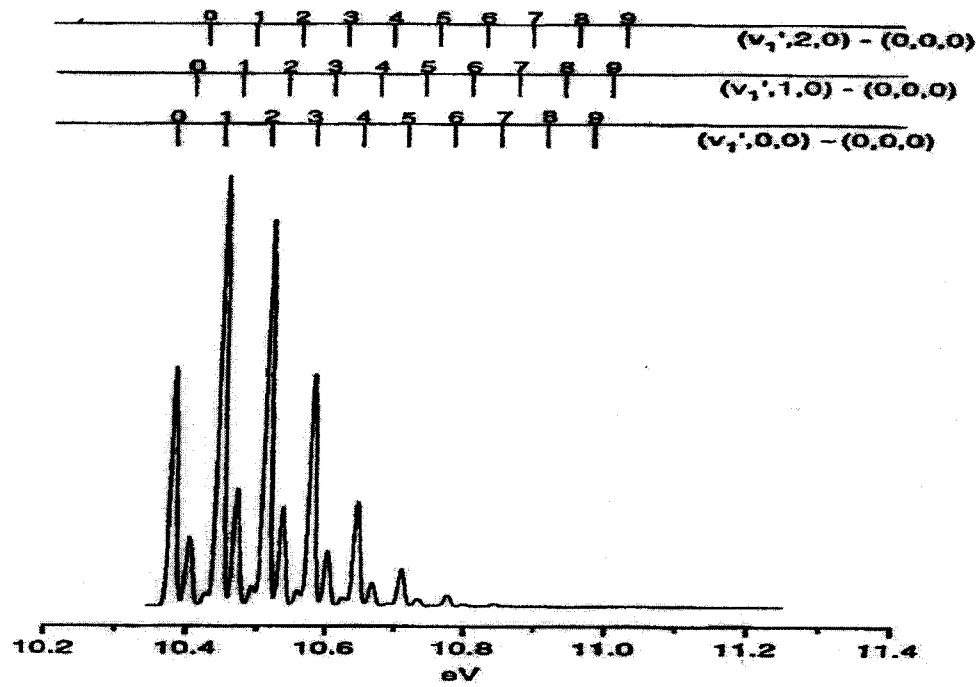

Figure 4.2. Simulated first photoelectron band of C_{2v} BrOBr using QCISD computed values for the neutral and ionic states involved (Table 4.1). Gaussian vibrational envelopes with a FWHM of 10 meV were used in this simulation.

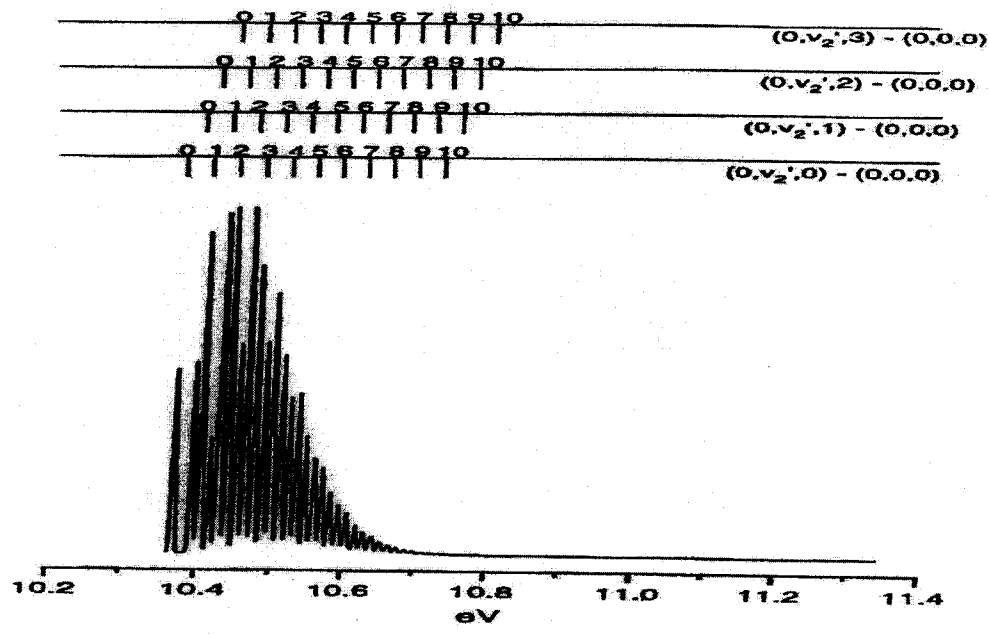

Figure 4.3. Simulated first photoelectron band of C_s BrBrO using QCISD computed values for the neutral and ionic states involved (Table 4.2). Gaussian vibrational envelopes with a FWHM of 5 meV were used in this simulation.

4.3.2. BrO_2: $OBrO(C_{2V})$ and its cation

Because a photoionization mass-spectrometry study (Thorn et al., 1996) derived the first AIE of Br_2O as (10.26 ± 0.01) eV, and this value happened to agree with 10.26 eV obtained from the He I photoelectron spectrum recorded for the O + Br_2 reaction. Therefore, it seemed reasonable to assume that the He I spectrum was due to an isomer of Br_2O. Very recently, a kinetic study of the reaction of OBrO with O_3 has been reported (Li, 1999). In this study, OBrO was produced via a number of reactions, including O + Br_2. This evidence and the lack of a completely satisfactory candidate for the assignment of the observed O + Br_2 photoelectron band of Dunlavey *et al.* (1978), have prompted us to consider OBrO. There are a number of previous ab initio studies on OBrO and one on the lowest singlet state of the cation (Francisco, 1998; Peterson, 1998; Alcami et al., 1998). The first AIE was calculated at the CCSD(T)/6-311+G(3df)//CCSD(T)/6-311G(2df) level to be 10.16 eV and the symmetric stretching frequency of the cation was computed to be 822 cm^{-1} at the CCSD(T)/TZ2P level (Francisco, 1998). Both the computed AIE and the vibrational frequency match reasonably well with those measured for the O + Br_2 10.26 eV band. However, as mentioned in the Background, the He I photoelectron spectrum of the valence iso-electronic molecule, OClO, has a much more complicated vibrational envelope in its first band, when compared with the 10.29 eV band of Dunlavey *et al.* (1978). In order to determine whether the latter is due to OBrO, spectral simulation would provide the most appropriate evidence.

Table 4.3. $BrO_2(X^2B_1)$ and $BrO_2^+(X^1A_1)$ computed minimum energy geometries and harmonic vibrational frequencies (cm^{-1}) at QCISD/6-311G(2d) level of theory

State	r_e/Å	ObrO/deg	Sym. str.	Sym. bend	Asym. str.
$BrO_2(X^2B_1)$	1.652	114.8	803	323	876
$BrO_2^+(X^1A_1)$	1.603	116.1	866	350	968

The simulated spectrum was obtained using the QCISD/6-311G(2d) geometries and force constants (Table 4.3). The main vibrational progression is the symmetric stretch in the cation, with very weak relative intensities of vibrational components in the symmetric bending mode. The simulated spectrum based on the ab initio geometries clearly matches with the 10.29 eV band of Dunlavey *et al.* (1978). Thus, it seems clear that the He I photoelectron band recorded by Dunlavey *et al.* (1978) is due to the BrO_2^+ $\tilde{X}\,^1A_1 \leftarrow BrO_2\ \tilde{X}\,^2B_1$ ionization. The IFCA procedure was carried out to obtain the simulated spectrum which matches best with the observed spectrum (Figure 4.1a) by varying the cationic geometry and employing the neutral experimental geometry (Muller et al., 1997) of r_e = 1.644 Å and θ_e = 114.3°. An experimentally estimated resolution (FWHM) of 65 meV was used for the Gaussian line-shape in the simulation. The final IFCA geometry used for the cationic state to produce Figure 4.1(b) is r_e = 1.6135 Å and θ_e = 117.5°. Although the vibrational components due to the bending mode were not resolved in the observed spectrum, the simulation suggested that the slightly asymmetric peak shape observed in the He I O + Br_2 band (on the high IE side) was most likely due to the contributions of the bending mode. The 10.26 eV O + Br_2 band was therefore assigned to the first ionization of BrO_2.

4.3.3. AlCN fluorescence spectra

The ab initio results on AlCN are given in Tables 4.4 and 4.5, together with the available experimental and theoretical values for comparison. In Table 4.4, the computed geometrical parameters and harmonic vibrational frequencies are reasonably consistent with each other, suggesting that they are reliable. The only exception is the CN-stretching frequency calculated at the MP2/6-31+G* level for the $\tilde{A}\,^1\Pi$ state, which is clearly too large. Comparing the computed vibrational frequencies of the $\tilde{X}^1\Sigma^+$ state with the observed values, the frequency of the CN stretching mode is consistently overestimated by about 200 cm^{-1} and the frequency of the AlC stretching mode is consistently underestimated by about 50 cm^{-1}. Considering the computed transition energies, T_e, in Table 4.5, the calculated values have a wide range from 2.56 eV to 3.77 eV. Comparing with the experimental T_0 values, the UMP2 values are reasonably good. The QCISD, CCSD and CCSD(T) methods do badly here, suggesting that the inadequacy of the UHF-based method for the open-shell $^1\Pi$ state is probably the major problem in the evaluation of relative energies for this type of system. The CASSCF/MRCI/cc-pVTZ//QCISD/6-311G(2d) T_e value of 3.774 eV for AlCN (the CAS space is all valence mos) is in reasonably good agreement with the observed T_0 values.

Table 4.4. The optimized geometries (Å) and harmonic vibrational frequencies (cm^{-1}) of the $\tilde{X}\,^1\Sigma$ and the $\tilde{A}\,^1\Pi$ states of AlCN.

AlCN, $\tilde{X}\,^1\Sigma$	AlC	CN	ω_1(CN)	ω_3(AlC)	$\omega_2(\pi)$
MP2/6-31+G*	2.0337	1.1919	2054	460	132
QCISD/6-31+G*	2.0353	1.1775	2214	461	146
QCISD/6-311G(2d)	2.0296	1.1642	2214	466	163
QCISD/cc-pVTZ	2.0269	1.1648	2224	470	165
QCISD/cc-pVQZ	2.0222	1.1609	2236	471	160
QCISD(T)/6-311+G(3df)[a]	2.0215	1.1712	2223	470	168
CCSD(T)/TZ2P+f[b]	2.014	1.171			
Expt (Gerasimov et al., 1999)			1974.5	523.5	132.9
Expt (Fukushima, 1998)			1974.5	523.5	131.9
AlCN, $\tilde{A}\,^1\Pi$					
CIS/6-311+G(2d)	1.9059	1.1472	2412	589	275; 260
MP2/6-31+G*	1.9188	1.1438	3180	582	263; 344
QCISD/6-31+G*	1.9291	1.1738	2193	568	232; 282
QCISD/6-311G(2d)	1.9270	1.1609	2197	565	228; 292
QCISD/cc-pVTZ	1.9237	1.1617	2209	570	234; 297
QCISD/cc-pVQZ	1.9172	1.1578			

[a] Fukushima, 1998
[b] Ma et al., 1995

Table 4.5. Calculated adiabatic excitation energies of the $\tilde{A}\,^1\Pi \rightarrow \tilde{X}\,^1\Sigma^+$ of AlCN. The values in square bracket are vertical excitation energies.

AEE [VEE]	eV	cm^{-1}
CIS/6-311+G(2d)	[4.01]	[32319]
UMP2/6-31+G*	3.43	27681
QCISD/6-31+G*	2.78	22398
QCISD/6-311G(2d)	2.78	22398
QCISD/cc-pVTZ	2.78	22448
UMP2/cc-pVTZ//QCISD/cc-pVTZ	3.44	27733
UMP2/cc-pVQZ//QCISD/6-311G(2d)	3.46	27928
CCSD/cc-pVQZ//QCISD/6-311G(2d)	2.76	22250
CCSD(T)/cc-pVQZ//QCISD/6-311G(2d)	2.56	20616
CASSCF/MRCI/cc-pVTZ//QCISD/6-311G(2d)	3.77	30440
Expt (Gerasimov et al., 1999)	3.57	28755.3
Expt (Fukushima, 1998)	3.57	28753.7

The AlCN $\tilde{A}\,^1\Pi$ (0,0,0) $\rightarrow$ $\tilde{X}\,^1\Sigma^+$ single vibronic level (SVL) emission was simulated, employing the QCISD/cc-pVTZ geometries and harmonic force constants (Table 4.4), and the result is shown in Figure 4.4(b). This is compared with the dispersed fluorescence spectrum excited at 28753.7 cm^{-1} observed by Fukushima (1998), given in Figure 4.4(a). It should be noted that the LIF spectrum of Fukushima is extremely complex and no vibrational assignment was given, except for the strongest LIF band at 28753.7 cm^{-1}, which was assumed to be the band origin. Comparison of the simulated and observed emission spectra in Figure 4.4 shows that there is reasonably

good agreement over the major vibrational series. This confirms that the LIF peak at 28753.7 cm^{-1} is the band origin of the AlCN $\tilde{A}\,^1\Pi \leftarrow \tilde{X}\,^1\Sigma^+$ absorption/excitation and the major part of the dispersed fluorescence spectrum at this excitation is due the AlCN $\tilde{A}\,^1\Pi$ (0,0,0) $\rightarrow$ $\tilde{X}\,^1\Sigma^+$ emission. However, it seems also clear that there are other emitters, which contribute to the dispersed fluorescence spectrum. Further investigation is required to identify these emitters.

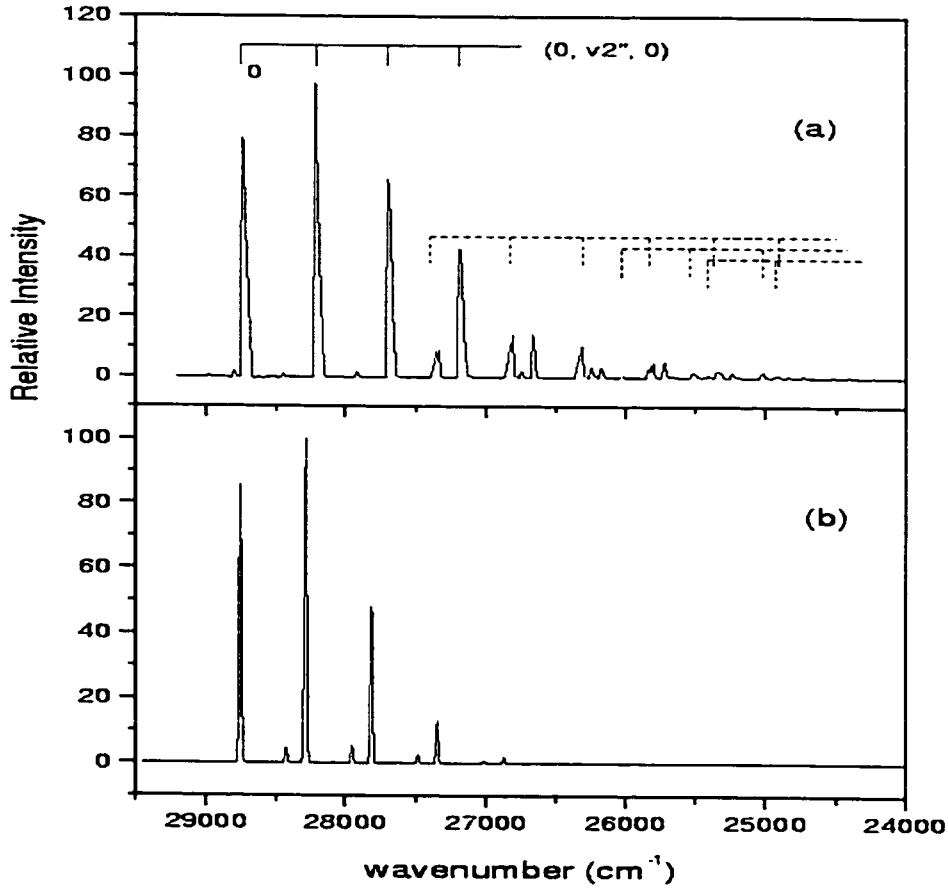

Figure 4.4. (a) The dispersed fluorescence spectrum of Fukushima at 28754 cm^{-1} (Fukushima, 1998) and (b) The simulated spectrum of the $\tilde{A}\,^1\Pi \leftarrow \tilde{X}^1\Sigma^+$ transition of AlCN. QCISD/cc-pVTZ ab initio geometries and harmonic force constants (Table 4.4) were used. The FWHM for the vibrational components is 14 cm^{-1} (0.1 nm).

4.4. Concluding remarks

The combined application of ab initio calculations and FC analysis to two difficult cases of spectral assignment has been demonstrated. In the first case, a band

recorded in the He I photoelectron spectrum by Dunlavey *et al.* (1978) for the O + Br_2 reaction, has been re-assigned to the BrO_2^+ $\tilde{X}\,^1A_1 \leftarrow BrO_2$ $\tilde{X}\,^2B_1$ ionization. A number of other possible candidates, which have their computed IEs and/or vibrational frequencies within the range of the observed values, were considered. Spectral simulations for these molecules and BrO_2 have provided unambiguous evidence for the assignment of the observed spectrum to BrO_2.

In the second case of the recently recorded AlCN fluorescence spectra, we have confirmed the assignments given by Gerasimov *et al.* (1999) that the 28754 cm^{-1} band systems are due to AlCN. For AlCN, the full experimental dispersed fluorescence spectra could not be assigned, because of the complexity of the spectra. Nevertheless, our spectral simulation has confirmed the assignment of the band origin [to be due to AlCN, rather than AlNC as suggested by Fukushima (1998)], and has also accounted for the major part of the observed emission spectrum excited at the band origin wavelength. Further ab initio calculations on the low-lying singlet states of AlCN need to be considered in order to identify other possible emitters.

CAPTER 5

The X^2B_1, A^2B_2, B^2A_1 and C^2A_2 states of Cl_2O^+: Ab initio Calculations and Simulation of the He I Photoelectron Spectrum

5.1. Background

The involvement of chlorine oxides in the loss of stratospheric ozone has motivated extensive studies into their photochemical, bonding and spectroscopic properties (Rowland, 1991; Sander et al., 1995). Dichlorine monoxide is thought to play only a minor role in the stratospheric ozone cycle. However, an understanding of the properties of this molecule can lead to an improved understanding of the more complex compounds of chlorine oxide which play a more important role in the ozone cycle. Cl_2O is also frequently used as a source of ClO in laboratory studies and in the synthesis of HOCl, a significant chlorine reservoir in the atmosphere. Furthermore, a correct interpretation of experiments, such as molecular beam studies to determine the yield of Cl and ClO fragments on photodissociation of Cl_2O, also requires characterization of Cl_2O photochemistry. Consequently, the photochemistry, and near ultraviolet (UV) spectroscopic properties of Cl_2O have received considerable attention in recent years from both experimentalists and theoreticians. Although the spectroscopy and photodissociation dynamics of Cl_2O have been extensively investigated using a wide range of techniques, there have been only a few studies on photoionization of Cl_2O.

The He I photoelectron (PE) spectrum of Cl_2O was first reported by Cornford et al. (1971). With a spectral resolution of ca 40 meV, only the lowest PE band of the spectrum was found to exhibit vibrational structure, which consisted of two progressions, assigned to excitation of the symmetric stretching vibrational mode, ν_1, and the bending vibrational mode, ν_2. The first adiabatic ionization energy (AIE) was measured to be 10.94eV. Twenty-five years later, Thorn et al. (1996) deduced an AIE value of 10.909 ± 0.016 eV from the photoionization efficiency (PIE) spectrum of Cl_2O. Very recently, Motte-Tollet et al. (1998) reported a higher resolution He I PE study

(with a full width at half maximum, FWHM, of 20 meV) of Cl_2O, where four structured bands were observed. New ionization energies were determined for the four lowest-lying electronic states of the molecular ion. Additionally, microwave spectroscopy (Herberich et al., 1966; Nakata et al., 1981) and electron diffraction experiments (Dunitz et al., 1950; Bru et al., 1952) have shown that Cl_2O is bent in its electronic ground state, $\tilde{X}\,^1A_1$, with its equilibrium bond length and bond angle being 1.6959 Å and 110.89° respectively.

Cl_2O possesses a complex manifold of electronically excited states. The four highest occupied molecular orbitals are nearly degenerate nonbonding and weakly antibonding orbitals, and excitation of electrons from these orbitals gives rise to several transitions in the visible and ultraviolet (Nelson et al., 1994). Nickolaisen et al. (1996) reported CASSCF/MRCI calculations on neutral Cl_2O, which studied the energy ordering and oscillator strengths for singlet-singlet and triplet-triplet transitions. In addition, the G2 and G2 (MP2) energies of ClO, Cl_2O, ClO_2 and Cl_2O_2 have been reported by Luke (Luke, 1995). However, to our knowledge, there has not been any ab initio study of the states of Cl_2O^+ or a simulation of the photoelectron spectrum of Cl_2O.

In the present study, we report ab initio calculations on the neutral ground state, and the $\tilde{X}\,^2B_1$, $\tilde{A}^2B_2$, $\tilde{B}\,^2A_1$ and $\tilde{C}\,^2A_2$ states of Cl_2O^+. From these calculations, the geometries and harmonic frequencies, for the neutral and cationic states are obtained, as well as the adiabatic ionization energies (AIE) and vertical ionization energies (VIE), for the first four bands in the ultraviolet photoelectron spectrum. Also, the first four bands in the He I photoelectron (PE) spectrum of Cl_2O has been simulated by employing the IFCA method (for details, see Chapter 2). The IFCA treatment makes use of ab initio force constants for both the neutral and a cationic state, and the experimental geometry (Herberich et al., 1966) of the neutral molecule. The geometrical parameters

were obtained for the cationic states, through a systematic variation of the cationic geometries, until the simulated spectra matched best with the observed He I PE spectra (Motte-Tollet et al., 1998). For two of the PE bands, the simulations, including the consideration of "hot" bands, have confirmed the assignments of the observed vibrational structure in the experimental spectrum (Motte-Tollet et al., 1998). In the case of the second band, the vibrational assignment has been revised.

5.2. Computational details

The main aims of the ab initio calculations in this work were to obtain reliable minimum-energy geometries and harmonic vibrational frequencies for the neutral electronic ground state of Cl_2O and its low-lying cationic states, so as to carry out subsequent FCF calculations and simulation of PE bands. The (U)MP2/6-311G(2d) level of calculation was first employed. Geometry optimization and vibrational frequency calculations on the ground states of the neutral and cation were completed. However, the MP2 level was found to be inadequate for the $\tilde{X}\,^2B_1$ cationic state, giving one imaginary frequency (for the b_2 asymmetric stretch). The QCISD/6-31G* (UQCISD/6-31G* for the cationic states) level of calculation was then employed and was found to be satisfactory for the neutral ground state and the four cationic states (see also next section), except for the harmonic vibrational frequency calculation of the $\tilde{C}\,^2A_2$ state of the Cl_2O^+. For the frequency calculation on the $\tilde{C}\,^2A_2$ cationic state at the QCISD level, there were excessive iterations in the QCISD energy evaluation at some point of the numerical second derivative calculations. Consequently, it was not possible to obtain the harmonic frequencies at the QCISD level for this state. In order to obtain the harmonic vibrational frequencies for the $\tilde{C}\,^2A_2$ state, CASSCF(7,6,nroot=2)/6-

311+G(2d) and CASSCF(7,8,nroot=2)/6-311+G(2d) geometry optimization and frequency calculations were carried out only for this state. Additionally, the AIEs and VIEs for the four lowest PE bands were computed using the RCCSD(T)/aug-cc-pVQZ method with the QCISD/6-31G* optimized geometry.

All the QCISD and CASSCF calculations were carried out using GAUSSIAN 98 (Frisch et al., 1998) and all RCCSD(T) calculations were carried out using MOLPRO98 (Werner et al., 1998), on the DEC8400 cluster at the Rutherford-Appleton Laboratory (EPSRC, UK) and SGI workstations at the Hong Kong Polytechnic University.

The principles and methods involved in the FCF calculations and spectral simulations have been described in Chapter 2. Briefly, the method is based on the harmonic oscillator model and includes the Duschinsky effect (Duschinsky, 1937). In the IFCA treatment, the ground state neutral geometrical parameters are held at the experimentally determined values (Herberich et al., 1966) and the initial ionic geometry is obtained from the ab initio computed geometry change on ionization. The ionic geometrical parameters are then varied slightly to give good agreement with the experimental vibrational band envelope. The ab initio force constant matrix (or F matrix) in the ionic state is assumed to be unchanged as the geometry (or G matrix) is changed slightly. Consequently, according to the Wilson GF formalism (Wilson, 1955), the vibrational frequencies will change, as the geometry is changed, but it was found that the differences between the refined and the ab initio values are less than 15 cm^{-1} in all cases of this work. The experimental structural parameters of the neutral molecule available in the literature (Herberich et al., 1966) were utilized in the IFCA computational procedure with no modification. Each vibrational component in a simulated photoelectron band was represented by a Gaussian function (with a FWHM of 20 meV, as estimated from the experimental spectra), with relative intensity of

vibrational components given by the computed Franck-Condon factors. "Hot" bands were included by assuming a Boltzmann distribution in the neutral initial state. The good agreement between the simulated and observed first band (see later text) suggests that the assumption of a Boltzmann distribution is a valid one. It was found that for the first PE band, where the "hot" bands were most clear, a temperature of 300 K gave the best match between the simulated and observed "hot" bands. Therefore, for the three higher IE bands, a vibrational temperature of 300 K was also used. The experimental AIEs (see Table 5.3) were used, except otherwise stated, in the simulation of each PE band.

5.3. Results and discussion

5.3.1. Ab initio calculations: Optimized geometry and vibrational frequencies

The results obtained from the ab initio calculations carried out on the neutral ground state and the four lowest lying cationic states of Cl_2O are summarized in Tables 5.1-5.3. For the $\tilde{X}\,^1A_1$ state, experimental values for the equilibrium geometrical parameters and vibrational frequencies are available for comparison. The agreement between the theoretical and experimental geometric parameters can be considered as satisfactory, particularly for the bond angle. Good agreement between the computed and observed vibrational frequencies provides confidence that the ab initio force constants obtained at the QCISD/6-31G* level of calculation should be reasonably reliable, and adequate for the subsequent FCF calculations.

Table 5.1. The calculated geometries (bond length in Å / bond angle in degrees) for the neutral and the four lowest-lying cationic states of Cl_2O.

States	Experimental values [a]	Ab initio values	IFCA values
$\tilde{X}\,^1A_1$	1.696 / 110.89	1.730 / 111.31 [b]	
$\tilde{X}\,^2B_1$		1.672 / 117.82 [b]	1.640±0.004 / 117.3±0.3
$\tilde{A}\,^2B_2$		1.726 / 94.84 [b]	1.705±0.007 / 100.1±0.4
$\tilde{B}\,^2A_1$		1.671 / 132.41 [b]	1.637 / 131.99 [e]
$\tilde{C}\,^2A_2$		1.782 / 104.22 [c]	1.725±0.004 / 108.9±0.5
		1.805 / 105.43 [d]	
		1.739 / 108.87 [b]	

[a] Herberich et al. 1966 & Nakata et al. 1981. [b] At the QCISD/6-31G* level. [c] At the CASSCF(7,8,nroot=2)/6-311+G(2d) level. [d] At the CASSCF(7,6,nroot=2)/6-311+G(2d) level. [e] These values are obtained by combining the experimental bond length and bond angle of the $\tilde{X}\,^1A_1$ state (column 2) with the computed geometric changes upon ionization to the $\tilde{B}\,^2A_1$ state at the QCISD/6-31G* level (column 3).

Table 5.2. The vibrational frequencies (ν_1 / ν_2 / ν_3 in cm^{-1}) [a] for the neutral and the four lowest energy cationic states of Cl_2O.

States	Experimental values [b]	Ab initio values	IFCA values
$\tilde{X}\,^1A_1$	642 / 296 / 686	653.8 / 299.6 / 717.4 [c]	657.3 / 303.9 / 716.0 [f]
$\tilde{X}\,^2B_1$	678 / 347 / --	681.7 / 320.3 / 648.3 [c]	686.0 / 324.5 / 646.8 [g]
$\tilde{A}^2B_2$	-- / 290 / --	749.9 / 278.8 / 652.1 [c]	726.0 / 291.4 / 671.1 [g]
$\tilde{B}\,^2A_1$	-- / 282 / --	561.8 / 283.6 / 579.7 [c]	564.3 / 288.2 / 578.9 [g]
$\tilde{C}\,^2A_2$	613 / 307 / --	569.5 / 262.1 / 411.6 [d]	559.0 / 275.8 / 421.0 [g]
		565.1 / 259.0 / 483.6 [e]	

[a] The two a_1 modes of ν_1 and ν_2 correspond to symmetric stretching and angle bending motions while the b_1 mode of ν_3 corresponds to the asymmetric stretching motion (see text also).

[b] Motte-Tollet et al. 1998.

[c] At the QCISD/6-31G* level.

[d] At the CASSCF(7,8,nroot=2)/6-311+G(2d) level.

[e] At the CASSCF(7,6,nroot=2)/6-311+G(2d) level.

[f] These frequencies correspond to the IFCA values at the experimental geometry (Motte-Tollet et al. 1998 & Herberich et al. 1966 (see text).

[g] These frequencies correspond to the values at the IFCA geometries as given in Table 5.1.

Table 5.3. The calculated adiabatic and vertical ionization energies (AIE / VIE in eV) of the four lowest energy cationic states.

States	AIE / VIE		
	Experimental values [a]	Ab initio values [b]	IFCA values
$\tilde{X}\,^2B_1$	10.887 / 10.971	11.007 / 11.199	
$\tilde{A}^2B_2$	12.016 / 12.297	11.983 / 12.371	12.159 / 12.304 [c]
$\tilde{B}\,^2A_1$	≤12.453 / 12.593	12.454 / 12.898	12.271 / 12.593 [d]
$\tilde{C}\,^2A_2$	12.742 / 12.742	12.842 / 12.851	

[a] Motte-Tollet et al. 1998.

[b] At the RCCSD(T)/aug-cc-pVQZ//QCISD/6-31G* level of calculation.

[c] The AIE value is the observed position of the fifth vibrational peak in the second band of the He I PE spectrum given by Motte-Tollet et al. (1998); see text.

[d] The VIE position was set to the observed VIE position given by Motte-Tollet et al. (1998); see text.

For the cationic states, there are no available experimentally derived geometrical parameters prior to this work. For the vibrational frequencies, some experimental values are available from the PE spectra (see Table 5.2). For the $\tilde{X}\,^2B_1$, $\tilde{A}^2B_2$, and $\tilde{B}\,^2A_1$ states, the agreement between the computed and observed values is very good. It seems clear that the QCISD/6-31G* force constants are adequate, at least for the subsequent FCF calculations. For the $\tilde{C}\,^2A_2$ state, where only CASSCF frequencies were obtained here, the agreement is not as good, but can be considered as reasonable. The two CASSCF calculations with different active spaces gave significantly different minimum-energy geometries, but similar vibrational frequencies. As the active space used in the CASSCF

method increases, the optimized geometrical parameters obtained appear to converge to the QCISD values (Table 5.1). Thus, the CASSCF(7,8,nroot=2)/6-311+G(2d) bond length (1.7821Å) is closer to its QCISD value (1.7391Å) than the CASSCF(7,6,nroot=2)/6-311+G(2d) value of 1.8045Å. The CASSCF(7,8,nroot=2)/6-311+G(2d) bending frequency of 262 cm^{-1} is slightly better than the CASSCF(7,6,nroot=2)/6-311+G(2d) value of 259 cm^{-1} (Table 5.2) when compared with the observed vibrational spacing of 307 cm^{-1} (Motte-Tollet et al., 1998). The CASSCF bond angles of 104.2° and 105.4° are probably too small. Because with the rather large computed change in the bond angle at the CASSCF level upon ionization to this cationic state, a longer vibrational progression in the bending mode ν_2' in the simulated spectrum than the observed one would be expected. It is clear that the QCISD bond angle of 108.9° for the $\tilde{C}\,^2A_2$ state is closer to the neutral QCISD angle of 111.3° than the CASSCF bond angles. The observed vibrational structure of the fourth band shows one major vibrational series, being assigned to the symmetric stretching mode, with only a weak shoulder being assigned to the bending mode (Motte-Tollet et al., 1998). Thus, it seems that the computed QCISD geometry change upon ionization for the fourth band, especially for the bond angle, is more consistent with the experimental observations than the CASSCF counterparts. In view of these considerations, for the $\tilde{C}\,^2A_2$ state, the CASSCF(7,8) force constants were used in the IFCA procedure, but the QCISD geometry was used as the initial geometry for the upper cationic state.

5.3.2. Adiabatic and vertical ionization energies of the PE bands

The AIEs/VIEs were calculated at the RCCSD(T)/aug-cc-pVQZ//QCISD/6-31G* level for the four PE bands of Cl_2O and are compared with the experimental AIEs

and VIEs in Table 5.3. It can be seen that, in general, all the computed AIEs and VIEs agree very well with the experimental values. Thus, the assignments of the cationic states to the PE bands can be confirmed unambiguously by the present ab initio calculations.

Examining the results in detail, the calculated AIEs and VIEs are slightly larger than the corresponding observed values for ionization to the cationic $\tilde{X}\,^2B_1$, $\tilde{B}\,^2A_1$ and $\tilde{C}\,^2A_2$ states. For ionization to the cationic $\tilde{A}^2B_2$ state, the computed AIE and VIE are slightly lower and higher than the corresponding measured values respectively. Nevertheless, for all four PE bands, the differences between the computed and observed AIEs and VIEs are within 0.12eV and 0.305eV respectively. In addition, the calculated AIE-VIE separations for each band agree to within 0.1 eV with the experimental values, except for the third band, where the observed AIE value reported in reference (Motte-Tollet et al., 1998) is an estimate (≥12.453 eV), because of being overlapped by the second band. The computed AIE-VIE separation for the third band suggests that the actual AIE position is lower than the experimentally estimated one by over 0.3 eV.

5.3.3. Simulation of vibrational structures of the PE bands of Cl_2O

Figure 5.1 shows the simulated (after application of the IFCA procedure for each band) and observed PE spectra of Cl_2O in the region of 10.6 to 13.2 eV. The relative band intensities have been chosen to match those in the experimental spectrum. It can be seen that the overall agreement is very good. The simulated spectrum, which matches best with the experimental spectrum (Motte-Tollet et al., 1998), has the IFCA geometries of the cationic states given in Table 5.1. The expanded, first and fourth

simulated PE bands and the corresponding experimental bands are compared in more detail in Figures 5.2 and 5.3. Since the second and third bands overlap extensively, it was not possible to study them separately (see later text) and their expanded simulated spectra are shown together in Figure 5.4.

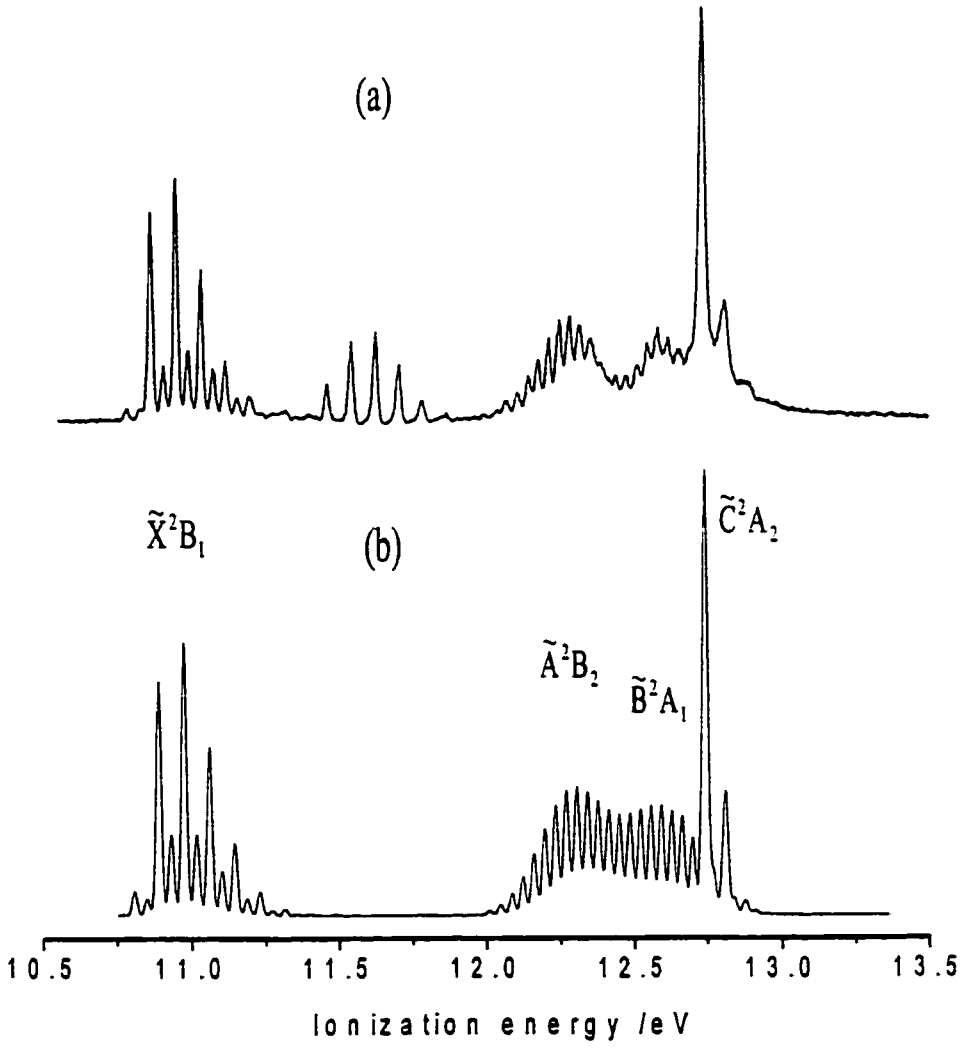

Figure 5.1. The full He I PE spectra of Cl_2O: (a) experimental and (b) simulated (see text for details). The vibrational progression in the 11.4 to 11.8eV region of the observed spectrum is due to Cl_2 (Motte-Tollet et al., 1998).

For the third band, the AIE position cannot be identified from the experimental spectrum. Consequently, the IFCA simulation procedure was not carried out for this

band. The ab initio geometry change upon ionization was employed together with the experimental geometry of the neutral molecule to produce the simulated spectrum (see footnote e of Table 5.1). The vibrational component, which was calculated to have the strongest, overall relative FCF, was set to match the observed strongest peak (the observed VIE position; see later text). Then the IFCA procedure was carried out for the second band, including the contribution from the simulated spectrum of third band obtained as described above. More details of the comparison between the simulated and observed spectra are given below.

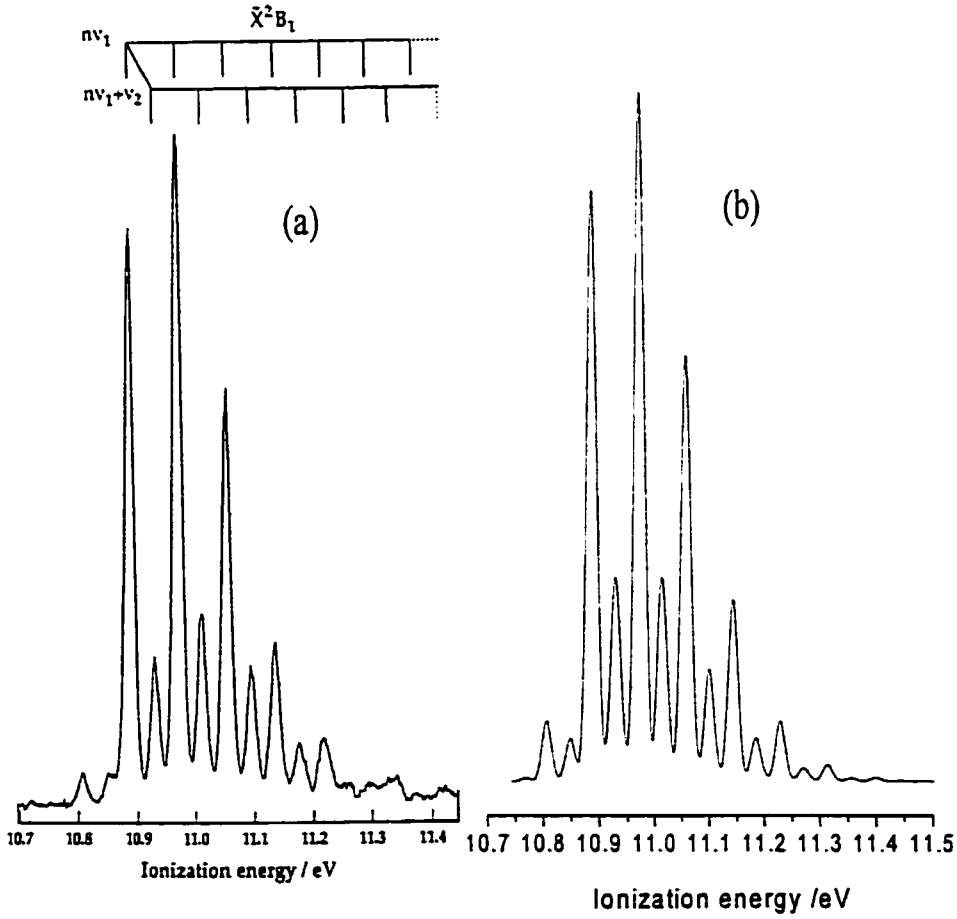

Figure 5.2. The expanded first band of the He I PE spectrum: (a) experimental spectrum given by Motte-Tollet et al. (1998) and (b) simulated spectrum, employing the IFCA geometry of the X^2B_1 state (see text and Table 5.1).

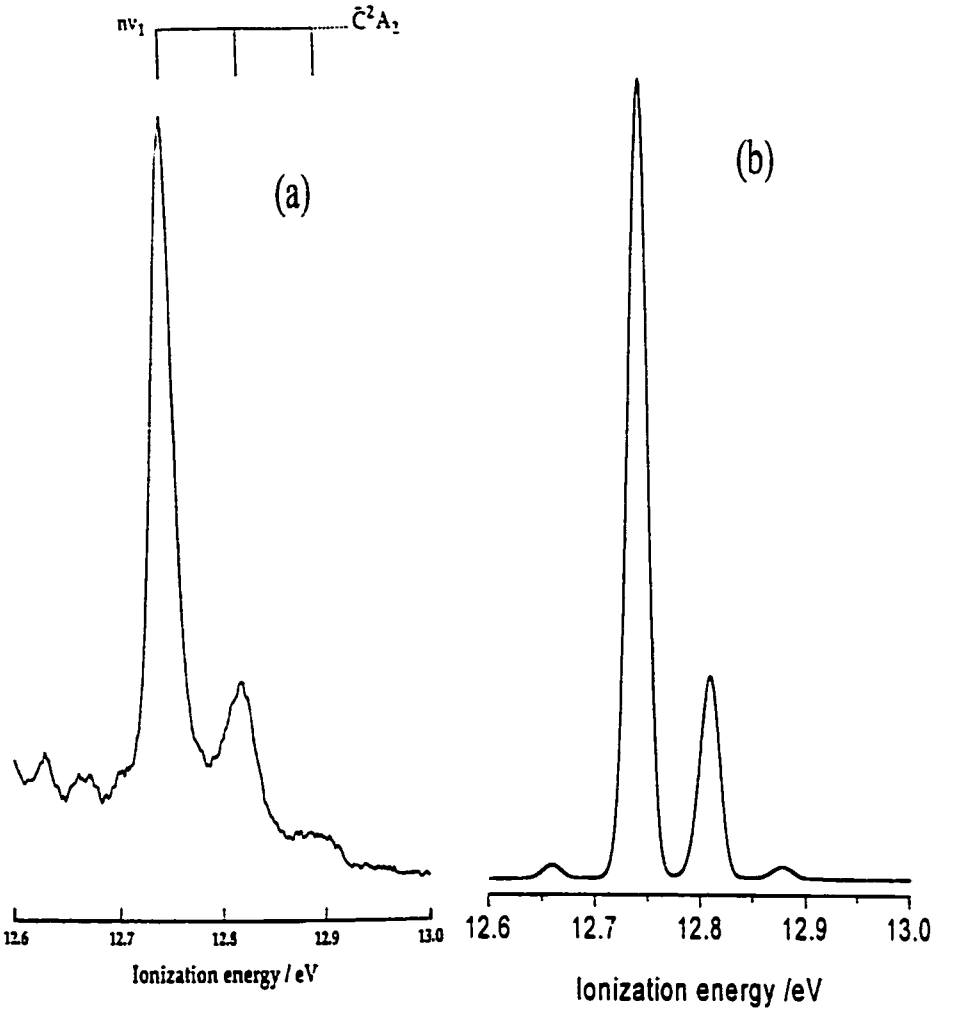

Figure 5.3. The expanded fourth band of the He I PE spectrum: (a) experimental spectrum given by Motte-Tollet et al. (1998); (b) simulated spectrum, employing the IFCA geometry of the C^2A_2 state (see text and Table 5.1). Note that the first weak peak in the simulated spectrum (b) at ca. 12.65 is a hot band, arising from the $v_1'' = 1$ level of the neutral molecule.

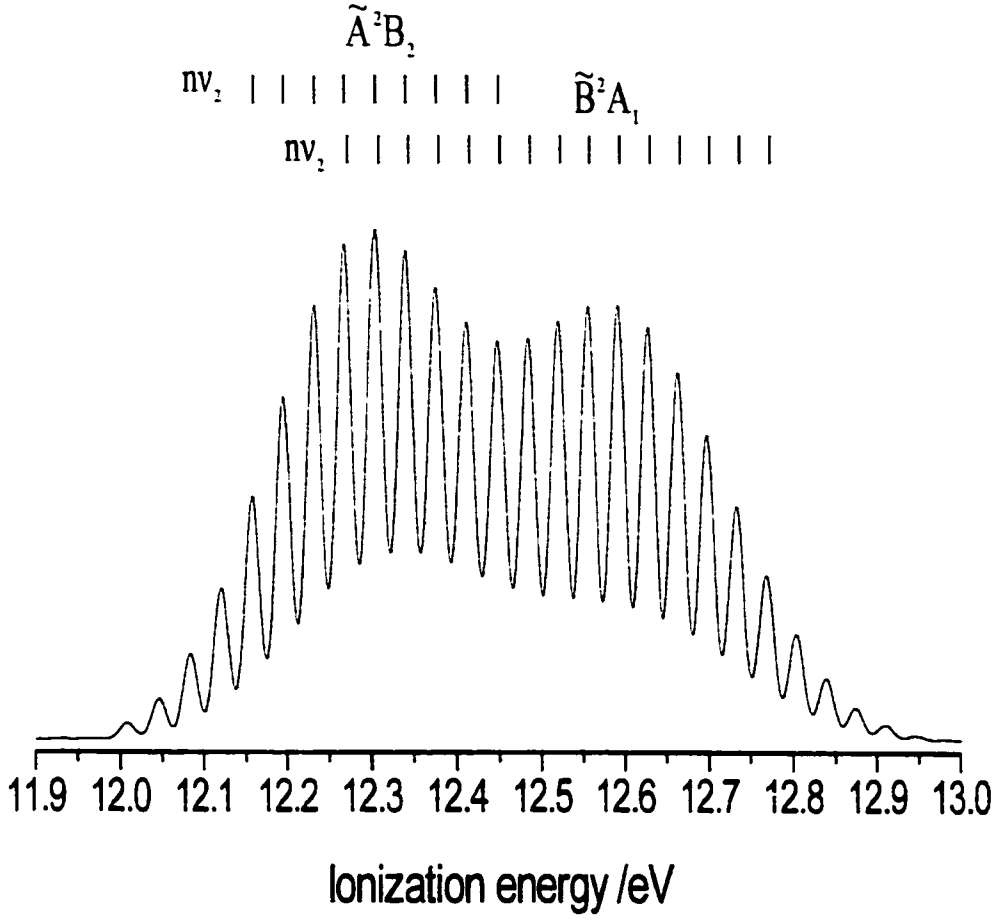

Figure 5.4. The expanded second and third bands of the He I PE spectrum: simulated spectrum, employing the IFCA geometry of A^2B_2 state (see Table 5.1 and text for details).

The IFCA procedure could be used for the first and fourth bands and the agreement between the simulated and observed spectra of these bands, as shown in Figure 5.2 and 5.3, is good (see also next section). The comparison between the simulated and observed spectra of the first band (Figure 5.2), in the low IE region, which included the effects of "hot" bands, enabled a vibrational temperature of 300 K to be reliably established, as mentioned above. When this temperature was used in the simulations of the other bands, it was found that the contributions of "hot" bands to the second and third bands are quite strong (from population of the excited vibrational

levels of the bending mode in the neutral molecule; see Figures 5.5 and 5.6). In order to show the various contributions of the different vibrational series, the computed FCFs of the vibrational progressions with reasonably strong intensities are displayed in bar diagrams for the second and third bands, respectively, in Figures 5.5 and 5.6. It can be seen that the FCF intensity patterns for the "hot" band series between these two PE bands are very different. In particular, for the second PE band (Figure 5.5), the low IE components of the "hot" band series are quite strong and are of comparable intensities to those in the high IE region. Consequently, the observed low IE components of the second band must be due to "hot" bands, rather than the main $(0,v_2',0) \leftarrow (0,0,0)$ series, as was assigned by Motte-Tollet et al. (1998). Based on FCF calculations and simulations carried out in this work, the first four observable components of the second band are almost certainly due to "hot" bands. In this connection, the AIE position of the second band would be at the fifth observed vibrational component, with a measured value of 12.159 eV, which was assigned to the $v_2'=4$ of the main series in the reference (Motte-Tollet et al., 1998). In addition, based on our spectral simulations, the observed VIE position at 12.297 eV is now due to the $(0,4,0) \leftarrow (0,0,0)$ ionization. It should be noted that for this feature, there are significant contributions from other vibrational series (see Figure 5.5), including those of the overlapping third band. For the main vibrational series $(0,v_2',0) \leftarrow (0,0,0)$, the $v_2' = 3$ component is the strongest within the series. However, contributions from "hot" bands and other series, as mentioned above, have changed the VIE position to the $v_2' = 4$ component.

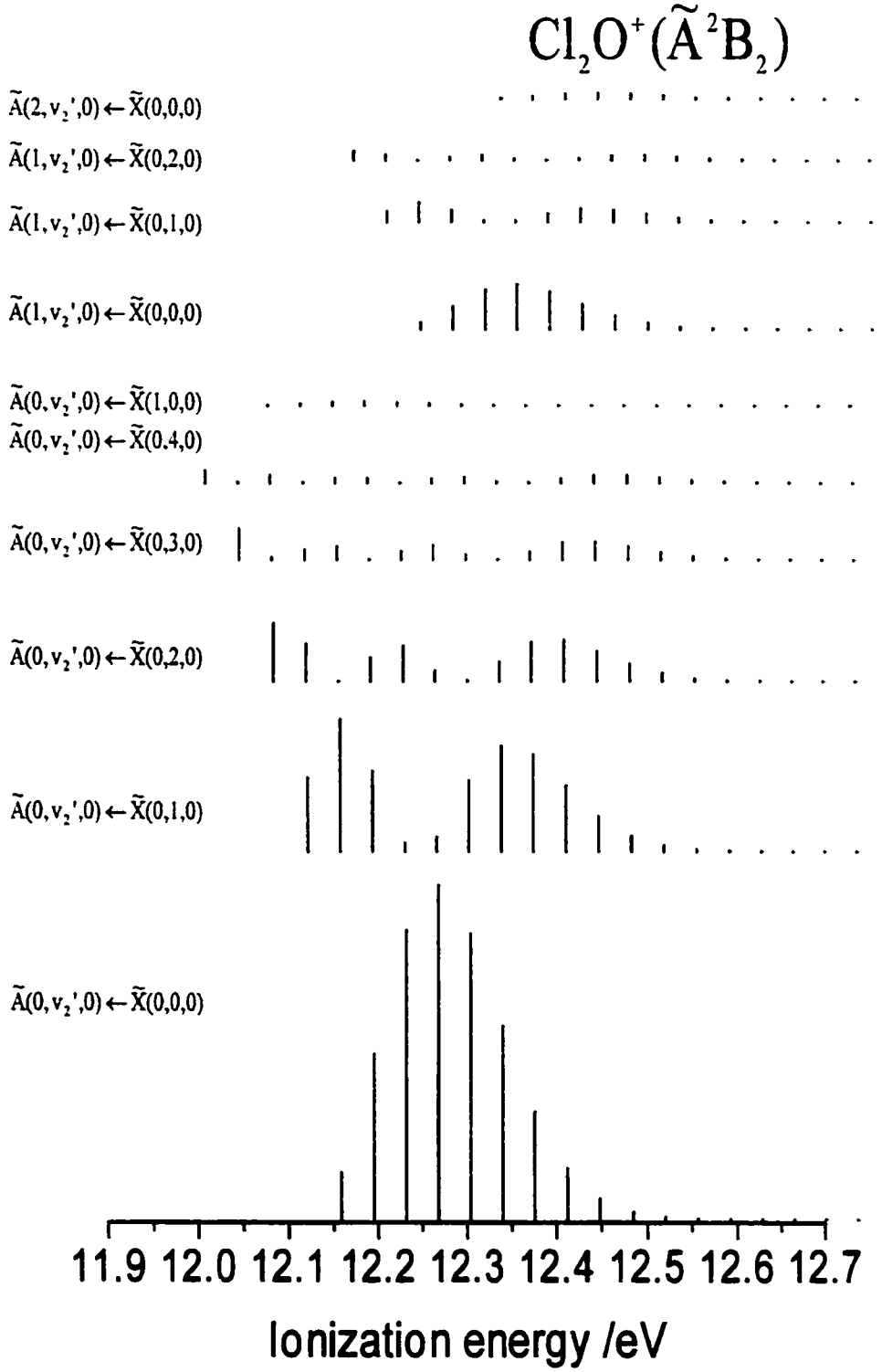

Figure 5.5. The computed FCFs of the vibrational series with relatively stronger intensities for the $A^2B_2 \leftarrow X^1A_1$ ionization, including hot bands, at a temperature of 300 K, assuming Boltzmann distributions.

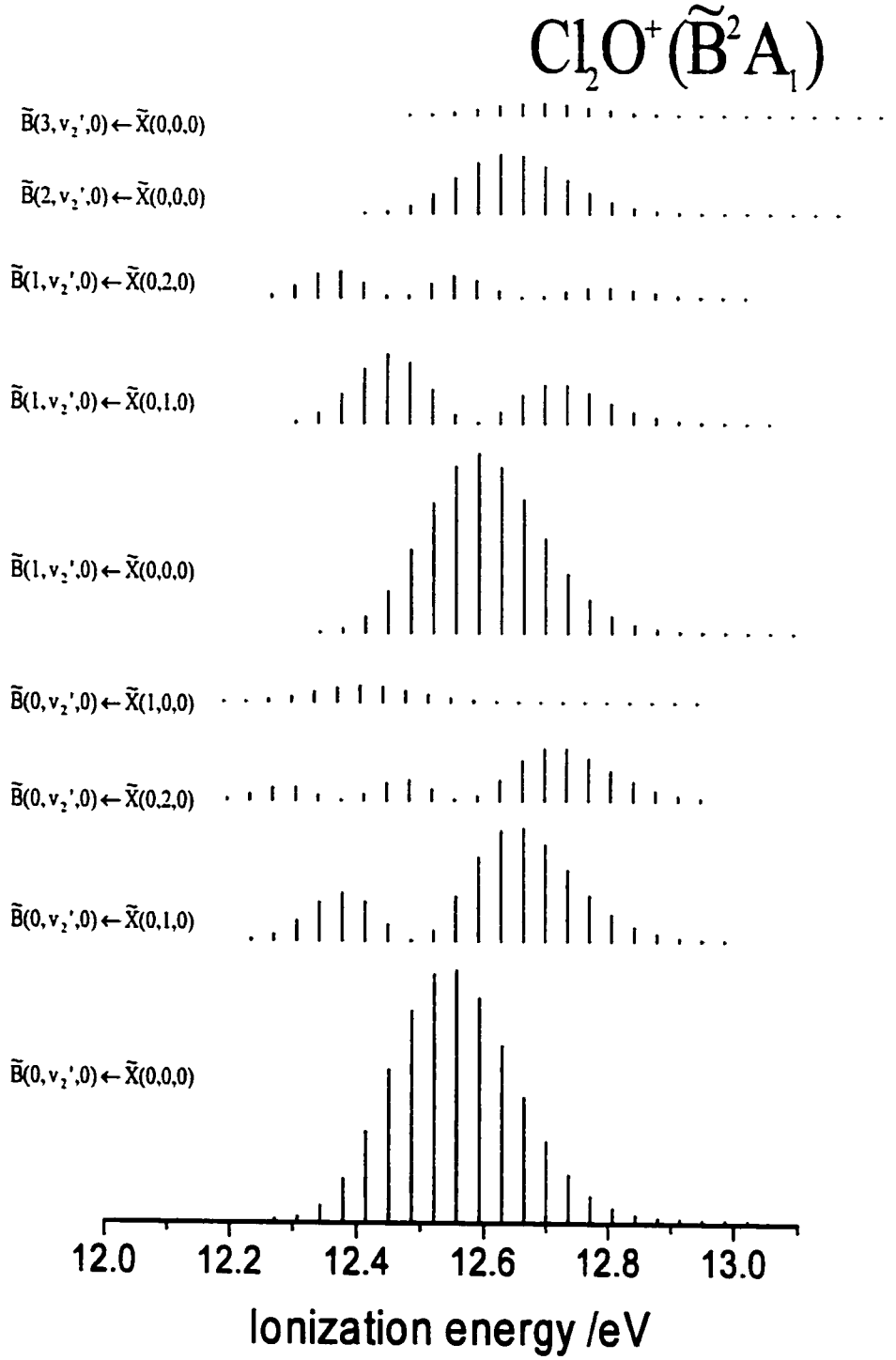

Figure 5.6. The computed FCFs of the vibrational series with relatively stronger intensities for the $B^2A_1 \leftarrow X^1A_1$ ionization, including hot bands, at a temperature of 300 K, assuming Boltzmann distributions.

For the third PE band, the contribution of "hot" bands seems to be slightly less strong, as compared with that to the second band (see Figures 5.5 and 5.6), and the pattern of the vibrational structure of the "hot" bands is quite different, as mentioned above. An attempt has been made to obtain the best simulation of the third band by matching the strongest component in the simulation with the observed VIE position, as the AIE position is not clear from the observed spectrum. In these simulations, contributions from the second and fourth bands were included. This is the best that can be done in view of the severe overlapping band problem that occurs with the third band. Because the IFCA procedure could not be carried out for this band, the main drawback in this simulation is the use of the ab initio geometry change upon ionization, which is assumed to be close to the true one. Based on the FCF calculations and simulations, the measured VIE position, 12.593 eV, of the third band can be assigned to the (0,9,0) ← (0,0,0) ionization, and the AIE position would then have a value of 12.271 eV, which is significantly lower than the experimentally estimated value (Table 5.3). Thus, the revised experimental AIE-VIE separation of 0.322 eV compares well with the RCCSD(T)/aug-cc-pVQZ//QCISD/6-31G* value of 0.444 eV.

5.4. Concluding Remarks

In this investigation, high-level ab initio calculations on the neutral ground state and the four lowest-lying cationic states of Cl_2O are reported. The assignments of the cationic states made in an earlier study of the He I PE spectra (Motte-Tollet et al., 1998) have been confirmed. FCF calculations and spectral simulations, which include allowance for "hot" bands, have led to revised assignments of the vibrational structure observed in the second PE band, the $\tilde{A}^2B_2 \leftarrow \tilde{X}^1A_1$ ionization. As a result of this

revision, the AIE position for this band is also revised. The error in the new AIE position depends on the reliability of the revised vibrational assignments, which is probably within one quantum in the bending mode. In this connection, the uncertainty associated with the revised AIE value (12.159 eV) can be estimated to be of the order of ±0.037 eV (≈ 300 cm^{-1}), which is the observed vibrational spacing of the bending mode of the upper state. In summary, the usefulness of FCF calculations and spectral simulations is clearly demonstrated in the study of the second PE band of Cl_2O.

For the third PE band of the $\tilde{B}\,^2A_1 \leftarrow \tilde{X}\,^1A_1$ ionization, despite being heavily overlapped by the second and fourth band, a major effort was made to simulate its PE spectrum. As a result, a more reliable AIE position than the estimate from the previous experimental study (Motte-Tollet et al. 1998) has been obtained. Although the uncertainty associated with this AIE value of 12.271 eV will be larger than that obtained above for the second band, for the $\tilde{A}^2B_2 \leftarrow \tilde{X}\,^1A_1$ ionization, the AIE-VIE separation obtained with this revised AIE value agrees with the RCCSD(T) AIE-VIE separation to within 0.122 eV. In this connection, an estimated uncertainty of 0.15 eV for the third AIE value seems reasonable. Although this uncertainty is rather large, it is at least possible to obtain a more reliable AIE position than previously, using the present FCF calculations and spectral simulations.

IFCA procedures were carried out for the first, second and fourth band of the He I PE spectrum of Cl_2O. With the experimental geometry of the neutral ground state, geometrical parameters of the $\tilde{X}\,^2B_1$, $\tilde{A}^2B_2$ and $\tilde{C}\,^2A_2$ states of Cl_2O^+ have been derived experimentally for the first time. For the first band, the overall agreement between the simulated and the observed spectra is very good, except for the (0,1,0) ← (0,0,0) peak, which has its simulated relative intensity slightly higher than the observed one (Figure 5.2). In the IFCA procedure, attempts were made to improve the agreement for this

peak. It was found that the IFCA r_e value was critical in affecting the relative intensity of this peak, and achieving a better agreement for this peak had led to a poorer agreement for the main ν_1 series. Because it seems reasonable to place more weight on the stronger main stretching series than the weaker bending progression in the comparison between the simulated and observed spectra, the simulation as shown in Figure 5.2 has been concluded to be the best match. With this simulation, the IFCA r_e value is 1.640 Å for the $\tilde{X}^2B_1$ cationic state (Table 5.1). A rather large uncertainty of ± 0.004 Å has been given for this IFCA r_e value (Table 5.1), including allowance for the slight discrepancy between the simulated and observed spectra. For the $\tilde{A}^2B_2$ and the $\tilde{C}^2A_2$ states, the uncertainties of the geometrical parameters obtained here are also large (Table 5.1). This is partly because of overlapping band problems, and also partly because only a vibrational series of one of the two symmetric modes is excited extensively in each case (the bending mode in the $\tilde{A}^2B_2$ state and the stretching mode in the $\tilde{C}^2A_2$ state). The lack of well-resolved vibrational structure in the other symmetric mode has hampered the extraction of information from the observed spectra. For the $\tilde{A}^2B_2$ state, the uncertainty in the revised vibrational assignments has been included in the estimation of the uncertainty associated with the IFCA bond angle. Nevertheless, the information derived in this study, notably the vibrational assignments, new AIEs, ionic state geometries and frequencies for the four lowest states of Cl_2O^+ represent a considerable body of new information.

CHAPTER 6

Simulation of the He I Photoelectron Spectrum of ClO_2 with the Consideration of Anharmonicity and the Duschinsky Effect

6.1. Background

The commonly used harmonic oscillator model, might be inadequate in cases, where anharmonicity effects are important, such as for vibronic transitions involving vibrational levels of high quantum numbers (Chau et al., 1998). In this chapter, the He I PE spectrum of ClO_2 (Flesch et al., 1993) has been chosen for spectral simulation, employing both the multi-dimensional harmonic FCF method and anharmonic FCF method developed in this work (see Chapter 2 for details). Other than the importance of ClO_2 in atmospheric chemistry, one main reason for the choice of simulating the PE spectrum of ClO_2 is that, highly accurate CASSCF/MRCI PEFs of the neutral ground state and low-lying cationic states of this intermediate are available (Peterson and Werner, 1993, 1996). Hence, the anharmonic FCF method developed in this work can be tested readily, without involving the demanding task of generating high-level ab initio PEFs.

Chlorine dioxides (ClO_2) have received much attention recently, because of their relevance in the destruction of the ozone layer in the upper atmosphere (Chau et al., 1998; Flesch et al., 1993; Peterson et al., 1993, 1996; Malmqvist et al., 1998). In contrast, there have been only two experimental studies on the ClO_2^+ cation in the gas phase. The first He I PE spectrum of ClO_2 was published in 1971 (Cornford et al., 1971). After more than two decades, Flesch *et al.* (1993) reported another He I PE spectrum (see Figure 6.1) of ClO_2, with a much improved resolution (quoted to be 15 meV; see later text). The spectral features in these two PE spectra are very similar in the low ionization energy (IE) region of 10-16 eV, but differ in the higher IE region. Since the later PE spectrum is of a better quality than the one published earlier, we will focus

on it from here onward and we will only investigate the PE bands observed in the low IE region.

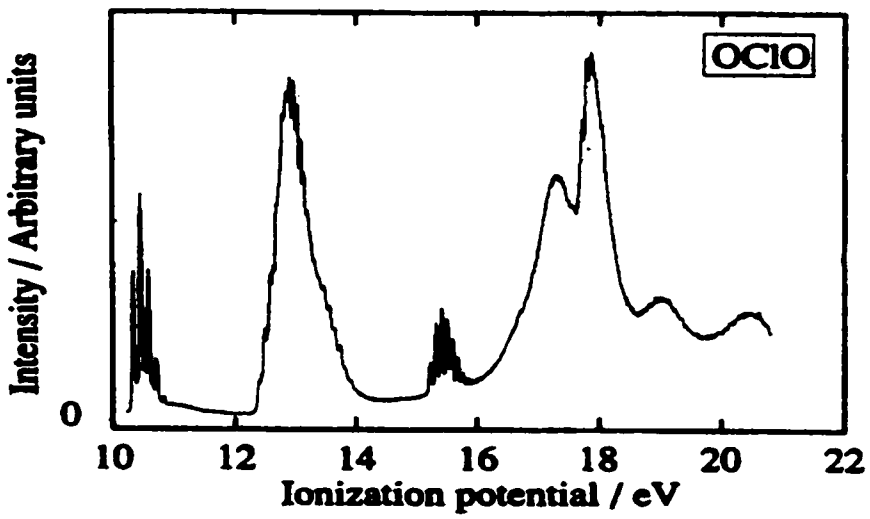

Figure 6.1. The experimental He I photoelectron spectrum of ClO_2 (Flesch et al., 1993).

In the low IE region, there are three observed PE bands (see Figure 6.1), which are well separated from each other. The first and third bands, with measured adiabatic ionization energies (AIE) of 10.345 and 15.440 eV, show simple and resolved vibrational structures, while the second band is a complex one, corresponding to several overlapped ionization structures. Based on considerations of the bonding nature of the high-lying occupied molecular orbitals of neutral ClO_2 molecule (from ab initio calculations) and comparison with the known PE spectrum of SO_2, assignments for all the observed bands were made by Flesch *et al.* (1993). Ionizations to five cationic states were associated with the second band (Flesch et al., 1993).

It should also be mentioned that Peterson and Werner (1993) reported high-level CASSCF/MRCI calculations (and PEFs; see the next section) on the ground electronic

state of ClO_2 and the low-lying cationic states of ClO_2^+. Based on their MRCI results, assignments for the PE spectrum of ClO_2 recorded by Fresch *et al.* were proposed. The assignments of Peterson and Werner (1993) differ from those of Fresch *et al.* (1993) in the ordering of the five cationic states associated with the second PE band. In the present study, it is hoped that spectral simulations may shed some light on the discrepancies between the two sets of assignments for the heavily overlapped second band in the He I PE spectrum of ClO_2, and may provide vibrational assignments for the first and third bands.

6.2. Computational details

The multi-dimensional anharmonic FCF method proposed in this investigation is based on that of Botschwina *et al.* (1995). One main reason for choosing the approach of Botschwina *et al.* is that, it can be readily incorporated into our developed harmonic FCF model (see Chapter 2 for details). In this way, the Duschinsky effect, which is lacking in the method of Botschwina *et al.*, as mentioned in Chapter 2, is included in the present anharmonic FCF method. At the same time, with the use of ab initio PEFs and the Cartesian coordinate approach (Chen, 1994; Chau, 1998) (which is good for an electronic transition even with a large geometrical change), many advantageous features of our harmonic FCF method are retained (see Chapters 3-5). Thus, with relatively straightforward modifications on our existing harmonic FCF method, anharmonicity can be incorporated into a multi-dimensional FCF calculation, which handles also the Duschinsky effect. It is therefore expected that the improved FCF method, which includes anharmonicity, should give more reliable results than the harmonic method.

The anharmonic FCF method encoded in this work has been described in details in Chapter 2.

The IFCA procedure with the harmonic FCF method has been applied successfully in the investigations of $SiCl_2$, BrO_2, AlCN and Cl_2O in Chapters 3-5. A similar IFCA procedure can be carried out employing the anharmonic FCF method. In this case, during the IFCA procedure, the shape/form of the ab initio PEF's of the two electronic states are kept unchanged. The equilibrium position of one of two states is fixed to the available experimental geometry, while the geometrical parameters of the other state are varied systematically (initially according to the computed geometry change from ab initio calculations), until the best match between the simulated and observed spectra is achieved. More technical details of the anharmonic IFCA procedure have been given in Chapter 2.

A*b initio* calculations were performed to provide the harmonic force constants required for the subsequent harmonic Franck-Condon calculations and for comparison with the CASSCF/MRCI calculations of Peterson and Werner (1993). In principle, from the MRCI PEFs available (Peterson and Werner, 1993), sufficient input data could be obtained for the harmonic FCF calculation. However, in order to compare the harmonic and anharmonic FCF methods in a consistent manner, ab initio calculations, which compute harmonic vibrational frequencies at the minimum-energy geometry, were performed for the former, as done in Chapters 3-5. Commonly used single-reference based correlation methods, such as MP2, QCISD and CCSD(T), were employed with standard basis sets. Geometry optimization and harmonic vibrational frequency calculations were carried out only for the ground (X^2B_1) state of the neutral ClO_2 radical, and the ground (X^1A_1) and the lowest $^1B_2$ states of the cation, as harmonic FCF calculations were carried out only for the ionization processes to these two ionic states.

All ab initio calculations were carried out with the GAUSSIAN98 (Frisch et al., 1998) suites of programs.

For the anharmonic FCF calculations, the PEFs of the electronic states involved in the electronic transition are required in the variational calculation for the vibrational wave function of each state. For the $\tilde{X}\,^2B_1$ state of ClO_2, the full three-dimensional PEF determined by Peterson (Peterson, 1998) was employed. This PEF was obtained by fitting 49 CASSCF/MRCI ab initio single point energies to a polynomial. For the cationic states, the two-dimensional CASSCF/MRCI PEFs of Peterson and Werner (Peterson and Werner, 1993) were used. [Basis sets of cc-pVQZ (without g functions) quality were employed.] For each cationic state, the PEF was obtained by fitting 13 computed energy values to a polynomial. These energy points are displacements from the equilibrium position of the symmetry coordinates $S_1 = (r_1 + r_2)/\sqrt{2}$ and $S_2 = \theta$ (Peterson and Werner, 1993). The above published PEFs were employed in our variational calculation. As the cationic PEFs are two-dimensional, the variational calculations performed are also two-dimensional. The asymmetric stretching mode ν_3 (the third mode) has been neglected in the FCF evaluation. In any case, it is of a different symmetry from the ν_1 and ν_2 modes in the C_{2v} symmetry.

For neutral ClO_2 vibrational levels with quantum number up to 6 were considered in the variational calculations. This should be sufficient, as there is no evidence for "hot" bands in the observed spectrum. To reduce the size of the three-dimensional basis, a further constraint that $\nu_1 + \nu_2 + \nu_3 \leq 6$ was applied in the selection of the harmonic basis. For ClO_2^+ vibrational levels with quantum number up to 12 were included, except where stated otherwise. This seems to be adequate for most cationic states considered here (see the later text). A further constraint of $\nu_1 + \nu_2 \leq 12$ was also applied in the variational calculations. The constraint (and hence the total size of the

basis) was chosen from a series of preliminary calculations on the $\tilde{X}\ ^1A_1$ state of ClO_2^+. Variational calculations were performed with the basis set constraints of $v_1 + v_2 \leq 6$, 8, 12, and 20. Results of these calculations are shown in Table 6.1. Only the energies of the progression of the stretching mode are given as the experimental spectrum is dominated by this progression. With the basis set constraint of up to $v_1 + v_2 \leq 12$, the computed vibrational energies of the levels (0,0,0) to (5,0,0) converge to within 1 cm^{-1}, while for the vibrational level (6,0,0), the computed energy converges to within 7 cm^{-1}. It seems that the basis set constraint of $v_1 + v_2 \leq 12$ is a reasonable compromise of accuracy and economy, at least for the $\tilde{X}\ ^1A_1$ state of ClO_2^+. This constraint has been applied for most of the cationic states considered here, unless otherwise stated.

Table 6.1. Computed vibrational energies (with respect to the ground vibrational state in cm^{-1}) from the ClO_2^- X^1A_1 potential surface of Peterson and Werner (1993) with different basis set sizes.

Constraints:	$v_1 + v_2 = 6$	$v_1 + v_2 = 8$	$v_1 + v_2 = 12$	$v_1 + v_2 = 20$
Zero point energy	1398.9	1398.9	1398.9	1398.9
(1,0,0)	997.8	997.8	997.8	997.8
(2,0,0)	1985.0	1984.8	1984.8	1984.8
(3,0,0)	2968.2	2962.0	2961.6	2961.6
(4,0,0)	3972.3	3933.4	3929.0	3929.0
(5,0,0)	5022.0	4930.1	4888.2	4887.7
(6,0,0)	6739.0	5978.0	5844.0	5838.6
basis set size	28	45	153	231

The variational calculations and the evaluation of anharmonic FCFs were performed using the software AN-FCF coded in FORTRAN. The computational time of the calculation increases tremendously with the size of the basis set, especially in the evaluation of the FCFs. For the second band of the ClO_2 photoelectron spectrum, a larger basis set size was required for the $^3A_2$ and the $^1A_2$ states as the computed FCFs suggest significant relative intensities for peaks of higher quantum numbers than 12 (see the next section). For these two states, the variational calculations had a basis set size of (12,18,0) with a constraint of $v_1 + v_2 \leq 18$. Thus, the largest FCF evaluations carried out in this work for ionization to these two cationic states involved 84 and 221 vibrational levels for the initial and the final electronic states, respectively. After evaluating the

FCFs, gaussian functions with a full-width-half-maximum (FWHM; see the next section) of 30 meV and relative intensities as given by the corresponding FCFs were used to simulate the vibronic peaks.

6.3. Results and Discussion

6.3.1. Ab initio calculations

The ab initio results obtained in this work are summarized in Tables 6.2 to 6.5 and compared with available experimental values and previous theoretical values. Briefly, it can be seen that, for the three electronic states studied no obvious trends in the computed geometrical parameters and harmonic vibrational frequencies are observed with the theoretical method used. This shows the difficulty in achieving convergence in the calculated parameters for this type of system. Nevertheless, for the ground states of the neutral and the cation, the computed bond angles at different levels of calculation are reasonably consistent. Therefore, they can be considered as reliable. However, for the open-shell singlet $^1B_2$ state the UHF based correlation methods used in this study are clearly inadequate for the minimum-energy geometry, particularly for the computed bond angles, which have a range of ca, 10°. Regarding the computed harmonic vibrational frequencies, the QCISD/6-311G(2d) values are the nearest to the available experimental values, and hence the corresponding force constants were used in the subsequent Franck-Condon calculations.

Table 6.2. The computed optimized geometries and harmonic vibrational frequencies (cm^{-1}) of the $\tilde{X}\,^2B_1$ state of OClO.

Method	r_e/Å	θ/°	$\omega_1(a_1)$	$\omega_2(a_1)$	$\omega_3(b_2)$	Reference
UMP2/6-311G(2d)	1.4976	119.09	966.3	431.0	1124.9	This work
UMP2/6-311G(3df)	1.4694	118.08	1037.6	452.2	3083.7	This work
UQCISD/6-311G(2d)	1.4968	117.62	904.9	435.8	1073.1	This work
UQCISD/6-311G(3df)	1.4653	116.90	[a]			This work
UCCSD(T)/6-311G(3df)	1.4760	117.46	[a]			This work
CASSCF/MRCI/ cc-pVQZ (no g)	1.480	117.8	945	452		Peterson and Werner, 1993
CASSCF/MRCI+Q/ cc-pVQZ (no g)	1.488	117.4	928	442		Peterson and Werner, 1993
CASSCF/MRCI+Q/ cc-pVQZ	1.4728	117.65	960.2	455.6	1127.9	Peterson, 1998
Expt	1.4698	117.41	963.5	451.7	1133.0	Muller et al., 1997; Richardson et al., 1969

[a] SCF convergence problems in the numerical second derivative calculations.

Table 6.3. The computed optimized geometries and harmonic vibrational frequencies (cm^{-1}) of the $\tilde{X}\,^1A_1$ state of $OClO^-$.

Method	r_e/Å	θ/°	$\omega_1(a_1)$	$\omega_2(a_1)$	$\omega_3(b_2)$	Reference
MP2/6-311G(2d)	1.4609	123.00	923.1	457.4	1189.6	This work
MP2/6-311G(3df)	1.4313	122.88	1006.9	477.8	1275.1	This work
QCISD/6-311G(2d)	1.4265	121.02	1019.2	503.6	1210.1	This work
QCISD/6-311G(3df)	1.4014	121.30	1127.5	527.6	1409.1	This work
CCSD(T)/6-311G(3df)	1.4176	121.50	1047.5	498.5	1330.5	This work
QCISD/6-311+G(2d)	1.428	121.0	1012	500	1280	Alcamí et al.,1999
CASSCF/MRCI/ cc-pVQZ (no g)	1.423	120.78	1012	511		Peterson and Werner, 1993
CASSCF/MRCI+Q/ cc-pVQZ (no g)	1.431	120.6	988	497		Peterson and Werner, 1993
CCSD(T)/cc-pVQZ	1.4252	120.81	1027.8	502.7	1300.9	Pak and Woods, 1996
IFCA (harmonic)	1.41	121.8				This work
IFCA (anharmonic)	1.414	121.8				This work
Expt			1020± 20	520± 20		Ruhl et al., 1999

Table 6.4. The computed optimized geometries and harmonic vibrational frequencies (cm^{-1}) of the $^1B_2$ state of $OClO^-$.

Method	r_e/Å	θ_e/°	$\omega_1(a_1)$	$\omega_2(a_1)$	$\omega_3(b_2)$	Reference
CIS/6-311G(2d)	1.4835	110.86	1034.6	368.8	470.2	This work
UMP2/6-311G(2d)	1.5405	119.53	1232.1	365.9	1058.3	This work
UMP2/6-311G(3df)	1.5260	118.99	1189.8	351.8	913.7	This work
UQCISD/6-311G(2d)	1.5991	107.78	690.8	322.6	416.7	This work
UQCISD/6-311G(3df)	1.5511	107.14	801.6	377.8	563.8	This work
UCCSD(T)/6-311G(3df)	1.5954	108.22	[a]			This work
CASSCF/MRCI/ cc-pVQZ(no g)	1.5619	113.58	775	225		Peterson and Werner, 1993
CASSCF/MRCI+Q/ cc-pVQZ(no g)	1.577	113.3	725	216		Peterson and Werner, 1993
IFCA (harmonic)	1.558	114.5				This work
IFCA (best estimate)[b]	1.56	114.0				This work
Expt			766			Flesch et al., 1993; Rockland et al., 1995

[a] SCF convergence problems in the numerical second derivative calculations.

[b] The best estimated geometry from anharmonic IFCA; Please refer to the discussion in the text.

Table 6.5. The computed AIE's [VIE's] (in eV) for the first ($\tilde{X}\,^1A_1$ $OClO^-$) and third bands ($^1B_2$ OClO+) in the He I photoelectron spectrum of OClO.

Method	$\tilde{X}\,^1A_1$ $OClO^-$	$^1B_2$ OClO+	Reference
UMP2/6-311G(2d)	9.68	15.52	This work
UMP2/6-311G(3df)	9.80	15.72	This work
UQCISD/6-311G(2d)	10.15	12.82	This work
UQCISD/6-311G(3df)	10.20	13.32	This work
UCCSD(T)/6-311G(3df)	10.04	12.37	This work
PMP2/cc-pVQZ//CCSD(T)/6-311G(3df)	10.07	15.76	This work
PMP3/cc-pVQZ//CCSD(T)/6-311G(3df)	10.67	16.68	This work
MP4SDQ/cc-pVQZ//CCSD(T)/6-311G(3df)	10.40	13.75	This work
UCCSD/cc-pVQZ//CCSD(T)/6-311G(3df)	10.50;[10.78]	13.73	This work
UCCSD(T)/cc-pVQZ//CCSD(T)/6-311G(3df)	10.30;[10.42]	12.57	This work
CASSCF/MRCI/cc-pVQZ	9.72; [9.86]	14.87; [15.12]	Peterson and Werner, 1993
CASSCF/MRCI+Q/cc-pVQZ	10.06; [10.11]	14.92; [15.25]	Peterson and Werner, 1993
Expt	10.345; [10.475]	15.250; [15.440]	Flesch et al., 1993; Rockland et al., 1995

Considering the computed AIEs and VIEs (see Table 6.5), for the ionization to the ground state of the cation, the CCSD(T)/cc-pVQZ values agree very well with the experimental values. This excellent agreement of within ca 0.05 eV is even better than that of the MRCI results from Peterson and Werner (1993). From Table 6.5, it is clear that basis size effect is important for the calculation of reliable AIE/VIE for this type of system. Other than the size-inconsistency problem with the MRCI method, the omission

of g functions in the cc-pVQZ basis set in the MRCI calculations of Peterson and Werner may be a reason for the relatively larger discrepancies of more than 0.3 eV between the MRCI AIE/VIE and the experimental values. However, for the ionization to the $^1B_2$ state, the UHF based correlation methods employed here are, again, clearly inadequate, as shown from the large discrepancies between their computed AIEs and the CASSCF/MRCI and experimental values.

6.3.2. Spectral simulation: First PE band

The simulations of the first band in the PE spectrum of ClO_2, employing the harmonic and anharmonic FCF codes, are shown in Figures 6.2(c) and 6.2(b) respectively, together with the experimental spectrum of Flesch *et al.* (1993) [Figure 6.2(a)]. This band is due to the ClO_2^+ $\tilde{X}\,^1A_1 \leftarrow ClO_2$ $\tilde{X}\,^2B_1$ ionization and has the best resolved vibrational structure. The experimental spectrum is dominated by the symmetric stretching progression. Although the bending progression is relatively weak, the resolution is good enough to reveal the bending feature. Thus, the observed vibrational structure provides sufficient information for both the bond angle and bond length of the ground cationic state to be extracted from the comparison between the simulated and observed spectra via the IFCA procedure. The details of the comparison are given in the following subsections for the harmonic and anharmonic FC simulations.

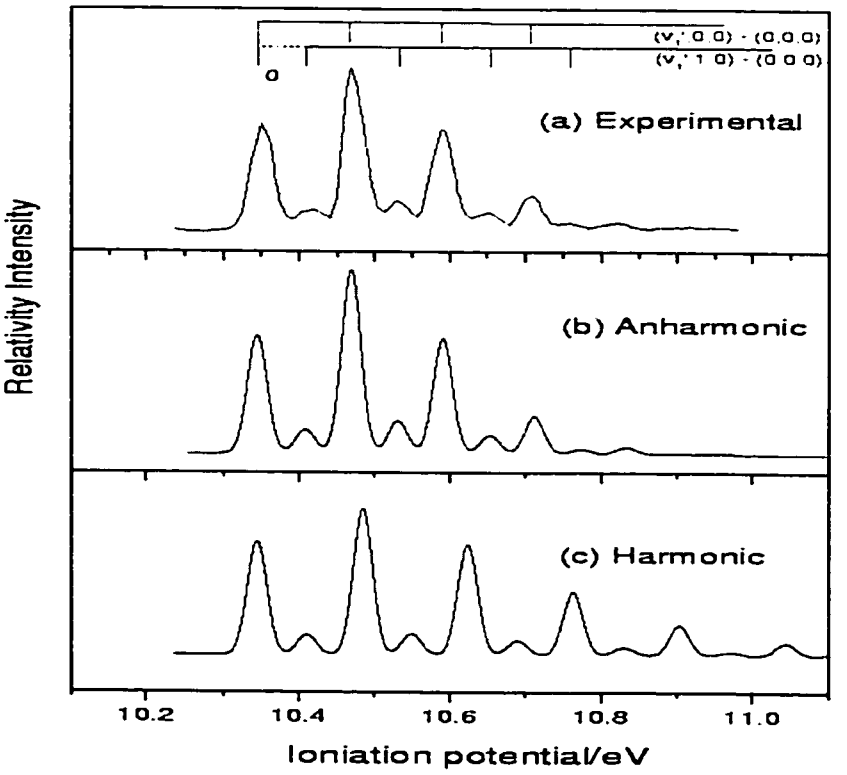

Figure 6.2. The first band of the ClO_2 photoelectron spectrum: (a) the experimental spectrum, (b) the simulated spectrum using the anharmonic FCFs, and (c) the simulated spectrum using the harmonic FCFs.

6.3.2.1. Harmonic FC simulation

The simulated first band [Figure 6.2(c)] with harmonic FCFs was obtained with the experimental AIE (Flesch et al., 1993) and experimental geometry of the $\tilde{X}\,^2B_1$ state (Muller et al., 1997; Richardson et al., 1969). The QCISD/6-311G(2d) and QCISD/6-311G(3df) harmonic force constants were used for the neutral and the cationic ground states respectively in the FCF calculations. The IFCA procedure has been applied and the geometry, R(Cl-O) = 1.410 ± 0.010 Å, ∠O-Cl-O = 121.8 ± 0.5°, is found to give the "best" match between the simulated and observed spectra. This simulated spectrum is

shown in Figure 6.2(c). However, it can been seen from Figures 6.2(c) and 6.2(a) that the match is far from perfect. Despite various attempts, it was not possible to match the relative intensity across the whole stretching progression over the whole PE band. The above IFCA geometry was obtained by matching the relative intensity of the first three most intense components, where the anharmonic effect would be expected to be the least important. With this IFCA geometry, simulated peaks of higher stretching levels are significantly stronger than the observed ones, suggesting that the harmonic oscillator model is probably inadequate. Apart from the stretching progression, the first bending peak (0,1,0) is too strong in the simulation. From the comparison between the anharmonic FC simulation and the observed first band to be discussed (see the next subsection), it seems clear that both the symmetric stretching and bending modes are significantly anharmonic in the ground cationic state of ClO_2^+. Consequently, the simulated spectrum using the harmonic FCFs failed to reproduce the overall intensity pattern of the two progressions observed in He I PE spectrum. In view of this inadequacy, rather large uncertainties have been included for the geometrical parameters given above. From the harmonic calculation, it was found that the FCFs for transitions involving the asymmetric stretching mode, ν_3, are negligible. This shows that the neglect of the asymmetric stretching mode in the anharmonic FCF calculation is a good approximation and should have little impact on the accuracy of the spectral simulation.

6.3.2.2. Anharmonic FC simulation

The expansion coefficients $c_{m,v'}$ obtained from the variational calculation are an indication of the degree of anharmonicity with the chosen PEF. The first three terms in

the anharmonic vibrational wave functions of the ground state of ClO_2^- with a basis set of $v_1 + v_2 \leq 12$ are given below

$$
\begin{aligned}
|0,0,0> &= 1.00\phi(0,0,0) - 0.06\phi(0,0,0) - 0.01\phi(0,0,0) + \ldots \\
|0,1,0> &= 1.00\phi(0,1,0) - 0.06\phi(1,1,0) + 0.04\phi(0,2,0) + \ldots \\
|1,0,0> &= 0.97\phi(1,0,0) - 0.15\phi(0,2,0) - 0.15\phi(2,0,0) + \ldots \\
|0,2,0> &= 0.98\phi(0,2,0) + 0.15\phi(1,0,0) - 0.07\phi(0,3,0) + \ldots \\
|2,0,0> &= 0.93\phi(2,0,0) - 0.26\phi(3,0,0) - 0.19\phi(1,2,0) + \ldots
\end{aligned}
\tag{6.1}
$$

where $\phi(v_1, v_2, v_3)$ stands for harmonic basis function $\phi(v_1)\phi(v_2)\phi(v_3)$. The deviation of the leading coefficient from unity shows the deviation from the dominant harmonic function, and is thus a measure of anharmonicity. From the above, the $|0,0,0\rangle$ and $|0,1,0\rangle$ states are very close to the case of a harmonic oscillator, as expected. Higher vibrational states are becoming more and more anharmonic. In addition, the stretching progression seems to be more anharmonic than the bending progression.

From Figure 6.2, it is clear that anharmonic FCF calculations have produced a much better simulated spectrum than the harmonic FCF calculations, when compared with the observed spectrum. The IFCA procedure as described in Chapter 2 has been carried out to obtain the experimentally derived IFCA geometry for the ground cationic state, which gave the best simulated spectrum, as shown in Figure 6.2b. The match between the anharmonic simulated and observed spectra is excellent. The IFCA geometry of the cation is R(Cl-O) = 1.414 ± 0.002 Å and ∠O-Cl-O = 121.8 ± 0.1°. It is of interest to note that the anharmonic IFCA geometry is close to that of the harmonic IFCA one.

6.3.3. Spectral simulation: Third PE band

The simulated third band using both the harmonic and anharmonic FCFs are shown in Figure 6.3. The third band of the ClO_2 PE spectrum is essentially a progression of the symmetric stretching mode. Although no expanded spectrum of the third band is given in the reference (Flesch et al., 1993), at least 7 peaks can be identified for this progression. Cornford *et al.* (1972) reported a measured bending frequency of 440 cm^{-1} in the third PE band of ClO_2. However, no bending vibrational frequency was reported in the experimental He I PE spectrum (Flesch et al., 1993) for this band. Although ab initio calculations have not given a consistent value of the bending frequency for the $^1B_2$ state of ClO_2^- (see Table 6.4), all the computed values are significantly smaller than the reported value of Cornford *et al.* (1972). In view of the superior quality of the observed spectrum of Flesch et al. (1993), it seems that the reliability of the bending frequency reported by Cornford *et al.* is doubtful.

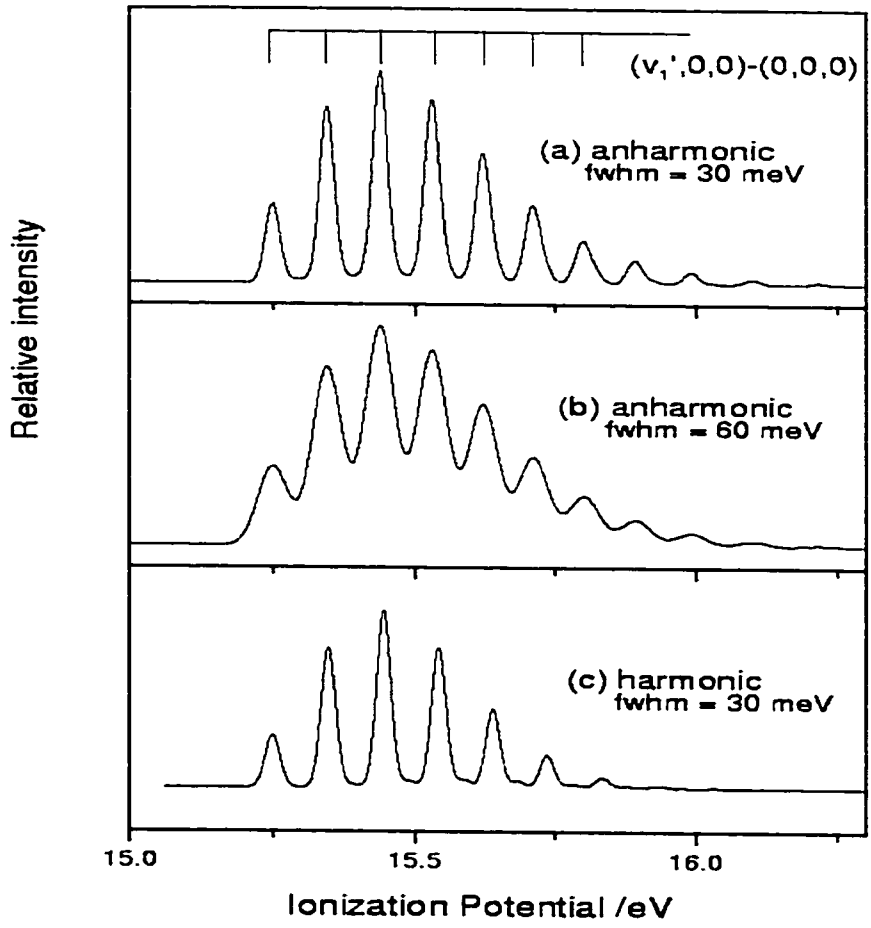

Figure 6.3. The third band of the ClO_2 photoelectron spectrum: (a) the simulated spectrum using anharmonic FCFs, (b) same as above, but with a fwhm of 60 meV, and (c) the harmonic simulated spectrum.

The harmonic FC simulation shown in Figure 6.3(c) was obtained with an IFCA geometry of R(Cl-O) = 1.558 Å and ∠O-Cl-O = 114.5° for the $ClO_2^+(^1B_2)$ state. The match between the simulated and observed spectra is mainly based on the first three vibrational components, and assuming that the relative intensity of bending mode is negligibly small. The IFCA procedure has not been performed for this PE band with the anharmonic simulation, because the match between the anharmonic FC simulated spectrum, obtained with the MRCI geometries, and the observed spectrum is already satisfactory. This suggests that the computed MRCI geometry change upon ionization to

the $^1B_2$ state is probably reliable. Considering both the IFCA results with the harmonic simulation discussed, and the good agreement between the MRCI anharmonic simulation with the observed spectrum, the best estimate of the geometry for the $^1B_2$ state from the present study is R(Cl-O) = 1.56 ± 0.01 Å and ∠O-Cl-O = 114.0 ± 1.0°. The large uncertainties associated with the estimated values of these geometrical parameters are mainly due to the relatively poorer quality of the observed third PE band.

The major difference between the anharmonic and harmonic FC simulations of the third PE band [Figures 6.3(a) and 6.3(c)] is that the former gives a longer stretching progression. Comparison between the simulated and experimental spectra suggests that the anharmonic simulation appears to be in slightly better agreement with experiment. In Figures 6.3(a) and 6.3(c), a FWHM of 30 meV has been used. This value was obtained by measuring the FWHM of a vibrational component in the first band given in the experimental He I PE spectrum (Flesch et al., 1993), and is significantly larger than the quoted resolution of 15 meV. The observed third band (Flesch et al., 1993) appears to be of even poorer resolution. Hence, a simulated spectrum with a FWHM of 60 meV is also given [Figure 6.3(b)] for comparison.

6.3.4. Spectral simulation: Second PE band

Based on the MRCI calculations of Peterson and Werner (1993), the second PE band of ClO_2 consists of ionizations to five electronic states of ClO_2^+, namely the $^3A_2$, $^3B_1$, $^3B_2$, $^1A_2$, and $^1B_1$ states. Both Flesch *et al.* (1993) and Peterson and Werner (1993) assigned these five cationic states to the second PE band of ClO_2, but the assignments of the relative energy ordering of these states and hence their adiabatic ionization energies (AIE's) are different. The two sets of assignments are shown in Table 6.6. In order to

confirm or revise these assignments, in particular, the relative energy ordering of these five cationic states, the ionizations to these five cationic states were simulated, employing the anharmonic FCF method with the MRCI PEFs of Peterson and Werner (1993). The simulated spectra are shown in Figures 6.4-6.6. The profiles of these simulated spectra are quite different, and it will be seen that they are very useful in clarifying the ionic state ordering, which is discussed in the following.

Table 6.6. The AIEs (VIEs) of the five cationic states in the second PE band of ClO_2 according to the assignments of Fresch et al. (1993), Peterson and Werner (1993) and the anharmonic FC simulations from this work (see text).

AIE (VIE) /eV	Fresch et al. (1993)	Peterson and Werner[a] (1993)	Anharmonic FC simulation
$^3B_2$	12.870 (12.990)	12.29 (12.7)	12.400 (12.693)
$^3A_2$	13.330 (13.330)	12.46 (12.8)	12.570 (13.040)
$^3B_1$	12.400 (12.590)	12.78 (13.0)	12.785 (12.872)
$^1A_2$	13.500 (13.590)	12.78 (13.1)	12.890 (13.386)
$^1B_1$	12.455 (12.635)	13.22 (13.6)	13.330 (13.579)

[a] The AIEs are the MRCI+Q/cc-pVQZ(with 1g) energies of the corresponding cationic states relative to the X^1A_1 state of ClO_2^+, plus the experimental AIE (10.350 eV) of the X^1A_1 state; the VIEs are the MRCI+Q/cc-pVQZ(with 1g) values shifted by 0.37 eV to approximate the match of the computed and observed first AIE.

6.3.4.1. New assignments based on comparison between simulated and observed vibrational structures

For convenience of discussion, the second band has been partitioned into three regions, the low-energy, mid-energy, and high-energy region. The low-energy region

covers 12.4 eV to about 12.8 eV, which exhibits resolved vibrational structures; there are essentially five pairs of peaks. A more careful inspection of the vibrational structures through this region suggests that the first pair through the fourth pair appear to be from the same ionization process, with a gradual increase and then decrease in their relative intensities. The fifth pair of peaks seems stronger than the forth pair, suggesting that another ionization starts from here and extends into the mid-energy region. The mid-energy region has the range of 12.9 eV to 13.2 eV. In this region, four or five peaks appear to be from the same vibrational progression. The high-energy region is from 13.2 eV onward and the vibrational structure is less obvious here.

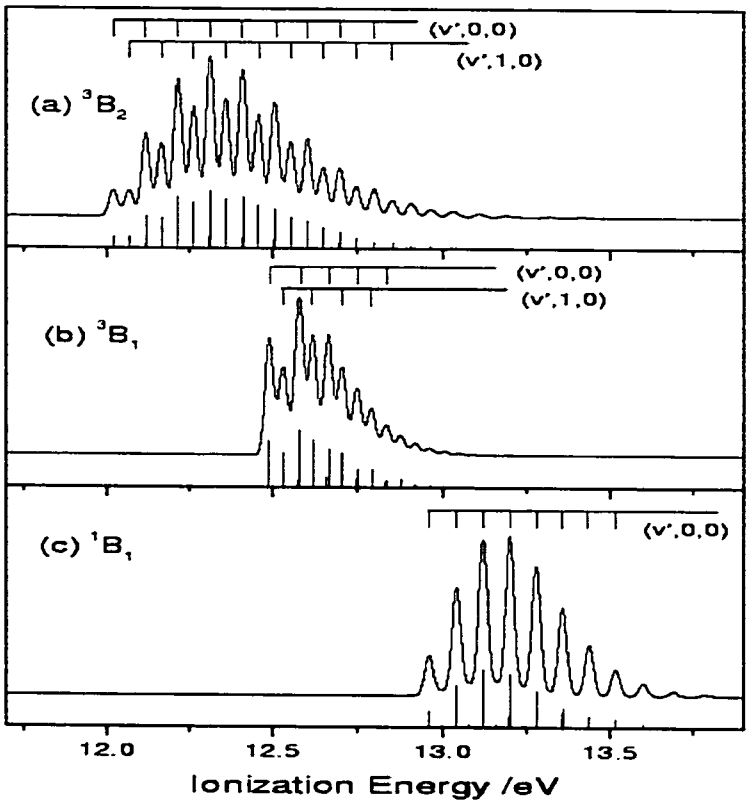

Figure 6.4. The simulated photoelectron spectra for the ionizations from ground state of ClO_2 to: (a) the $^3B_2$ state of ClO_2^+, (b) the $^3B_1$ state of ClO_2^+, and (c) the $^1B_1$ state of ClO_2^+ (see the text for further details).

We first consider the low-energy region, where the well-resolved vibrational structure is observed. The simulated ClO_2^+ $^3B_1 \leftarrow ClO_2$ X^2B_1 and ClO_2^+ $^3B_2 \leftarrow ClO_2$ X^2B_1 bands [Figures 6.4(b) and 6.4(a), respectively] are both dominated by the stretching (v', 0, 0) and the combination bands (v', 1, 0), giving two vibrational progressions. They clearly resemble the vibrational structure observed in the low-energy region of the second band with five 'pairs' of peaks. Flesch *et al.* (1993) assigned these two progressions (pairs of peaks) to the ionizations to the $^{3,1}B_1$ electronic states (i.e.,

two nearby cationic states, each with a single vibrational progression, instead of two vibrational progressions of the same electronic state). However, both the computed MRCI triplet/singlet splitting (and/or the AIEs; see Table 6.6) and our simulations of these two states [Figures 6.4(b) and 6.4(c)] do not support the assignments of Fresch *et al.* (1993). (The assignments of Peterson and Werner (1993) will be considered later.)

Based on the simulated spectra, the low-energy region of the second PE band is now re-assigned to the ionizations to the $^3B_2$ and $^3B_1$ states, with the pairwise structures assigned to the symmetric stretch and bending modes. The $^3B_1$ simulation [Figure 6.4(b)] shows a sharp adiabatic peak in the vibrational structure, while the relative intensities of the two vibrational progressions of the $^3B_2$ simulation [Figure 6.4(a)] increase gradually. These simulated vibrational envelopes support the assignments that the observed onset of the second PE band at 12.400 eV is the AIE position of the $^3B_2$ state. The MRCI calculations (Peterson and Werner, 1993) also give the $^3B_2$ state as the lowest state of the five cationic states assigned to the second PE band. The AIE position of the ionization to the $^3B_1$ state is then assigned to the fifth pair of vibrational components in the low-energy region measured at 12.785 eV. These assignments give a relative energy (T_0) between the $^3B_2$ and $^3B_1$ state of 0.385 eV, which compares reasonably well with the MRCI+Q/cc-pVQZ(with g) relative T_e value of 0.49 eV.

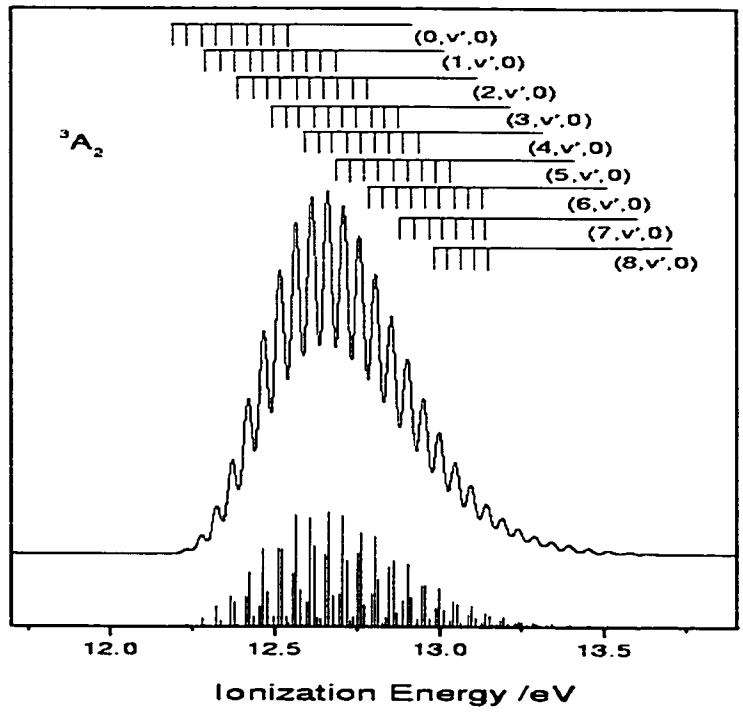

Figure 6.5. The simulated photoelectron spectrum of the ClO_2^+ $^3A_2 \leftarrow ClO_2$ $\tilde{X}\,^2B_1$ ionization (see the text for further details).

From the MRCI calculations, the AIE of the $^3A_2$ state was computed to be in between those of the $^3B_2$ and $^3B_1$ state. However, our simulation of the ClO_2^+ $^3A_2 \leftarrow$ ClO_2 X^2B_1 ionization (Figure 6.5) shows long progressions in the symmetric bending and stretching vibrations, suggesting a very weak relative intensity at the adiabatic position of the $^3A_2$ ionization, which would probably be too weak to be identified in the observed spectrum. Nevertheless, if the vertical ionization position (strongest overall relative intensity) of the simulated spectrum is aligned to the observed peak at 13.050 eV (having the strongest resolved relative peak intensity) in the mid-energy region, an AIE of 12.580 eV can be obtained from the simulation. This AIE value corresponds

very well with the MRCI value of 12.46 (see Table 6.6). This assignment of the $^3A_2$ state would then account for the observed single progression in the mid-energy region.

Before the whole second PE band is considered, we look briefly at the simulated spectra of the two singlet states. The simulations of the $^1A_2$ and $^1B_1$ states are shown in Figure 6.6 and 6.4(c) respectively. These singlet states are expected to be weaker than their corresponding triplet states (with a statistical ratio of 1:3). The vibrational structure of the $^1A_2$ state is very similar to the triplet counterpart (Figures 6.5 and 6.6), but the $^1B_1$ simulated spectrum, dominated by the stretching (v', 0, 0) progression, is quite different from that of the $^3B_1$. The latter difference is not surprising, as the triplet and singlet states have considerably different bond angles from the MRCI calculations (Peterson and Werner, 1993).

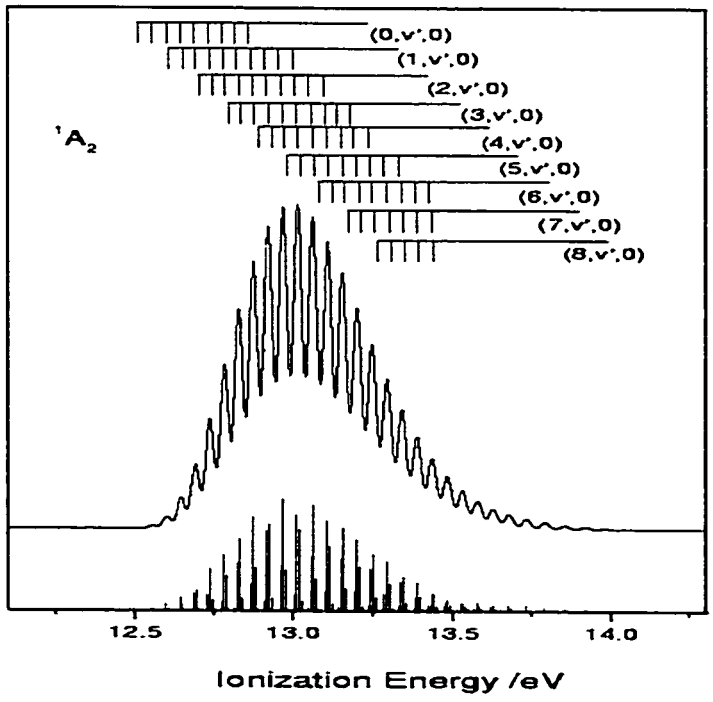

Figure 6.6. The simulated photoelectron spectrum of ClO_2^+ $^1A_2 \leftarrow ClO_2$ $\tilde{X}\,^2B_1$ ionization (see the text for further details).

6.3.4.2. The simulation of the second PE band

Considering the assignments of Peterson and Werner (1993), which were mainly based on computed MRCI AIEs/VIEs, the whole second band of the ClO_2 PE spectrum was synthesized by a weighted sum of the five constituent simulated spectra. The MRCI+Q AIEs, shifted by 0.38 eV in order to match approximately the observed values, were used. Thus, for the $^3B_2$, $^3A_2$, $^3B_1$, $^1A_2$, and $^1B_1$ states, the AIEs after the shift are 12.40, 12.57, 12.87, 12.89, and 13.33 eV, respectively. In Figure 6.7(c), the simulated spectrum (lower trace) was generated by simple addition of the five simulated spectra, assuming the same photoionization cross section for each ionization, but with allowance for the statistical weights of spin-multiplicity. That is, the total relative intensities between the $^3A_2$ and $^1A_2$ spectra and that of the $^3B_1$ and $^1B_1$ spectra were assumed to be 3 to 1, while the three triplet states were assumed to have the same intensity. The agreement between the spectrum synthesized in this way [the lower trace in Figure 6.7(c)] and the experimental spectrum [the upper trace in Figure 6.7(c)] is reasonably good, particularly for the resolved vibrational structures. In general, most of the observed vibrational features can be accounted for by the simulations, suggesting that the assignments of Peterson and Werner (1993) are reasonably reliable.

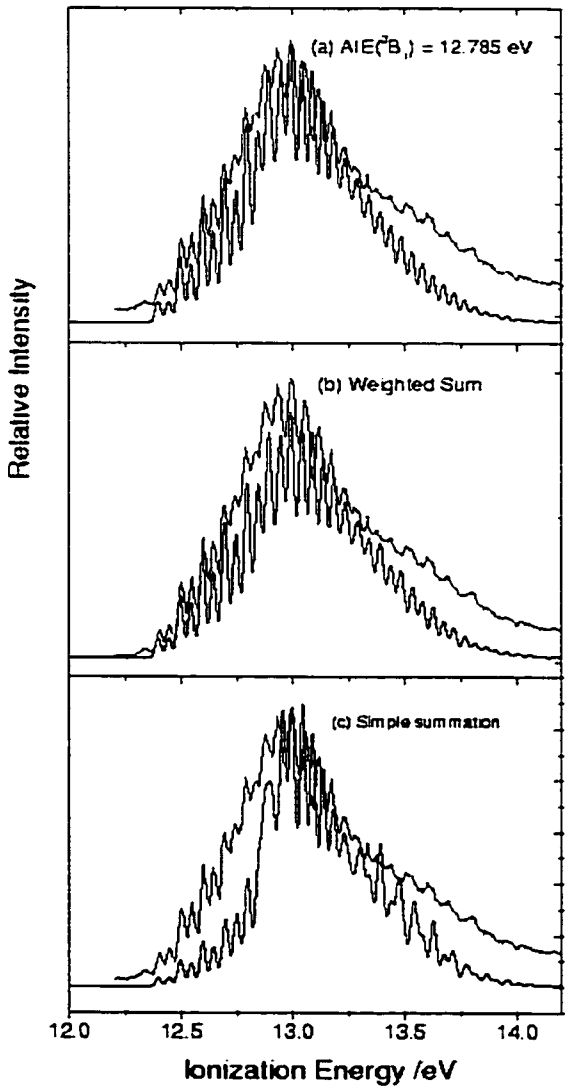

Figure 6.7. The synthesized second band of the ClO_2 photoelectron spectrum (lower trace) and the experimental spectrum (upper trace) of Flesch et al. (1993) (see the text for details): (a), the best match, as (c) and (b), but with AIE ($^3B_1$) set to 12.785 eV; (b), as (c) but with adjusted relative photoionization cross sections (see the text); (c) with MRCI+Q AIEs + 0.38 eV shift.

A better agreement between the simulated second band and the observed one can be obtained by varying the relative intensities between the $^3B_2$, the $^3A_2$ and $^1A_2$ pair, and

the $^3B_1$ and $^1B_1$ pair, and also the AIEs. Figure 6.7(b) shows the best matching spectrum (lower trace) obtained by varying the relative intensities. The relative intensities for the $^3B_2$, $^3A_2$, and $^3B_1$ ionizations used are 3, 0.3, and 1.5, respectively (assuming a triplet to singlet statistical ratio of 3:1). Efforts were also made to improve the agreement by changing the AIE of each ionization. From the previous subsection, we have assigned the 12.785 eV peak to the AIE of the $^3B_1$ ionization. The simulated second PE band employing this AIE for the $^3B_1$ ionization is shown in Figure 6.7(a). In the low- and mid-energy region, this simulation seems to be in marginally better agreement with the experimental band than the one using the shifted MRCI+Q AIEs. Further attempts were made in varying each AIE of the individual ionizations in order to obtain a better match with the experimental band. However, no further improvement could be achieved and the synthesized second PE band shown in Figure 6.7(a) is the best match that can be obtained. Thus, the best AIEs to the $^3B_2$, $^3A_2$, $^3B_1$, $^1A_2$, and $^1B_1$ states are estimated to be 12.400, 12.570, 12.785, 12.890, and 13.330 eV, respectively. These values are tabulated together with the corresponding VIE values obtained from the simulated spectra in Table 6.6. The AIEs to the triplet states obtained in this way are very similar to those obtained above, by considering the comparison between the simulated and observed vibrational structure of individual ionizations to the triplet states. For the $^3A_2$ ionization, the difference is only 0.01 eV.

6.4. Concluding Remarks

In summary, in this work both the harmonic and anharmonic FCF methods were applied to study the first and third bands of the He I PE spectrum of ClO_2. These two PE bands of ClO_2 have rather simple and well-resolved vibrational structures. For the first

band of the PE spectrum, the harmonic FC model even after applying the IFCA procedure was shown to be inadequate and the anharmonic FC simulation gave a much-improved agreement with the observed spectrum.

The IFCA procedure was applied with the anharmonic FC method to refine the published MRCI geometry of the $\tilde{X}\,^1A_1$ state of ClO_2^+. The first experimentally derived geometry obtained for this cationic state is R(Cl-O) = 1.414 ± 0.002 Å and ∠O-Cl-O = 121.8 ± 0.1° and this should be the most reliable one to date. Although the agreement of the harmonic FC simulated spectrum with the observed spectrum is not as good as that of the anharmonic one, the IFCA geometrical parameters of the $\tilde{X}\,^1A_1$ state of ClO_2^+ obtained with the harmonic FC calculations are very close to those with the anharmonic calculations. In this connection, and in view of the different computational resources required for the harmonic and anharmonic FC calculations, the harmonic FCF method can still be considered very useful in obtaining experimentally derived geometrical parameters as done in Chapters 3-5. However, in the IFCA procedure with the harmonic method, care should be taken in the comparison between the simulated and observed spectra (Chau et al., 1998). It should also be mentioned that the ab initio calculations, required for the harmonic and anharmonic FCF calculations, are very different. For the latter, multi-dimensional PEFs, obtained from energy surface scans, are required. These scans are expected to be considerably more expensive than geometry optimization and harmonic frequency calculations at the minimum-energy geometry, which are required for the harmonic FC method. Summarizing, there are different theoretical and practical advantages and disadvantages associating with the harmonic and anharmonic FC methods and the method chosen will depend on the problem under consideration, the quality of the experimental information, and the available computational resources.

The second band of the ClO_2 He I PE spectrum revealed complicated vibrational structures because it involves ionizations to five low-lying electronic states of the cation. The spectral simulations reported here clearly support the MRCI assignments of Peterson and Werner (1993). The simulated spectrum of the second band has reproduced the main vibrational features of the experimental spectrum. However, a perfect match has not been obtained, even with the variations of the AIEs and the relative ionization cross sections of the ionizations to the five cationic states. A better match may be obtained, if the IFCA procedure were carried out for each of the five ionizations. However, this has not been carried out, because well-resolved vibrational structure in the observed spectrum is required for doing this, but this is not available from the observed spectrum. Nevertheless, with the spectral simulations reported here, the ordering of the $^3B_2$, $^3A_2$, $^3B_1$, $^1A_2$, and $^1B_1$ states in the second PE band of ClO_2 seems clear and their AIEs were determined. The usefulness of the powerful combination of high-level ab initio calculation and FC analysis in the interpretation of a seriously overlapping spectrum has been clearly demonstrated. In the case of the He I PE spectrum of ClO_2, the combination of MRCI PEFs and the anharmonic FC method has been shown to work well.

CHAPTER 7

Ab initio Studies of the Geometry, Ionization Potentials and Anharmonic Properties of Oxygen Difluoride (F_2O) and Spectral Simulation of its He I Photoelectron Spectrum

7.1. Background

The He I photoelectron (PE) spectrum of F_2O was first reported by Cornford et al. (1971). With a spectral resolution of ca. 45 meV (full width at half-maximum, FWHM), only the first PE band of the spectrum was found to exhibit vibrational structure, which consisted of one progression, assigned to excitation of the symmetry stretching vibrational mode ν_1. The first adiabatic ionization energy (AIE) was measured to be 13.13eV. The observed bands were assigned with the aids of INDO and CNDO/2 calculations, and previous ab initio calculations [see the reference (Cornford et al., 1971) for details]. A year later, Brundle et al. (1972) reported another very similar He I PE study of F_2O, perhaps with a improved resolution (quoted to be ca. 30meV, see the later text), in which the new AIE for the first PE band was determined as 13.11eV. Ab initio calculations were also performed; both the Koopman's Theorem (KT) and the ΔSCF method were utilized to assign the observed spectrum. The assignments of the first four PE bands from these two studies are essentially identical, giving the order of the lowest four cationic states of F_2O^+ as $^2B_1$, $^2A_1$, $^2B_2$ and $^2A_2$. These cationic states were assigned to four distinct PE bands observed in the He I PE spectra, with measured VIEs of 13.25, 16.10, 16.44 and 18.50 eV respectively (Brundle et al., 1972; see also Table 7.1). However, Brundle et al. mentioned also an alternative assignment that the ionization of an electron from the nonbonding a_2 molecular orbital, leading to the $^2A_2$ state, might be preferred to be assigned to the relative sharp third PE band at 16.44 eV, rather than the broad band at 18.50 eV. Thus, the lowest $^2A_1$, $^2B_2$ and the $^2A_2$ cationic states of F_2O^+ would be assigned jointly to the observed overlapping second and third PE bands with measured VIEs of 16.10 and 16.44 eV respectively. With this alternative

assignment, the precise positions of the lowest $^2A_1$, $^2B_2$ and the $^2A_2$ cationic states of F_2O^+ are unclear, as three states are now assigned to two observed bands. Since the later PE spectrum is of a better quality with a higher resolution than the one published in 1971, we will focus on the second PE spectrum given by Brundle et al., and we will only investigate the PE bands observed in the low IE region (see Figure 7.1).

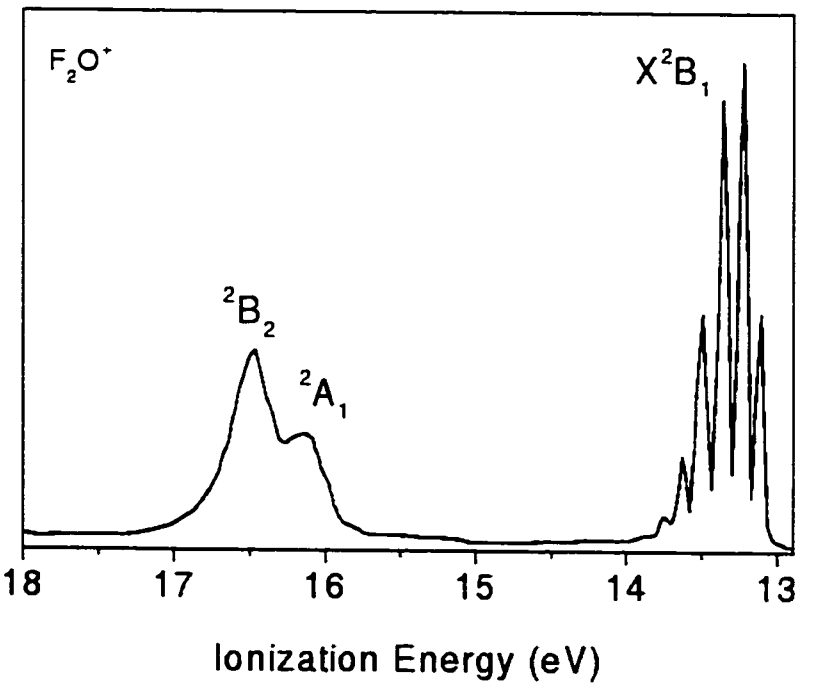

Figure 7.1. The experimental He I photoelectron spectrum within the range of 13-18 eV (Brundle et al., 1972).

Table 7.1. The vertical ionization energies (VIEs in eV) of the first four cationic states of F_2O^+ from previous calculations

Method[a]	$^2B_1$	$^2B_2$	$^2A_1$	$^2A_2$	First author/Year
INDO[b]	14.3	16.7	15.8	18.1	Cornford/1971
ΔSCF/DZ[c]	13.5	16.9	16.3	18.3	Brundle/1972
MRDCI/DZP+bp[d]	13.43	16.17	16.36	17.41	Valenta/1980
ROCI+Q[e]/DZP	13.18	16.01	16.59	16.62	Langhoff/1981
RSPT-KT[f]/DZ-STO	13.29	16.54	16.33	16.69	Chong/1974
GF[g]	13.06	16.46	16.37	16.95	Von Niessen/1979
RSPT-KT[h]/DZP	13.14	16.78	16.75	17.14	Langhoff/1982
pGW2[i]	13.39	16.27	16.61	16.54	Hu/1997
Observed[j]	13.26	16.47	16.17	18.68	Cornford/1971
Observed[k]	13.25	16.44	16.10	18.50	Brundle/1972

[a] The highest level of calculation from the respective reference.

[b] For earlier calculations, see the reference (Cornford et al., 1971) and references therein.

[c] Whether the irreducible representation b_1 or b_2 in the C_{2v} point group corresponds to being symmetrical with respect to the molecular plane, depends on the choice of the axes system. Brundle et al employed an axes system, which differs from others. Here, the convention that b_2 corresponds to being symmetrical with respect to the molecular plane is used.

[d] sp bond functions (exponent=1.0) at the centre of mass of the two OF bond were included in the basis set.

[e] RO refers to relaxed orbitals, which mean that the molecular orbitals of the ground state of the cation (instead of those of the neutral molecule) were employed as the many particle basis set in the CI calculation. Q refers to the Davidson correction for quadruple excitations.

[f] Third order Rayleigh-Schrodinger perturbation corrections to Koopman's Theorem (KT).

[g] Green Function calculation.

[h] As footnote e; $\Delta(E^{GA})$ values (see original work for details).

[i] Parametrized second order Green Function (pG) times screened interaction (W2) approximation (see original work for details). It should be noted that in this work, the assignments given for the observed VIEs from Cornford et al are not the same as those in the original paper. Some typing errors in Table 2 of this paper of Hu et al are suspected. In addition, an observed VIE value of 16.32 eV was given to the $^2B_2$ state, which was not found in the original work of Cornford et al. We are unable to trace the origin of this value.

[j] Assignments based on KT from previous ab initio and their own semi-empirical calculations.

[k] Assignments based on KT and ΔSCF results; an alternative assignment of the $^2A_2$ state to the relatively sharp peak at 16.44 eV was given, because of the nonbonding character of the $1a_2$ molecular orbital.

Since the publication of these two He I photoelectron studies on F_2O (Cornford et al., 1971; Brundle et al., 1972), numerous theoretical studies, which calculated the ionization energies (IEs) of the low-lying cationic states of F_2O^+ by various methods, have appeared in the literature. Some of the reported, computed vertical ionization energies (VIEs) for the lowest four cationic states (Cornford et al., 1971; Brundle et al., 1972; Valenta et al., 1980; Langhoff and Chong, 1981; Chong et al., 1974; Niessen, 1979; Langhoff and Chong, 1982; Hu et al., 1997) are summarized in Table 7.1. From Table 7.1, the assignment of the $^2B_1$ state of F_2O^+ to the observed first PE band is reasonably certain. However, based on available calculations, the order of the next three cationic states is far from unambiguously clear. Regarding the alternative assignment of the position of the $^2A_2$ state mentioned by Brundle et al. (1972), some calculated IEs (e.g. ROCI+Q and pGW2; see Table 7.1) clearly support it, but for the others, there is no clear preference between the original (Cornford et al., 1971; Brundle et al., 1972) and the alternative assignments (Brundle et al., 1972). With a MRDCI VIE of 17.41 eV for the $^2A_2$ state, which may be considered as the computed value obtained from the highest level of calculation prior to the present study, Valenta et al.(1980) support the original assignment of the $^2A_2$ state to the broad band at 18.50 eV. In view of the above considerations, it is the purpose of the present investigation to clarify the situation by performing high-level ab initio calculations and carrying out spectral simulations. For the $^2A_2$ state, the two proposed assignments would have their respective observed VIEs differed by over 2 eV. It is expected that near state-of-the-art quantum chemical calculations at present should give IEs, with uncertainties of less than 0.2 eV, and hence should be able to determine which of the two proposed assignments of the $^2A_2$ state is more reliable. With the high level ab initio calculations and spectral simulations in this

work, it is hoped that the assignments of the low-lying cationic states of F_2O^+ could be firmly established.

In Chapter 5 and Chapter 6, we have reported related investigations on the He I PE spectra of Cl_2O and ClO_2 by ab initio calculations and spectral simulations. For the former, the first four observed PE bands are well resolved with vibrational structures (see Figure 5.1), and their assignments have been firmly established to be due to the lowest $^2B_1$, $^2B_2$, $^2A_1$ and $^2A_2$ cationic states respectively (see Table 7.2 for details). Comparing the assignments of the observed bands in the PE spectrum of Cl_2O with those of F_2O (Cornford et al., 1971; Brundle et al., 1972), the following points should be noted (see Table 7.2). Firstly, the order of the second and third cationic states is reversed. Secondly, the fourth PE band assigned to the $^2A_2$ state of Cl_2O^+ has a very strong (0,0,0 – 0,0,0) vibrational component, while the third PE band assigned to the $^2A_1$ state is broad and relatively weak (see Figure 5.1). In addition, the third and fourth bands are close and overlapping. In the present study on the He I PE spectrum of F_2O, an approach similar to the above two investigations has been employed.

The structure of neutral F_2O has been determined by microwave spectroscopy (Pierce et al., 1963; Morino and Saito, 1966); the O-F bond distance is 1.4053 Å, and the bond angle is 103.07°. The harmonic and anharmonic force fields of F_2O have received considerable attention (Lee et al., 1996; Thiel et al., 1988; Dressler and Thiel, 1997; Breidung et al., 1999; Saarinen et al., 1990). Since F_2O is in the test set of molecules, whose heats of formations were calculated by the composite method, G2 (Curtiss et al., 1991), many calibration studies (Petersson et al., 1998; Kieninger et al., 1998) on new methods, such as RI-MP2 (Bernholdt and Harrison, 1998), G3 (Curtiss et al., 1998) and some new density functionals (Abu-Awwad and Politzer, 2000; Politzer and Abu-Awwad, 1998; Schmider and Becke, 1998; Voorhis and Scuseria, 1998; Kafafi

et al., 1998; Kafafi, 1998), have included F_2O. However, the cation, F_2O^+, has received significantly less attention.

Table 7.2. The comparison of the electronic structures between F_2O^+ and Cl_2O^+ in the low IE region

States	Cl_2O^+ Expt Values[a] (AIE) in eV	Cl_2O^+ Ab initio[b] (AIE) in eV	F_2O^+ Spectral simulation[c] (AIE) in eV	F_2O^+ Ab initio[d] (AIE) in eV	F_2O^+ Expt values[e] (VIE) in eV	F_2O^+ Expt values[f] (VIE) in eV
X^2B_1	10.89	11.01	13.11	12.87	13.26	13.25
$^2B_2$	12.02	11.98	15.72	15.59	16.17	16.10
$^2A_1$	≤12.45	12.45	16.19	15.99	16.47	16.44
$^2A_2$	12.74	12.84	16.46	16.26	18.68	18.50

[a] Motte-Tollet et al., 1998.

[b] At the RCCSD(T)/aug-cc-pVTZ//QCISD/6-31G* level of calculation.

[c] See the text for details.

[d] At the MRCI+D/cc-pVQZ//RCCSD(T)/cc-pVQZ level of calculation (see the text).

[e] Cornford et al., 1971.

[f] Brundle et al., 1972; see also the footnote k of Table 7.1.

In this investigation, we report ab initio calculations on the neutral ground state X^1A_1 and the X^2B_1, $^2B_2$, $^2A_1$ and $^2A_2$ states of F_2O^+ at various high-levels of theory. From these calculations, the geometries and harmonic frequencies, for the neutral and cationic states are obtained, as well as the adiabatic ionization energies, for the first four cationic states involved in the He I PE spectrum. Also, the first three bands in the He I PE spectrum of F_2O have been simulated by employing the FCF calculation with the

Duschinsky effect. For the first PE band, the IFCA procedure incorporated with the multi-dimensional harmonic simulation and anharmonic simulation has been performed, respectively, in order to obtain the more reliable cationic geometry. The simulations have confirmed the assignment of the observed vibrational structure of the first band in the experimental PE spectrum. The experimentally derived geometry of F_2O^+ (X^2B_1) was obtained, for the first time, via the IFCA method, which includes anharmonicity and Duschinsky effect. Based on the ab initio calculations and the spectral simulations of the overlapping 2nd and 3rd PE bands in this work, the discrepancy in the assignment for the order of the lowest three cationic states ($^2B_2$, $^2A_1$ and $^2A_2$) in the previously experimental and/or theoretical investigations has been clarified. This investigation has also led to a re-assignment of the heavily overlapping second and third bands in the experimental He I PE spectrum (Brundle et al., 1972). It firmly concludes that the experimental overlapping second and third bands are due to ionizations to three cationic states ($^2B_2$, $^2A_1$ and $^2A_2$) instead of the two cationic states ($^2A_1$ and $^2B_2$) as given in the experimental PE spectrum (Brundle et al., 1972). The RCCSD(T) anharmonic potential energy functions (PEFs) for the neutral ground state and the lowest four cationic states obtained in this work have been used in the anharmonic FC simulations of the first three PE bands of F_2O.

7.2. Theoretical Considerations and Computational Details

7.2.1. Ab initio calculations

A*b initio* calculations were performed to provide the minimum energy geometries, harmonic frequencies, the AIEs and the single point energies required for the

subsequent harmonic FCF calculations, the spectral simulations and the fitting of multi-dimensional anharmonic potential energy functions, respectively. Geometry optimization and harmonic vibrational frequency calculations were carried out for the ground state (X^1A_1) of the neutral F_2O radical and the first four ionic states (X^2B_1, $^2B_2$, $^2A_1$ and $^2A_2$) of F_2O^+ at various levels of theory for obtaining reliable input data for the subsequent spectral simulations. Comparisons between the sensitivities of geometry optimization and frequency calculation with the used vavrious levels of calculation can also be made from these computations. For relative energies, AIEs and/or VIEs were evaluated at up to the RCCSD(T)/cc-pV5Z//RCCSD(T)/cc-pVQZ level. The best optimized geometries and computed force constants (see next section for details) were then employed in the subsequent Franck-Condon factor calculations. The ab initio energy scans for the neutral state X^1A_1 and the lowest four cationic states (X^2B_1, $^2B_2$, $^2A_1$ and $^2A_2$) in the symmetric stretching and bending coordinates have been performed at the CCSD(T) level with the aug-cc-pVQZ or aug-cc-pVTZ basis. All the ab initio calculations were carried out with the GAUSSIAN98 suites of programs (Frisch et al., 1998) or the MOLPRO program (Werner et al.).

7.2.2. The least squares fitting of potential energy surfaces

For the anharmonic FCF calculations, the PEFs of the electronic states involved in the electronic transition are required in the variational calculations for the vibrational wave function of each state (see Chapter 2 for details). In order to obtain reasonably reliable PEFs, a total of 26 ab initio single-point energies at the CCSD(T) level of theory were used to fit the following polynomial for the neutral state (X^1A_1) and the cationic states (X^2B_1, $^2B_2$, $^2A_1$ and $^2A_2$), respectively,

$$V = \sum_{ij} C_{ij} (S_1)^i (S_2)^j + V_{eqm} . \quad (7.1)$$

The PEFs are expressed in the displacements of symmetry coordinates

$$S_1 = (\Delta r_1 + \Delta r_2)/\sqrt{2}, \quad (7.2)$$

and the bending coordinates suggested by Carter and Handy (1987),

$$S_2 = \Delta\theta + \alpha * \Delta\theta^2 + \beta * \Delta\theta^3, \quad (7.3)$$

where $\Delta r_{1,2}$ and $\Delta\theta$ are displacements in FO bond lengths (for the symmetric stretch, $\Delta r_1 = \Delta r_2$) and F-O-F bond angle, respectively. By restricting the energy gradient in S_2 to zero when the molecule is linear (i.e. when $\theta = \pi$), an expression relating α and β can be obtained:

$$\beta = [1 + 3 * \alpha(\pi - \theta_{eqm})^2]/[-2 * (\pi - \theta_{eqm})]. \quad (7.4)$$

This condition is imposed to make sure that the gradient of the resulting potential energy function takes a value of zero when the molecules is linear. The non-linear least squares fit procedure, NL2SOL (Dennis et al., 1981) was employed to obtain the C_{ij}'s, V_{eqm}, r_{eqm}, θ_{eqm} and α from the computed single point energies. In these energy scans, the aug-cc-pVQZ basis set was employed for the ground states of the neutral and cation, while for the excited cationic states, the aug-cc-pVTZ basis set was used. The reason for using a smaller basis set for the latter states is that the vibrational structures observed in the second and third PE bands are poorly resolved, and hence only qualitative comparison between the simulated and observed spectra is required.

These ab initio single-point energies used in the fitting of the above PEFs have ranges of –0.21 Å ≤ Δr ≤ +0.35 Å and -30° ≤ Δθ ≤ +30° in the CCSD(T)/aug-cc-pVQZ calculations, and of –0.14 Å ≤ Δr ≤ +0.21 Å and -15° ≤ Δθ ≤ +15° in the CCSD(T)/aug-

cc-pVTZ calculations. The asymmetric stretching mode, ν_3, had not been considered in the anharmonic FCF calculations, because harmonic FCF calculations gave negligible intensities for this vibrational mode upon ionization to all four lowest cationic states. From these energy scans, equilibrium geometrical parameters and fundamental frequencies of the symmetric stretch and bending modes were also obtained (see next subsection).

In all the PEFs, all terms up to the fourth order and also C_{05} and C_{06} are included. For the ground states of F_2O and F_2O^+, as the vibrational structure observed in the He I PE spectrum is essentially due to the symmetric stretching mode, the fifth and sixth order terms for stretching, C_{50} and C_{60}, are included as well. A higher level of theory, CCSD(T)/aug-cc-pVQZ was employed to determine the PEFs of the neutral and cationic ground states, so that a more reliable cationic geometry can be deduced using the iterative Franck-Condon analysis procedure. For $^2B_2$, $^2A_1$ and $^2A_2$ cationic states, the CCSD(T)/aug-cc-pVTZ level of calculation was used, as mentioned above.

The method of combination of ab initio calculation and FC analysis for spectral simulation with harmonic and anharmonic IFCA procedures is the same as used in Chapter 6 and the details have been described in Chapter 2. The IFCA procedure was applied to the first PE band, where well resolved vibrational structure was observed. Experimentally derived geometrical parameters of the X^2B_1 state were thus obtained for the first time (see next section). For the second and third bands, the vibrational structures observed are poorly resolved and the AIE positions of the three cationic states involved are uncertain from the observed spectrum. Consequently, the IFCA procedure was not considered in the second and third PE bands. For the $^2B_2$, $^2A_1$ and $^2A_2$ states, their total simulated band areas were assumed to be the same. For the first PE band of F_2O, the experimental AIE was used in the simulation. For the three excited cationic

states considered in this work, the RCCSD(T)/cc-pVTZ, RCCSD(T)/cc-pVQZ, RCCSD(T)/cc-pV5Z//RCCSD(T)/cc-pVQZ and MRCI+D/cc-pVQZ//RCCSD(T)/cc-pVQZ AIEs were respectively employed for comparison with the experimental He I PE spectrum.

7.2.3. The basis used in the variational calculations of the vibrational wave functions

For neutral F_2O, vibrational levels with quantum number of up to 8 were considered in the variational calculations, with a further constraint of $v_1 + v_2 \leq 8$. This was shown to be more than sufficient from a series of calculations including different numbers of vibrational levels. Similarly, for $F_2O^+(X^2B_1)$, vibrational levels with quantum number of up to 25 were included, with a further constraint of $v_1 + v_2 \leq 25$. Thus, a total of 45 harmonic basis functions for the neutral $F_2O(X^1A_1)$ and of 351 harmonic basis functions for the cationic $F_2O^+(X^2B_1)$ have been used in the variational calculations to obtain the anharmonic vibrational wavefunctions. FCF calculations employing vibrational wavefunctions obtained with larger harmonic basis sets for the ground neutral state and ground cationic state were also carried out to test the sensitivity of calculated FCFs and simulated PE band to the selected basis sets. These calculations show that larger basis sets than the ones mentioned above do not alter the quality of the calculated FCFs or spectral simulation to any significant extent. Similarly, for the excited cationic states, vibrational levels with quantum number of up to 25 were also included in the variational calculation, with a further constraint of $v_1 + v_2 \leq 25$. It seems that the basis set constraint of $v_1 + v_2 \leq 25$ for the four cationic states involved in this

work is a reasonable compromise of accuracy and economy. Therefore, this constraint was applied for all four lowest cationic states considered here.

7.3. Results and discussion

7.3.1. Ab initio calculations and anharmonic PEFs

The minimum-energy geometry, computed harmonic vibrational frequencies and IEs obtained in this work for $F_2O(X^1A_1)$ and the low-lying states of F_2O^+ are summarized in Tables 7.3 to 7.5, respectively, and compared with available experimental values. From Table 7.3, the calculated geometrical parameters of neutral $F_2O(X^1A_1)$ converge to the available experimental values readily as the level of calculation improves. At the highest level of CCSD(T)/aug-cc-pVQZ, the calculated geometrical parameters are very close to the experimental values though no obvious trends are observed with the theoretical methods used, for the harmonic vibrational frequencies of $F_2O(X^1A_1)$ (see Table 7.4).

Table 7.3. The calculated minimum-energy geometries (bond length in Å / bond angle in degrees) for the neutral (X^1A_1) and the four lowest-lying cationic states (X^2B_1, $^2B_2$, $^2A_1$ and $^2A_2$) of F_2O.

Methods	X^1A_1	X^2B_1	$^2B_2$	$^2A_1$	$^2A_2$
experimental values[a]	1.4053/103.07				
MP2/6-311+G(2df)	1.398/103.15	1.2715/107.99	1.3714/79.92	1.3177/ 121.25	1.5096/ 104.93
B3LYP/cc-pVTZ	1.4036/103.97	1.3186/108.01	1.4280/84.96	1.3777/ 118.71	1.4462/ 98.48
QCISD/cc-pVTZ	1.3945/103.15	1.3178/107.29	1.4200/83.48	1.3794/ 119.17	b
CCSD(T)/cc-pVTZ	1.4056/103.04	1.3238/107.43	1.4416/82.71	1.3660/ 118.89	1.4681/ 98.54
CCSD(T)/cc-pVQZ			1.4383/82.46	1.3613/ 118.88	1.4644/ 98.20
CCSD(T)/aug-cc-pVTZ[c]			1.4437/82.28	1.3689/ 118.57	1.4698/ 97.94
CCSD(T)/aug-cc-pVQZ[c]	1.4056/103.04	1.3190/107.28			
CASSCF(7, 6)/6-311+G(2d)					1.5098/ 94.70
CASSCF(7, 6)/cc-pVTZ					1.5023/ 95.08
CCSD(T)/cc-pVQZ(fc)[d]	1.4056/103.09				
IFCA[e]		1.3303/107.3			
IFCA[f]		1.3219/107.3			

[a] Pierce et al., 1963.
[b] QCISD excessive iterations in the numerical second derivative calculations.
[c] The optimized geometrical parameters were from energy scans and PEF fittings.
[d] Breidung et al., 1999.
[e] The best estimated geometry from the harmonic IFCA procedure (see the text for details).
[f] The best estimated geometry from the anharmonic IFCA procedure (see the text for details).

Table 7.4. The calculated harmonic vibrational frequencies {$\omega_1(a_1$ symmetric stretch) / $\omega_2(a_1$ symmetric bending) / $\omega_3(b_2$ asymmetric stretch) in cm^{-1}} for the neutral (X^1A_1) and the four lowest energy cationic states (X^2B_1, $^2B_2$, $^2A_1$ and $^2A_2$) of F_2O.

Methods	X^1A_1	X^2B_1	$^2B_2$	$^2A_1$	$^2A_2$
experimental values	928.07[a]/460.56[b] /828.69[c]				
MP2/6-311+G(2df)	977.5/485.5/ 902.8	1490.0/664.2 /1336.8	1760.8/707.6 /1353.7	1109.3/ 485.7 /1811.4	946.9/ 323.8 /251.1i
B3LYP/cc-pVTZ	1018.7/480.1/ 893.8	1125.0/570.0 /993.5	1029.5/445.0 /538.9	821.9/ 429.7/ 385.1	959.2/ 424.6 /723.3i
QCISD/cc-pVTZ	1007.5/494.0/ 951.0	1146.3/573.8 /1059.0	1089.5/479.6/ 484.3	799.0/ 427.3 /6495.0	
CASSCF(7,6)/6-311+G(2d)					769.2/ 366.0/ 575.9
CASSCF(7,6)/cc-pVTZ					794.6/ 372.1/ 573.9
CCSD(T)/aug-cc-pVTZ[d]			957.3/454.6/--	862.1/ 414.9/--	879.2/ 378.9/-
CCSD(T)/aug-cc-pVQZ[d]	952.4/466.9/--	1068.3/556.7/ --			
CCSD(T)/cc-pVQZ(fc)[e]	951 / 471 / 865				

[a] Taubmann et al., 1986.

[b] Burger and Schippel, 1987.

[c] Taubmann and Naturforsch, 1987.

[d] Fundamental frequencies from the ab initio scans in this work.

[e] Breidung et al., 1999.

Table 7.5. The observed and calculated adiabatic and vertical ionization energies (AIE / VIE in eV) of the four lowest energy cationic states (X^2B_1, $^2B_2$, $^2A_1$ and $^2A_2$) in the He I PE spectrum of F_2O.

Methods	X^2B_1	$^2B_2$	$^2A_1$	$^2A_2$
experimental values	13.13 / 13.26[a]	-- / 16.47[a]	-- / 16.17[a]	-- / 18.68[a]
	13.11 / 13.25[b]	-- / 16.44[b]	15.74 / 16.10[b]	17.9 / 18.50[b]
QCISD/cc-pVTZ	12.84 / --	15.76 / --	15.99 / --	
RCCSD/aug-cc-pVQZ //QCISD/cc-pVTZ	-- / 13.40	-- / 16.28	-- / 16.74	
RCCSD(T)/cc-pVTZ	12.93 / --	15.72 / --	16.19 / --	16.46 / --
RCCSD(T)/cc-pVQZ	13.07 / --	15.78 / --	16.36 / --	16.63 / --
RCCSD(T)/cc-pV5Z// RCCSD(T)/cc-pVQZ	13.13 / --	15.85 / --	16.43 / --	16.71 / --
MRCI+D/cc-pVQZ// RCCSD(T)/cc-pVQZ		15.59 / 15.97	15.99 / 16.18	16.26 / 16.41
Spectral simulation[c]	13.11 / -	15.72 / --	16.19 / --	16.46 / --

[a] Cornford et al., 1971.

[b] Brundle et al., 1972; see also the footnote k of Table 7.1.

[c] See the text for details.

For the cationic states considered here, no experimentally derived geometry was available prior to the present study. From Table 7.3, it seems clear that, for all the cationic states considered the optimized geometrical parameters are rather sensitive to

the levels of calculation in obtaining them. This is particularly true for the $^2A_2$ state. A higher level of calculation is clearly required to obtain reliable geometrical parameters for the cationic states than the neutral ground state. A similar conclusion can be drawn from Table 7.4 for the computed vibrational frequencies. In particular, the MP2 level is inadequate for all the cationic states studied, giving both geometrical parameters and harmonic vibrational frequencies significantly different from those obtained from higher levels of calculation. In Contrast, the B3LYP results are in closer agreement with the QCISD and/or RCCSD(T) results. For the $^2A_2$ state, CASSCF calculations were carried out to obtain the minimum-energy geometry and harmonic vibrational frequencies, because QCISD geometry optimization on this state faced excessive QCISD iteration problems; in addition, both MP2 and B3LYP frequency calculations yielded an imaginary frequency for the b_2 asymmetric stretching mode. The CASSCF calculations on the $^2A_2$ state considered seven electrons in six active orbitals. The second CI root was requested in order to obtain the $^2A_2$ state (a similar approach was employed in our study on the $^2A_2$ state of Cl_2O^+; see Chapter 5). With both the 6-311+G(2d) and cc-pVTZ basis sets, the CASSCF calculations gave all real frequencies at their respective optimized geometries. The most reliable computed geometrical parameters and fundamental vibrational frequencies of the symmetric stretch and bending modes were, however, obtained from calculations at the highest levels {CCSD(T)/aug-cc-pVTZ and/or CCSD(T)/aug-cc-pVQZ} from the scans/PEFs.

The computed ionization energies are given in Table 7.5. Firstly, the first AIE is considered, as reliable experimental values are available. All the computed values obtained in this work agree with the experimental values to within 0.3 eV. If only the RCCSD(T) values are considered, the agreements are within 0.2 eV. At the highest level of calculation {RCCSD(T)/cc-pV5Z}, the computed AIE value agrees with available

experimental values to ≤ 0.02 eV. The difference between the RCCSD(T)/cc-pVQZ and RCCSD(T)/cc-pV5Z levels is only 0.06 eV, suggesting near exhaustion of basis set effect. All these comparisons support the expectation mentioned in the Introduction that near state-of-the-art quantum chemical calculations on relative energies are reliable to within 0.2 eV.

For the order of the low-lying cationic states and the position of the $^2A_2$ state (the alternative assignment of Brundle et al., 1972), it gives a clearer picture, if the T_e's (the relative electronic energy of the excited cationic state with respect to the ground cationic state), rather than the AIEs, are considered. From Table 7.6, the consistency in the computed T_e values of the low-lying cationic states of F_2O^+ obtained at various levels of calculation is remarkably high. Therefore, it can be concluded that the reliability of these values is beyond any reasonable doubt. The order of the low-lying cationic states of F_2O^+ is conclusively $^2B_1$, $^2B_2$, $^2A_1$ and $^2A_2$, which is the same as for Cl_2O^+ (see Chapter 5), but different from the original assignments of Cornford et al. (1971) and Brundle et al. (1972). From the present systematic investigation on the computed IEs, it can be concluded that this order would very unlikely be changed with any further improvement in the level of calculation.

Table 7.6. The computed relative electronic energies, T_e (in eV), of the low-lying cationic states of F_2O^+ (with respect to the X^2B_1 state).

Method	$^2B_2$	$^2A_1$	$^2A_2$
RCCSD(T)/cc-pVTZ	2.79	3.26	3.53
RCCSD(T)/cc-pVQZ	2.71	3.29	3.56
RCCSD(T)/cc-pV5Z// RCCSD(T)/cc-pVQZ	2.72	3.30	3.58
MRCI+D/cc-pVQZ// RCCSD(T)/cc-pVQZ	2.72	3.12	3.39

Regarding the position of the $^2A_2$ state, from Table 7.6, the range of the computed T_e values is from 3.4 to 3.6 eV. Combining the experimental AIE of the first band with the computed T_e values, the AIE range for the $^2A_2$ state is then from 16.5 to 16.7 eV. In addition, the differences between the computed T_e values of the $^2A_1$ and $^2A_2$ states obtained at various levels of calculation (Table 7.6) are remarkably consistent. The average computed AIE/T_e separation between the $^2A_1$ and $^2A_2$ state is 0.27 ± 0.01 eV. The CASSCF/MRCI separation is 0.27 eV, in excellent agreement with RCCSD(T) values. Based on all these highly consistent computed results, it can be concluded that the $^2A_1$ and $^2A_2$ states should be very close, with a separation of ≤ 0.3 eV. This conclusion clearly favours the alternative assignment of the $^2A_2$ state suggested by Brundle et al. (1972), that the ionization leading to the $^2A_2$ state has to be assigned together with the $^2B_2$ and $^2A_1$ states to the second and third PE bands. However, the detailed assignments of these two observed bands and the precise AIE/VIE positions of the three cationic states involved could not be deduced without the aids of spectral simulations, which will be discussed later. Higher computed IE values from previous

calculations for the $^2A_2$ state of F_2O^- (for examples, Brundle et al.. 1972; Valenta et al., 1980; Langhoff and Chong, 1982; see Table 7.1) are almost certainly due to a lack of sufficient electron correlation in their calculations.

The C_{ij}, α, r_e and θ_e obtained from the fitting are given in Table 7.7 for all the electronic states studied. The root mean square (RMS) deviations in the fitting are smaller than 11 cm^{-1} in all the PEFs reported here. For the X^1A_1 state of neutral F_2O, the anharmonic force fields at the CCSD(T) level (quadratic force field from CCSD(T)/cc-pVQZ, cubic and quartic force fields from CCSD(T)/cc-pVTZ calculations) have been reported by Breidung et al. (1999). Variational calculation of vibrational wavefunction was also performed employing the best PEF from the reference (Breidung et al., 1999). A basis size limit of v_1, $v_2 \leq 8$ and a further constraint of $v_1 + v_2 \leq 8$ were imposed, when only the two symmetric modes were considered. When all three vibrational modes are considered, a basis limit of v_1, v_2, $v_3 \leq 8$ with a constraint of $v_1 + v_2 + v_3 \leq 8$ were imposed. The computed vibrational energies thus obtained are compared with those obtained using the PEF of the present study for the neutral ground state of F_2O, as shown in Table 7.8. The agreement among the computed vibrational energies (and with available experimental values) is generally very good. The effect of including the asymmetric mode, v_3, in the variational calculation on the computed vibrational energies of the two symmetric modes (v_1 and v_2) seems small. The present PEF for the ground state of F_2O may be considered to be of a slightly higher quality than those reported by Breidung et al. (1999), as the basis set used here (aug-cc-pVQZ), which includes diffuse valence and polarization functions, is of higher quality than those (cc-pVTZ and cc-pVQZ) used in the reference (Breidung et al., 1999).

Table 7.7. The calculated anharmonic potential energy functions (PEFs) (in units of Hartree $Å^{-m}$ rad^{-n} for m stretching and n bending coordinates) for the neutral ground state (X^1A_1) and cationic states (X^2B_1, $^2B_2$, $^2A_1$ and $^2A_2$) of F_2O.

C_{ij}[a]	X^1A_1[b]	X^2B_1[b]	A^2B_2[c]	B^2A_1[c]	C^2A_2[c]
20	0.5722	0.7628	0.5545	0.6165	0.4712
11	0.0630	0.1005	0.2042	0.1081	0.0436
02	0.1683	0.2000	0.1927	0.0996	0.1250
30	-0.9291	-1.3654	-0.8852	-1.0596	-0.7307
21	-0.2450	-0.3649	-0.5370	-0.2215	-0.1763
12	-0.4573	-0.5425	-0.7579	-0.2653	-0.3924
03	0.0405	0.0614	-0.1597	-0.0219	0.0191
40	0.8944	1.4570	0.7510	0.9484	0.5865
31	0.4298	0.5556	0.7623	0.2837	0.3495
22	0.5696	0.6467	0.8996	0.3399	0.5480
13	0.0328	0.0008	0.2398	0.1019	0.0670
04	0.1922	0.2293	0.2822	0.1012	0.1717
50	-0.7661	-1.2534			
05	0.2009	0.3029	1.0120	0.0455	0.1584
60	0.4288	0.6481			
06	0.1404	0.2155	1.1904	0.0474	0.1013
r_e	1.4056	1.3190	1.4437	1.3689	1.4698
θ_e	1.7975	1.8714	1.4345	2.0699	1.7099
α	0.0703	0.0706	0.1868	-0.1193	0.1047
V_{eqm}	-274.4461	-273.9632	-273.7956	-273.7732	-273.7648

[a] See text for the definition of coefficient C_{ij}.

[b] Using the CCSD(T)/aug-cc-pVQZ level of theory (see the text).

[c] Using the CCSD(T)/aug-cc-pVTZ level of theory (see the text).

Table 7.8. The observed and calculated vibrational terms (with respect to the ground vibrational state in cm^{-1}) of the X^1A_1 state of F_2O

v_1 v_2 v_3 [a]	Obs[b]	Calc[c]	Breidung et al[d]	Breidung et al[e]
0 1 0	460.56	464.1	461.7	465.1
0 2 0	916.04	924.7	928.1	925.9
1 0 0	928.07	943.2	943.9	937.6
1 1 0		1382.7	1388.5	1384.4
0 3 0		1406.8	1408.4	1403.1
0 4 0		1838.1	1846.6	1840.1
1 2 0		1864.7	1868.9	1859.5
2 0 0		1878.4	1880.2	1871.2
0 5 0		2291.4	2302.7	2294.5
1 3 0		2320.6	2327.5	2317.6
2 1 0		2342.4	2345.4	2337.6

[a] The vibrational quantum numbers v_1 v_2 and v_3 correspond to the symmetric stretching, bending and asymmetric stretching, respectively.

[b] Jones et al., 1951; Taubmann et al., 1986; Burger et al., 1987.

[c] This work; see text for details.

[d] From the "best" PEF of the reference (Breidung et al., 1999) with the asymmetric mode ignored in the basis set.

[e] From the "best" PEF of the reference (Breidung et al.,1999).

It should be noted that for the neutral ground state of F_2O there are significant mixings of harmonic basis functions of the stretching and bending modes in the computed anharmonic vibrational levels. This is expected, as the $2v_2$ and v_1 levels (for $v_2 = v_1$) have close vibrational energies ($2v_2 \approx v_1$) for almost all the electronic states considered. The labels given in Table 7.8 are based on the computed largest coefficients of the harmonic basis function in the respective anharmonic vibrational wavefunctions.

However, for highly excited vibrational levels, the mixings could become so strong that their labels cannot be unambiguously certain. Nevertheless, for all the cationic states considered here, mixing between the symmetric stretching and bending mode is negligible.

The computed fundamental frequencies obtained from the PEFs of this work are given in Table 7.4. In general, they are in closer agreement with available experimental values than the computed harmonic frequencies, as expected.

7.3.2. Spectral simulation: first PE band

The simulations of the first band in the He I PE spectrum of F_2O, employing the harmonic and anharmonic FCF methods with the IFCA procedures, are shown in Figures 2(b), 2(c) and 2(d) respectively, together with the experimental spectrum of Brundle et al. in Figure 2(a). This band is due to the $F_2O^+(X^2B_1) \leftarrow F_2O(X^1A_1)$ ionization and has the most clearly resolved vibrational structure mainly in the symmetric stretching progression. The structure in the bending progression is relatively weak. Thus, the observed vibrational structure provides sufficient information for the bond length of the ground cationic state to be extracted from comparison between the simulated and observed spectra via the IFCA procedure. The details of the comparison are given in the following subsections for the harmonic and anharmonic FCF simulations respectively.

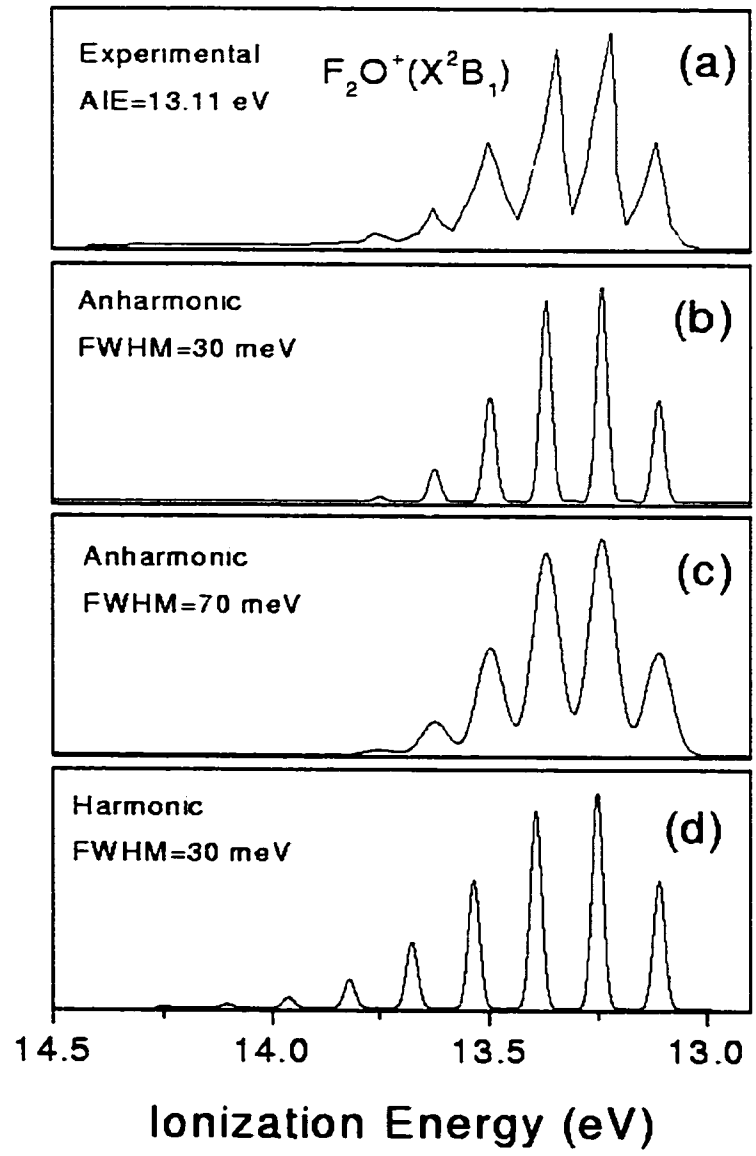

Figure 7.2. The first band of the F_2O photoelectron spectrum: (a) the experimental spectrum (Brundle et al., 1972); (b) and (c) the simulated spectrum obtained using anharmonic FCFs with the resolutions (FWHM) of 30 meV and 70 meV respectively; (d) the simulated spectrum using harmonic FCFs with the resolution of 30 meV. The IFCA geometries (see Table 7.3) which best match with experimental PE band have been used in the harmonic and anharmonic FCF calculations respectively (see the text for details).

7.3.2.1. Harmonic FCF simulation

The simulated first band [(Figure 7.2(d)] was obtained with the experimental AIE of 13.11 eV and the experimental geometry of the X^1A_1 state (Pierce et al., 1963; Morino and Saito, 1966). The QCISD/cc-pVTZ harmonic force constants were used for the neutral and the cationic ground states in the FCF calculations. The IFCA procedure has been applied and the geometry, R(F-O) = 1.3303 ± 0.001 Å and ∠F-O-F = 107.3 ± 0.05 ° for the cationic ground state, is found to give the "best" match between the simulated and observed spectra. The large uncertainty associated with the estimated value of the bond length is mainly due to the poor match between the IFCA harmonic simulated and the observed first PE bands. It can be seen from Figures 7.2(a) and 7.2(d) that, the match is not very perfect. Despite various attempts, it was not possible to match the component relative intensities across the whole stretching progression within the whole PE band. The above IFCA geometry was obtained mainly by matching the relative intensities of the most intense components in the low IE region, and assuming that the relative intensities of bending mode components are negligibly small. Since the bending progression is very weak in the observed PE spectrum, the IFCA bond angle used above is obtained based the change in calculated bond angle at the CCSD(T)/aug-cc-pVQZ level (see Table 7.3) and its uncertainty is also given by comparing the corresponding calculated value of the neutral state X^1A_1 with the experimental value (see Table 7.3). With this IFCA geometry, the simulated components involving higher stretching levels are significantly stronger than the observed ones. Comparison between the harmonic IFCA simulated and experimental spectra suggests that the harmonic oscillator model is probably inadequate for this system. Since the stretching progression

is dominant in the first PE band, while the bending progression completely disappeared in the observed spectrum [Figure 7.2(a)], the IFCA procedure has been performed completely by varying the bond length of the cationic state X^2B_1 systematically, with the bond angle change of X^2B_1 upon ionization fixed at the value predicted by the CCSD(T)/aug-cc-pVQZ calculation. From the comparison between the anharmonic FC simulation and the observed first band (see next subsection), it seems apparent that the symmetric stretching is significantly anharmonic in the ground state of F_2O^+. Therefore, the simulated spectrum using the harmonic FCFs failed to reproduce the overall intensity pattern of the first observed band in He I PE spectrum.

7.3.2.2. Anharmonic FCF simulation

Comparing Figures 7.2(a) and 7.2(b), it is apparent that the simulated first PE band, with the anharmonic FCF calculations in the IFCA procedure, has very satisfactorily produced the observed spectrum. The anharmonic IFCA procedure as described in the previous section has been carried out to obtain the experimentally derived IFCA geometry for the ground state of F_2O^+. This experimentally derived geometry of the X^2B_1 state thus obtained in the anharmonic IFCA procedure, for the first time, is R(F-O) = 1.3219 ± 0.0001 Å, ∠F-O-F = 107.3 ± 0.05 °. Also, the given uncertainty for the calculated bond angle of the X^2B_1 state is based on the deviation between the CCSD(T)/aug-cc-pVQZ calculated and experimental values in the neutral state X^1A_1, as pointed out in above section. The adjusted quantity in the anharmonic IFCA procedure is the bond length in the cationic state X^2B_1, with the geometry of neutral state X^1A_1 fixed at the experimental value and the change in bond angle predicted by the CCSD(T)/aug-cc-pVQZ calculations. In Figures 7.2(b) and 7.2(c), the

experimental AIE of 13.11 eV (Brundle et al., 1972) and the FWHM of 30 meV and 70 meV have been used respectively. It should be noted that the simulated spectrum with a FWHM of 70 meV [Figure 7.2(c)] is more satisfactory to reproduce the observed base line [Figure 7.1(a)] than that with a higher resolution of 30 meV [Figure 7.2(b)]. Therefore, the quoted FWHM of 30 meV in the experimental PE spectrum (Brundle et al., 1972) is very doubtful and a FWHM of 70 meV or 90 meV might be more true in the observed PE spectrum. So a FWHM of 90 meV will be used in the simulations of the overlapping second and third PE bands (see next subsection), except their extended PE bands will still use a higher FWHM of 30 meV for assignments in their vibrational structures. It is really of interest to find that the anharmonic IFCA geometry is very close to the harmonic IFCA one for the cationic ground state X^2B_1 (see the Table 7.3).

7.3.3. Spectral simulation: the second and third PE bands (ionizations to the $^2B_2$, $^2A_1$ and $^2A_2$ states)

Based on the ab initio AIEs (see Table 7.5) of the lowest three excited states at the high levels of theory used in this work, the second and third PE bands of F_2O consist of ionizations to three electronic states of F_2O^+, namely the $^2B_2$, $^2A_1$ and $^2A_2$ states. In order to confirm or revise the assignments arisen from the previous investigations (see the discussions in Background), particularly, the relative energy ordering of these three cationic states, the ionizations to these three cationic states were simulated, employing the harmonic and anharmonic methods with the PEFs obtained in this work. The simulated spectra were shown in Figures 7.3-7.9.

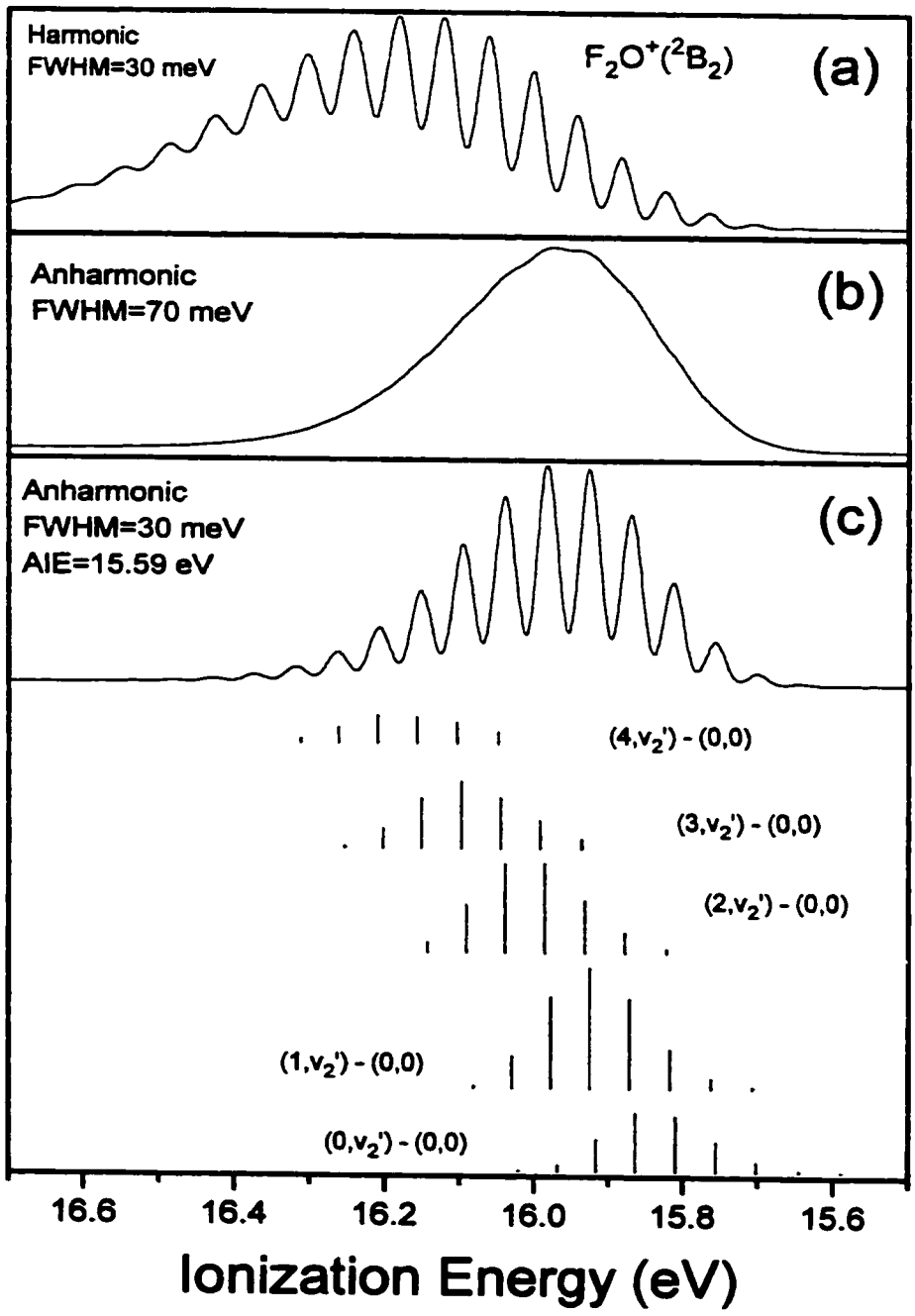

Figure 7.3. The simulated photoelectron spectra for the ionization from ground state of F_2O to the $^2B_2$ state of F_2O^+: (a) harmonic simulation with the CCSD(T)/aug-cc-pVQZ cationic geometry and the experimental neutral geometry; (b) anharmonic simulation with the same geometries as (a); (c) as (b) but with a higher resolution of 30 meV.

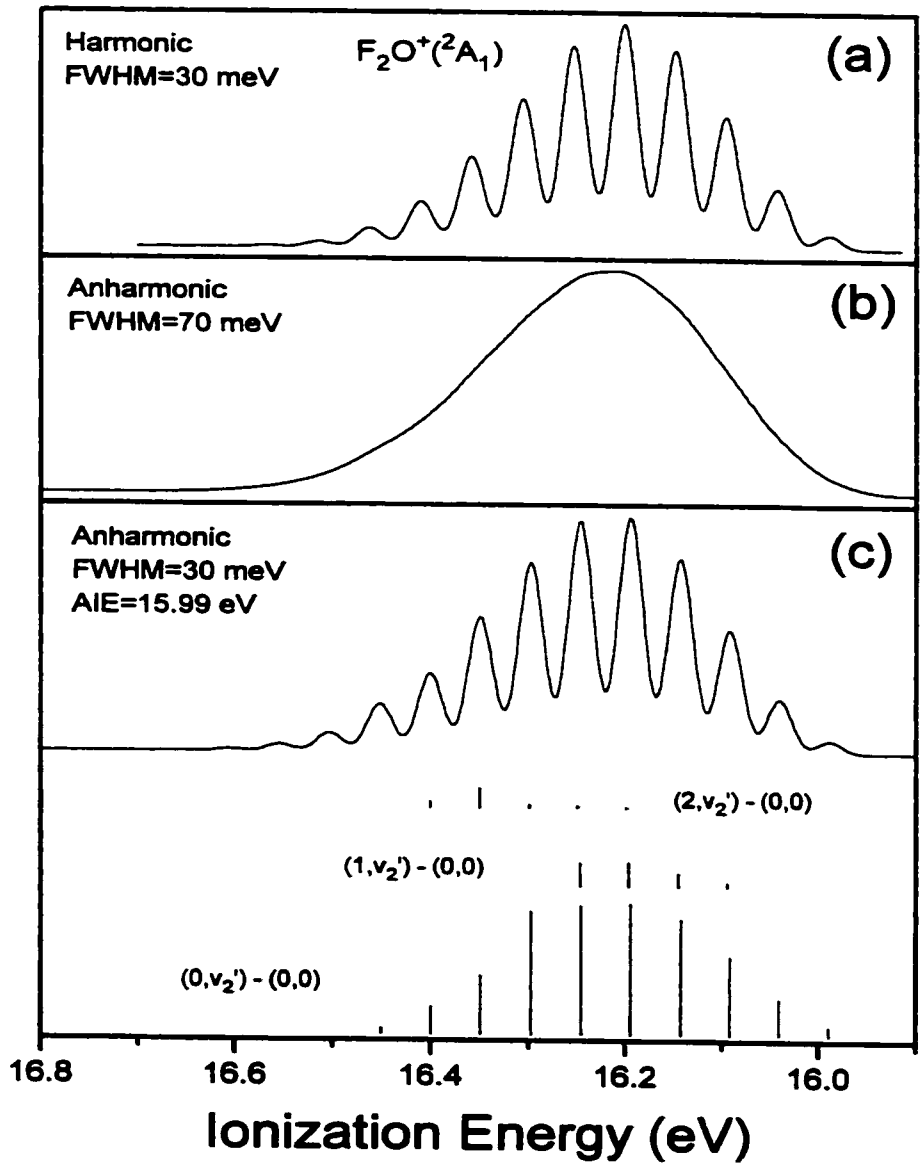

Figure 7.4. The simulated photoelectron spectra for the ionization from ground state of F_2O to the $^2A_1$ state of F_2O^+: (a) harmonic simulation with the CCSD(T)/aug-cc-pVQZ cationic geometry and the experimental neutral geometry; (b) anharmonic simulation with the same geometries as (a); (c) as (b) but with a higher resolution of 30 meV.

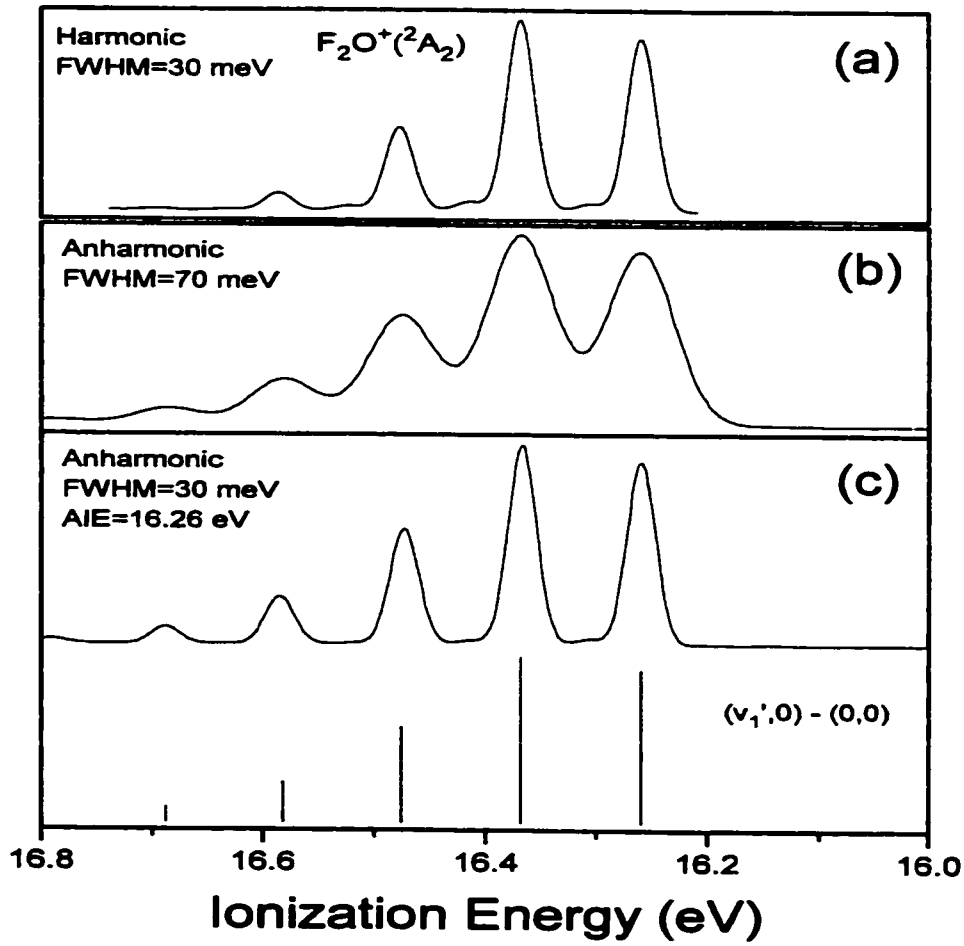

Figure 7.5. The simulated photoelectron spectra for the ionization from ground state of F_2O to the $^2A_2$ state of F_2O^+: (a) harmonic simulation with the CCSD(T)/aug-cc-pVQZ cationic geometry and the experimental neutral geometry; (b) anharmonic simulation with the same geometries as (a); (c) as (b) but with a higher resolution of 30 meV.

From Figures 7.3-7.5, it can be seen that the bending progressions are dominated in both the ionizations to $^2B_2$ and $^2A_1$, while the dominant progression of ionization to $^2A_2$ is the stretching mode. Comparing the harmonic and anharmonic simulations of these ionizations, both two simulations are almost the same in reproducing the vibrational envelopes, except that for the ionization to $^2B_2$ state, the anharmonic simulation gives a shorter vibrational progression than the harmonic simulation. As

anharmonic simulation of the first band agrees with the observation much better than the harmonic one, therefore, in the following investigations, only the anharmonic simulations would be considered, as they should be more reliable. It is also noted that because the first two peaks are too weak to appear in the $^2B_2$ band (see Figure 7.3), the first peak appeared in this band is actually due to the (0,2) ← (0,0) vibrational component, rather than the (0,0) ← (0,0) adiabatic position. So the measured AIE value (15.74 eV) of the second band in the experimental He I PE spectrum (Brundle et al., 1972), which is actually the AIE value of the $^2B_2$ band (see the discussions in Background and ab initio results in Table 7.5), should be more small. In this connection, the RCCSD(T)/cc-pVTZ AIE value of 15.72 eV (see Table 7.5) might be more reliable. The simulated vibrational shapes of ionizations to the $^2B_2$ and $^2A_1$ states are very similar, while the ionization to $^2A_2$ has a very sharp vibrational shape, which just confirms the non-bonding property of the $^2A_2$ molecular orbital and the alternative assignment of Brundle et al. (1972) that the $^2A_2$ ionization should contribute to the very sharp third band at 16.44 eV in the experimental PE spectrum (Brundle et al., 1972).

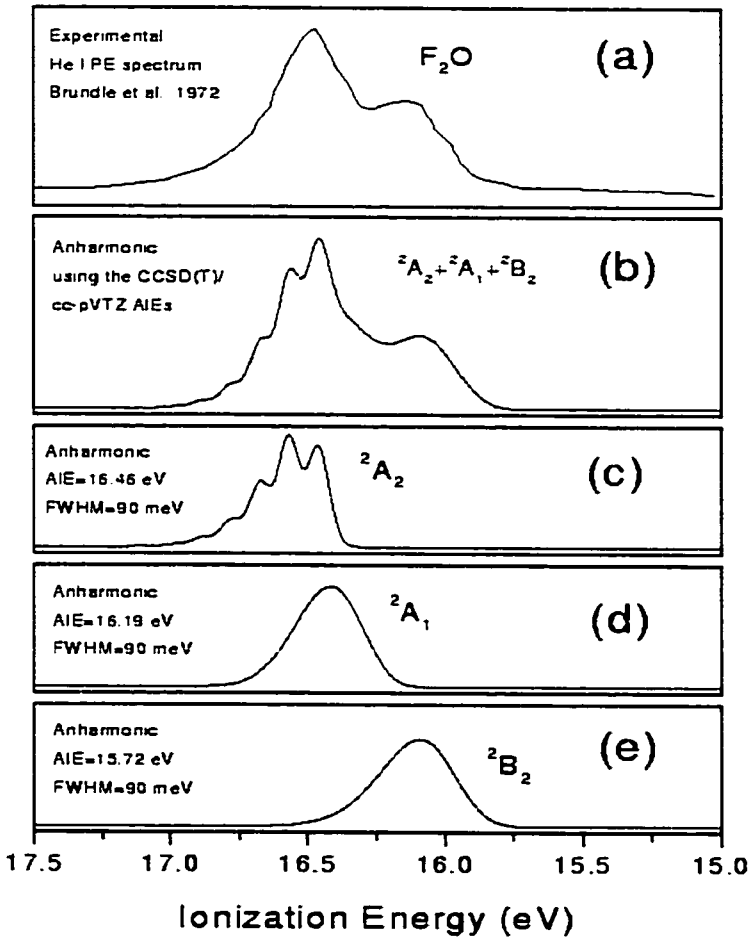

Figure 7.6. The synthesized second and third bands of the F_2O photoelectron spectrum and the experimental spectrum (Brundle et al., 1972): (a) the experimental spectrum; (b) the simulated second and third bands by synthesizing up the $^2B_2$ band as (e), the $^2A_1$ band as (d), and the $^2A_2$ band as (c) with equal relative photoionization cross sections (see the text). The anharmonic FCFs with the CCSD(T)/aug-cc-pVQZ geometries (see Table 7.3) and the RCCSD(T)/cc-pVTZ AIEs (see Table 7.5) were used in the simulations.

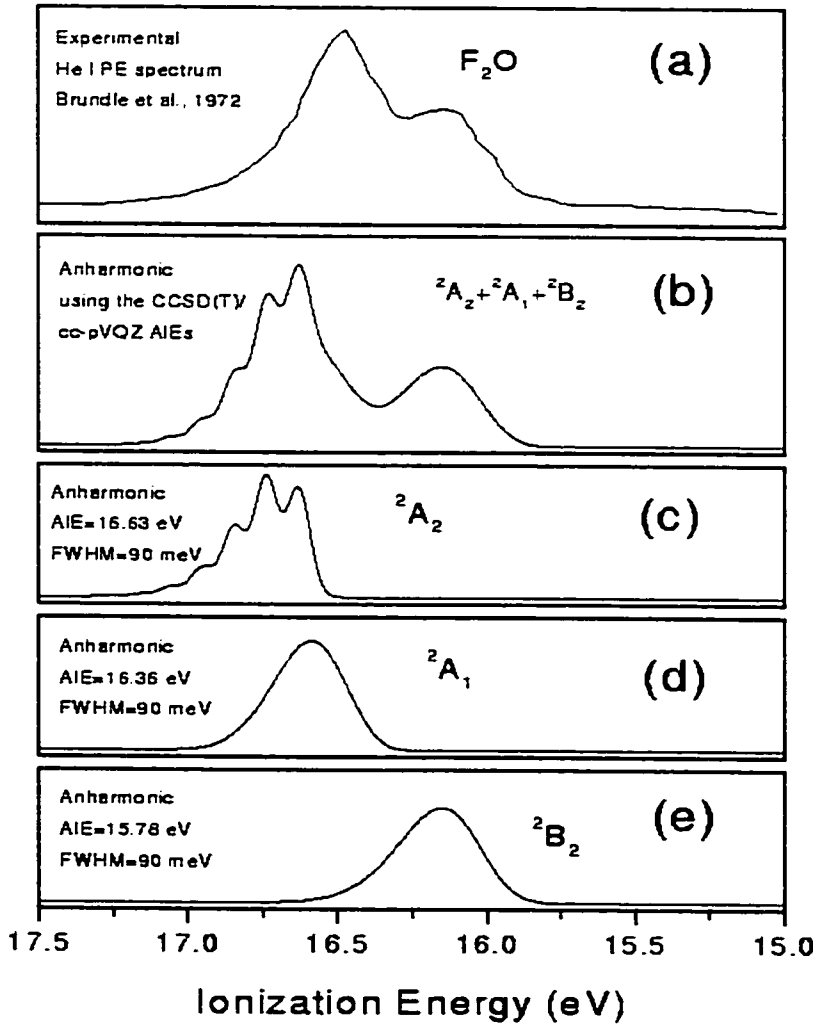

Figure 7.7. The same as Figure 7.6 but with the RCCSD(T)/cc-pVQZ AIEs (see Table 7.5).

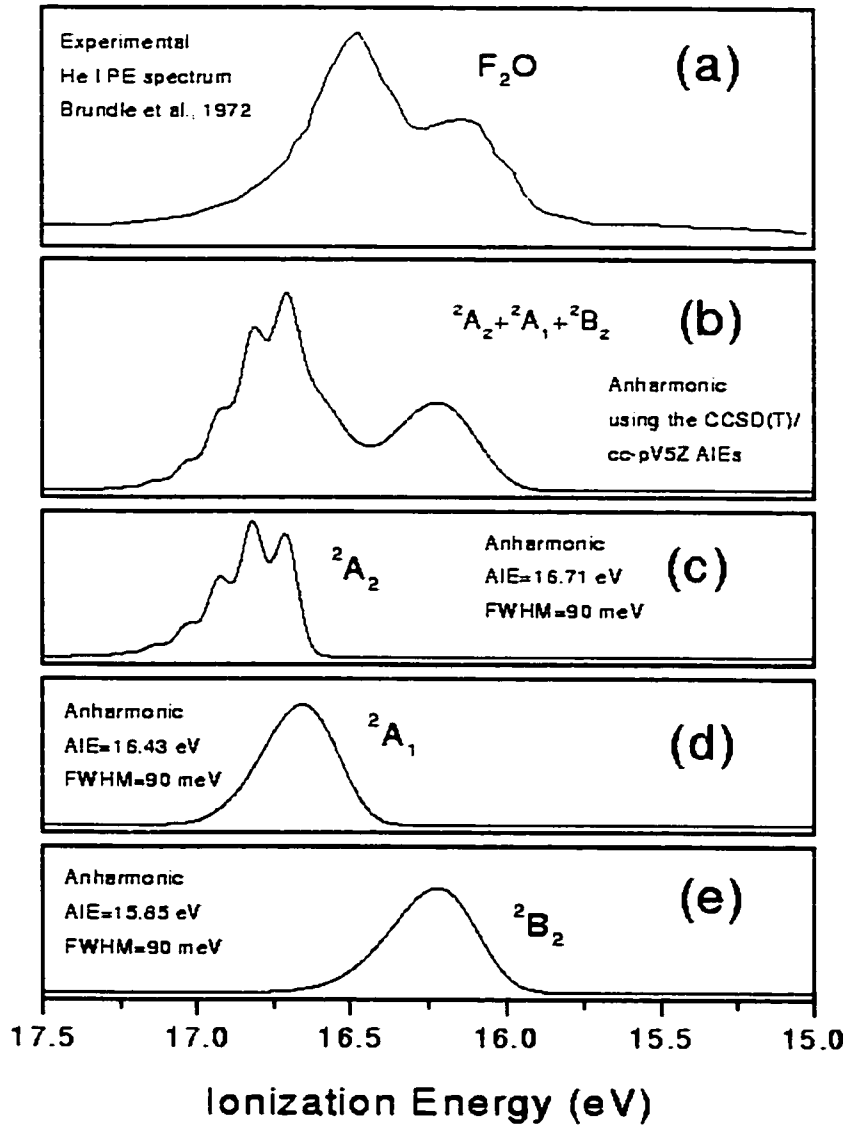

Figure 7.8. The same as Figure 7.7 but with the RCCSD(T)/cc-pV5Z//RCCSD(T)/cc-pVQZ AIEs (see Table 7.5).

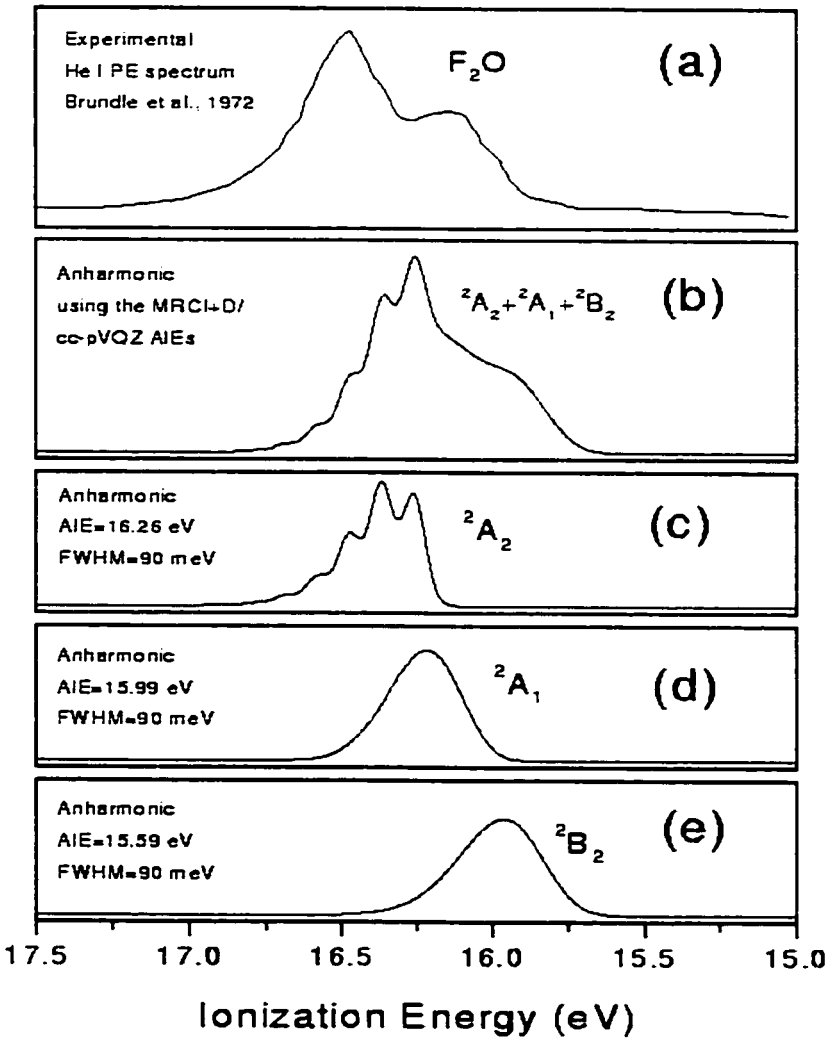

Figure 7.9. The same as Figure 7.8 but with the MRCI+D/cc-pVQZ//RCCSD(T)/cc-pVQZ AIEs (see Table 7.5).

Regarding the comparison between the simulated and observed spectra, ionization to all three states, namely the $^2B_2$, $^2A_1$ and $^2A_2$ states, have to be considered together, as they overlap to form the observed second and third PE bands. Since the

overlapping second and third bands in the observed PE spectrum (Brundle et al., 1972) have a very low resolution without any vibrational structure except the two obvious VIE peaks respectively at 16.10 eV and 16.44 eV, the IFCA procedure was not considered in the simulations. Based on the ab initio AIE values of the $^2B_2$, $^2A_1$ and $^2A_2$ states respectively at the four different high levels of calculation (see Table 7.5) and the CCSD(T)/aug-cc-pVQZ geometries (see Table 7.3), some attempts with anharmonic FCF calculations were performed in order to simulate the experimentally overlapping second and third PE bands. In Figures 7.6-7.9, the whole second and third bands of the F_2O PE spectrum were synthesized by a equal weighted sum of the three constituent simulated spectra [see Figures (c)-(e) of Figures 7.6-7.9]. These simulated spectra (Figures 7.6-7.9) were generated by simple addition of the three simulated spectra (i.e., the $^2B_2$, $^2A_1$ and $^2A_2$ bands), assuming the same photoionization cross section for each ionization, with the calculated AIEs respectively at four different high levels of calculation (see Table 7.5). Comparing the synthesized spectra [Figures (b) of Figures 7.6-7.9] with the different calculated AIEs, it is clear that the agreement between the spectrum synthesized in this way with the RCCSD(T)/cc-pVTZ AIEs and the experimental spectrum is reasonably good, particularly for the observed two VIE positions. With the ab initio geometries and AIEs, the good agreement of the simulated spectrum [Figure 7.6(b)] and the experimental spectrum [see Figure 7.6(a)] suggests that the RCCSD(T)/cc-pVTZ AIEs are reasonably reliable and the energy ordering of the lowest four ionic states (X^2B_1, $^2B_2$, $^2A_1$ and $^2A_2$) is certain. Attempts were also performed to smooth the third band in the simulated spectrum [Figure 7.6(b)] using IFCA procedure to $^2A_2$ band, but it was found that the third band would become very sharp and the relative intensity ratio of these two bands would be far from the observed value. Therefore, more works will be required in order to improve the simulated

spectrum and extract reliable experimentally derived geometries of the $^2B_2$, $^2A_1$ and $^2A_2$ states using IFCA procedure, if a higher resolution He I PE spectrum can be obtained experimentally.

7.4. Concluding Remarks

Geometry optimization and frequency calculations were carried out for the X^1A_1 state of F_2O and the X^2B_1, $^2B_2$, $^2A_1$ and $^2A_2$ states of F_2O^+. The order and positions of the lowest four cationic states of F_2O^+ have been studied by near state-of-the-art ab initio calculations. Anharmonic PEFs for the ground neutral state $\tilde{X}\,^1A_1$ of F_2O and the four lowest cationic states have been obtained at the RCCSD(T)/aug-cc-pVQZ or RCCSD(T)/aug-cc-pVTZ level of theory. Spectral simulations based on both the harmonic and anharmonic oscillator models were carried out to assist assignment of the observed PE spectrum. The order of the first four cationic state of F_2O^+ has been firmly established as X^2B_1, $^2B_2$, $^2A_1$ and $^2A_2$, which is the same as that of the valence isoelectronic Cl_2O^+.

For the first band, it has a well-resolved vibrational structure. The multi-dimensional harmonic oscillator model and the anharmonic model with the anharmonic potential energy functions for the ground neutral state and the ground cationic state obtained in this study, have been used in the IFCA procedure to obtain the reliable experimentally derived geometry of $F_2O^+(X^2B_1)$. The harmonic FCF simulation can not give an overall match with the observed first band even after applying the IFCA procedure. Comparing the simulated and observed first PE band, it is apparent that the anharmonic FCF model is superior to the harmonic model to this system and the anharmonic effect is important even at low vibrational levels for the symmetry

stretching mode of $F_2O^+(X^2B_1)$ state. Also, it is clear that the agreement between the simulated and observed first PE band by employing the anharmonic IFCA procedure is very perfect. The first experimentally derived geometry, for the cationic ground state X^2B_1 obtained in the anharmonic IFCA procedure is R(F-O) = 1.3219 ± 0.0001 Å and <F-O-F = 107.3 ± 0.05° and this should be the most reliable one to date. Although the agreement of the harmonic FC simulated spectrum with the observed spectrum is not as good as that of the anharmonic one, the IFCA geometrical parameters of the X^2B_1 state of F_2O^+ obtained with the harmonic FC calculations are very close to those with the anharmonic calculations. In this connection and in view of the different computational resources required for the harmonic and anharmonic FC calculations, the harmonic FCF method can be still considered to be very useful in obtaining experimentally derived geometrical parameters. It should also be mentioned that the ab initio calculations, required for the harmonic and anharmonic FC calculations, are very different. For the latter, multi-dimensional PEFs, obtained from energy surface scans, are required. These scans are expected to be considerably more expensive than geometry optimization and harmonic frequency calculations at the minimum-energy geometry, which are required for the harmonic FC simulation. Summarizing, there are different theoretical and practical advantages and disadvantages associating with the harmonic and anharmonic FC methods. The method chosen will depend on the problem under consideration, the quality of the experimental information and the available computational resources.

The second and third PE bands are heavily overlapping with each other in the observed spectrum. However the VIE positions of these two bands and their relative envelope are clear. Consequently, it is probable to perform a spectral simulation with a high level ab initio calculation to determine the AIE positions and the energy ordering of the related three cationic states in the overlapping bands. It is clear that the simulated

second and third bands in the He I PE spectrum with high level ab initio calculations have firmly clarified the discrepancies on the assignment of the lowest cationic states in the previous investigations (see discussions in Background). The spectral simulations and ab initio calculations reported here have confirmed that the energy ordering of the lowest four cationic states are X^2B_1, $^2B_2$, $^2A_1$ and $^2A_2$. Also, the spectral simulation in this work has revised the AIE position of the $^2B_2$ band (or the second band) in the experimental He I PE spectrum (Brundle et al., 1972) and given a more reliable AIE value (16.72 eV) for this PE band.

CITED REFERENCES

Abu-Awwad, F. and Politzer, P. Journal of Computational Chemistry, Vol. 21, pp. 227 (2000).

Alcami, M. and Cooper, J.L. Journal of Chemical Physics, Vol. 108, pp. 9414 (1998).

Alcamí, M., Mó, O., Yáñez, M. and Cooper, I.L. Journal of Physical Chemistry A, Vol. 103, pp. 2793 (1999).

Allen, W.D. and Csaszar, A.G. Journal of Chemical Physics, Vol. 98, pp. 2983 (1993).

Ansbacher, F.Z. Naturforsch, Vol. 14a, pp. 889 (1959).

Aoki, K., Hoshina, K.N. and Shibuya, K. Journal of Chemical Physics, Vol. 105, pp. 2228 (1996).

Arnold, D.W., Bradforth, S.E., Kim, E.H. and Neumark, D.M. Journal of Chemical Physics, Vol. 102, pp. 3493 (1995).

Baltzer, P., Chau, F.T., Eland, J.H.D., Karlsson, L., Lundqvist, M., Rostas, J., Tam, K.Y., Veenhuizen, H. and Wannberg, B. Journal of Chemical Physics, Vol. 104, pp. 8922 (1996).

Bangert, S., Kle ·ns, S., Little, J., Moler, C. "MATLAB, High-Performance Numeric Computation and V. · ·alization Software", the MATH WORKS Incorporation, 1993.

Barker, J. R. (World Scientific, Singapore, 1995).

Bernholdt, D.E. and Harrison, R.J. Journal of Chemical Physics, Vol. 109, pp. 1593 (1998).

Born, M. and Oppenheimer, J.R. Annual Physik, Vol. 84, pp. 457 (1927).

Botschwina, P. in "Ion and Cluster Ion Spectroscopy and Structure", edited by Maier, J.P. Elsevier, Amsterdam, 1989.

Botschwina, P., Schulz, B., Horn, M. and Matuschewski, M. Chemical Physics, Vol. 190, pp. 345 (1995).

Botschwina, P., Seeger, S., Mladenovic, M., Schulz, B., Horn, M., Schmatz, S., Jörg, F. and Oswald, R. International Reviews in Physical Chemistry, Vol. 14, pp. 169 (1995).

Botschwina, P., Heyl, A., Oswald, M. and Hirano, T. Spectrochimica Acta Part A - Molecular and Biomolecular Spectroscopy, Vol. 53, pp. 1079 (1997).

Bowman, J.M. Accounts of Chemical Research, Vol. 19, pp. 202 (1986).

Bradforth, S.E., Arnold, D.W., Neumark, D.M. and Manolopoulos, D.E. Journal of Chemical Physics, Vol. 99, pp. 6345 (1993).

Breidung, J., Thiel, W., Gauss, J. and Stanton, J.F. Journal of Chemical Physics, Vol. 110, pp. 3687 (1999).

Bru, L., Rodriguez P. and Cubero M. Journal of Chemical Physics, Vol. 20, pp. 1069 (1952).

Brundle, C.R., Robin, M.B., Kuebler, N.A. and Basch, H. Journal of American Chemical Society, Vol. 94, pp. 1451 (1972).

Bunker, P.R. and Sears, T.J. Journal of Chemical Physics. Vol. 83, pp. 4860 (1985).

Burger, H. and Schippel, G. Journal of Molecular Spectroscopy, Vol. 121, pp. 238 (1987).

Butcher, V., Costa, M.L., Dyke, J.M., Ellis, A.R. and Morris, A. Chemical Physics, Vol. 115, pp. 261 (1987).

Carney, G.D. and Porter, R.N. Journal of Chemical Physics, Vol. 65, pp. 3547 (1976).

Carter, S. and Handy, N.C. Molecular Physics, Vol. 57, pp. 175 (1986).

Carter, S. and Handy, N.C. Computational Physics Review, Vol. 5, pp. 115 (1986).

Carter, S. and Handy, N.C. Journal of Chemical Physics, Vol. 87, pp. 4294 (1987).

Cederbaum, L.S. and Domcke, W. Advance Chemical Physics, Vol. 36, pp. 205 (1977).

Chau, F.T. Journal of Molecular Structure, Vol. 94, pp. 155 (1983).

Chau, F.T. Journal of Molecular Spectroscopy, Vol. 103, pp. 66 (1984).

Chau, F.T. Spectrochimica Acta, Vol. 40A, pp. 629 (1984) and references therein.

Chau, F.T. Journal of Molecular Structure (Theochem), Vol. 119, pp. 281 (1985) and references therein.

Chau, F.T. and McDowell, C.A. Spectroscopy Acta, Vol. 46A, pp. 723 (1990) and references therein.

Chau, F.T., Dyke, J.M., Lee, E.P.F., Ridha, A. and Wang, D.C. Chemical Physics, Vol. 224, pp. 157 (1997).

Chau, F.T., Lee, E.P.F. and Wang, D.C. Journal of Physical Chemistry A, Vol. 101, pp. 1603 (1997).

Chau, F.T., Dyke, J.M., Lee, E.P.F. and Wang, D.C. Journal of Electron Spectroscopy and Related Phenomena, Vol. 97, pp. 33 (1998).

Chau, F.T., Dyke, J.M., Lee, E.P.F. and Wang, D.C. Journal of Electron Spectroscopy and Related Phenomena, Vol. 97, pp. 33 (1998).

Chau, F.T. To be published (2001).

Chen, K.M. and Pei, C.C. Chemical Physics Letters, Vol. 165, pp. 523 (1990).

Chen, P. in "Unimolecular and Biomolecular Ion-Molecule Reaction Dynamics", edited by Ng, C.Y., Baer, T. and Powis I. Wiley, Chichester, 1994.

Chong, D.P., Herring, F.G. and McWilliams, D. Journal of Chemical Physics, Vol. 61, pp. 958 (1974).

Coon, J.B., DeWames, R.E. and Loyd, C.M. Journal of Molecular Spectroscopy, Vol. 8, pp. 285 (1962).

Cornford, A.B., Frost, D.C., Herring, F.G. and McDowell, C.A. Journal of Chemical Physics, Vol. 55, pp. 2820 (1971).

Cornford, A.B., Frost, D. C., Herring, F.G. and McDowell, C.A. Faraday Discussions, Vol. 54, pp. 56 (1972).

Curtiss, L.A., Raghavachari, K., Trucks, G.W. and Pople, J.A. Journal of Chemical Physics Vol. 94, pp. 7221 (1991).

Curtiss, L.A., Raghavachari, K. and Pople, J.A. Journal of Chemical Physics, Vol. 98, pp. 1293 (1993).

Curtiss, L.A., Redfern, P.C., Smith, B.J., Radom, L. Journal of Chemical Physics, Vol. 104, pp. 5148 (1996).

Curtiss, L.A., Raghavachari, K., Redfern, P.C., Rassolov, V. and Pople, J.A. Journal of Chemical Physics, Vol. 109, pp. 7764 (1998).

Dennis, J.E., Gay, Jr.D.M. and Welsh, R.E. ACM Transactions on Mathematical Software, Vol. 7, pp. 348, ibid, 369 (1981).

Doktorov, E.V., Malkin, I.A. and Man'ko, V.I. Journal of Molecular Spectrometer, Vol. 56, pp. 1 (1975).

Dressler, S. and Thiel, W. Chemical Physics Letters, Vol. 273, pp. 71 (1997).

Du, K. Chen, X. and Setser, D.W. Chemical Physics Letters, Vol. 181, pp. 344 (1991).

Dunitz, J. D. and Jedberg, K. Journal of Chemical Society, Vol. 72, pp. 3108 (1950).

Dunlavey, S.J., Dyke, J.M. and Morris, A. Chemical Physics Letters, Vol. 53, pp. 382 (1978).

Dunning, T.H.Jr. Journal of Chemical Physics, Vol. 90, pp. 1007 (1989).

Duschinsky, F. Acta Physicochim URSS, Vol. 7, pp. 551 (1937).

Faulkner, T.R. and Richardson, F.S. Journal of Chemical Physics, Vol. 70, pp. 1201 (1979).

Flesch, R., Rühl, E., Hottmann, K. and Baumgärtel, H. Journal of Physical Chemistry, Vol. 97, pp. 837 (1993).

Francisco, J.S. Chemical Physics Letters, Vol. 288, pp. 307 (1998).

Francisco, J.S., Parithiban, S. and Lee, T.J. Journal of Chemical Physics, Vol. 109, pp. 10818 (1998).

Frisch, M.J., Trucks, G.W., Schlegel, H.B., Gill, P.M.W., Johnson, B.G., Robb, M.A., Cheeseman, J.R., Keith, T.A., Petersson, G.A., Montgomery, J.A., Raghavachari, K., Al-Laham, M.A., Zakrzewski, V.G., Ortiz, J.V., Foresman, J.B., Cioslowski, J., Stefanov, B.B., Nanayakkara, A., Challacombe, M., Peng, C.Y., Ayala, P.Y., Chen, W., Wong, M.W., Andres, J.L., Replogle, E.S., Gomperts, R., Martin, R.L., Fox, D.J., Binkley, J.S., Defrees, D.J., Baker, J., Stewart, J.P., Head-Gordon, M., Gonzalez, C. and Pople, J.A. "Gaussian 98", Gaussian Inc., Pittsburgh PA, (1998).

Fukushima, M. Chemical Physics Letters, Vol. 283, pp. 337 (1998).

Gerasimov, I., Yang, X. and Dagdigian, P.J. Journal of Chemical Physics, Vol. 110, pp. 220 (1999).

Gosavi, R.K. and Strausz, O.P. Chemical Physics Letters, Vol. 123, pp. 65 (1996).

Göthe, M.C., Chau, F.T., Baltzer, P., Suensson, S., Wannberg, B. and Karlsson, L. Chemical Physics Letters, Vol. 174, pp. 109 (1990).

Ha, T.K., Nguyen, M.T., Kerins, M.C. and Fitzpatrick, J. Chemical Physics, Vol. 103, pp. 243 (1986).

Hargittai, I., Schultz, G., Tremmel, J., Kagramov, N.O., Maltsev, A.K. and Nefedov, O.M. Journal of American Chemical Society, Vol. 105, pp. 2895 (1983).

Heilbronner, G., Muszkat K.A. and Schaublin J. Helv Chimica Acta, Vol. 54, pp. 58 (1971).

Herberich, G. E., Jackson, R.H., Millen, D.J. Journal of Chemical Societry A, pp. 336 (1966).

Herzberg, G. "Electronic Spectra and Electronic Structure of Polyatomic Molecules", van Nostran Reinhold, New York, (1966).

Ho, J., Ervin, K.M. and Lineberger, W.C. Journal of Chemical Physics, Vol. 93, pp. 6987 (1990).

Hollas, J.M. and Sutherley, T.A. Molecular Physics Vol. 22, pp. 213 (1971).

Horn, M., Oswald, M., Oswald, R. and Botschwina, P. Ber. Bunsenges Physical Chemistry, Vol. 99, pp. 323 (1995).

Horn, M., Seeger, S., Oswald, R. and Botschwina, P. Z. Physics D, Vol. 36, pp. 293 (1996).

Hrusak, J. Schröder, D. and Iwata, S. Journal of Chemical Physics, Vol. 106, pp. 7541 (1997).

Hu, C.H., Chong, D.P., and Casida, M.E. Journal of Electron Spectroscopy and Related Phenomena, Vol. 85, pp. 39 (1997).

Jensen, P. Journal of Molecular Spectroscopy, Vol. 128, pp. 478 (1988).

Jensen, P. Journal of Chemical Society Faraday Transaction II, Vol. 84, pp. 1315 (1988).

Jensen, P. Journal of Molecular Spectroscopy, Vol. 133, pp. 438 (1989).

Jones, E. A., Kirby-Smith, J.S., Woltz, P.J.H. and Nielsen, A.H. Journal of Chemical Physics, Vol. 19, pp. 337 (1951).

Kafafi, S.A. and El-Gharkawy, E.-S. R.H. Journal of Physical Chemistry, Vol. 102, pp. 3202 (1998).

Kafafi, S.A. Journal of Physical Chemistry, Vol. 102, pp. 10404 (1998).

Karolczak, J. and Clouthier, D.J. Chemical Physics Letters, Vol. 201, pp. 409 (1993).

Kieninger, M., Segovia, M. and Ventura, O.N. Chemical Physics Letters, Vol. 287, pp. 597 (1998).

Kolm, J., Schrems, O. and Beichart, P. Journal of Physical Chemistry A, Vol. 102, pp. 1083 (1998).

Kupka, H. and Cribb, P.H. Journal of Chemical physics, Vol. 85, pp. 1303 (1986).

Langhoff, S.R. and Chong, D.P. Chemical Physics, Vol. 55, pp. 355 (1981).

Langhoff, S.R. and Chong, D.P. Chemical Physics Letters, Vol. 86, pp. 487 (1982).

Lee, E.P.F., Wang, D.C. and Chau, F.T. Journal of Physical Chemistry, Vol. 100, pp. 19795 (1996).

Lee, T.J. Journal of Physical Chemistry, Vol. 99, pp. 15074 (1995).

Lee, T.J., Rice, J.E. and Dateo, C.E. Molecular Physics, Vol. 89, pp. 1359 (1996).

Li, Z. Journal of Physical Chemistry A, Vol. 103, pp. 1206 (1999).

Luke, B.T. Theochem-Journal of Molecular Structure, Vol. 332, pp. 283 (1995).

Ma, B., Yamaguchi, Y. and Schaefer, H.F. Molecular Physics, Vol. 86, pp. 1331 (1995).

Malmqvist, P.-A. and Forsberg, N. Chemical Physics, Vol. 228, pp. 227 (1998).

Manneback, C. Physica, Vol. 17, pp. 1001 (1951).

Mass, G., Hauge, R.H. and Margrave, J.L. Chemistry, Vol. 392, pp. 295 (1972).

Mayer, M. Cederbaum, L.S. and Köppel, H. Journal of Chemical Physics, Vo. 100, pp. 89 (1994).

McIntosh, D.F., Peterson, M.R. and O'Leary, T.J. "QCMP012 program", QCPE, University of Indiana, Bloomington, (1977).

McIntosh, D.F. and Peterson, M.R. "Program BMAT (QCMP067)", QCPE, University of Indiana, Bloomington, (1992).

McIntosh, D.F. and Peterson, M.R., "Program UMAT (QCMP067)", QCPE, University of Indiana, Bloomington, (1992).

Mebel, A.M., Chen, Y.T. and Lin, S.H. Journal of Chemical Physics, Vol. 105, pp. 9007 (1996).

Mejier, G., Henze, J. Meerts, W.L. and Ter Meulen, J.J. Journal of Molecular Spectroscopy, Vol. 138, pp. 251 (1989).

Microsoft, "Fortran Powerstation Version 1.0", (1993).

Miller, C.E., Nickolaisen, S.L., Francisco, J.S. and Sander, S.P. Journal of Chemical Physics, Vol. 107, pp. 2300 (1997).

Milligan, D.E. and Jacox, M.E. Journal of Chemical Physics, Vol. 49, pp. 1938 (1968).

Monks, P.S., Stief, L.J., Krauss, M., Kuo, S.C. and Klemm, R.B. Chemical Physics Letters, Vol. 211, pp. 416 (1993).

Morino, Y. and Saito, S. Journal of Molecular Spectroscopy, Vol. 19, pp. 435 (1966).

Morse, P.M. Physical Review, Vol. 34, pp. 57 (1929).

Motte-Tollet, F., Delwiche, J., Heinesch, J., Hubin-franskin, M.-J., Gingell, J.M., Jones, N.C., Mason, N.J. and Marston, G. Chemical Physics Letters, Vol. 284, pp. 452 (1998).

Muller, H.S.P., Miller, C.E. and Cohen, E.A. Journal of Chemical Physics, Vol. 107, pp. 8292 (1997).

Muller, H.S.P., Sorenson, G.O., Birk, M. and Friedl, R.R. Journal of Molecular Spectroscopy, Vol. 186, pp. 177 (1997).

Muller, T., Vaccaro, P.H., Perez-Bernal, J. and Iachello, F. Journal of Chemical Physics, Vol. 111, pp. 5038 (1999).

Nakata, M., Sugic, M., Takeo, H., Matsumura, C., Fukuyama, T. and Kuchitsu, K. Journal of Molecular Spectroscopy, Vol. 86, pp. 241 (1981).

Negri, F. and Zgierski, M.Z. Journal of Chemical Physics, Vol. 107, pp. 4827 (1997).

Nelson, C.M., Moore, T.A., Okumura, M. and Minton, T.K. Journal of Chemical Physics, Vol. 100, pp. 8055 (1994).

Nickolaisen, S.L., Miller, C.E., Sander, S.P., Hand, M.R., Williams, I.H. and Francisco, J.S. Journal of Chemical Physics, Vol. 104, pp. 2857 (1996).

Niessen, W.V. Journal of Electron Spectroscopy and Related Phenomena, Vol. 17, pp. 197 (1979).

Orlandi, G., Zerbetto, F. and Zgierski, M.Z. Chemical Review, Vol. 91, pp. 867 (1991).

Özkan, I. Journal of Molecular Spectroscopy, Vol. 139, pp. 147 (1990).

Pak, Y. and Woods, R.C. Journal of Chemical Physics, Vol. 104, pp. 5547 (1996).

Peric, M., Engels, B. and Peyerimhoff, D. Journal of Molecular Spectroscopy, Vol. 171, pp. 494 (1995).

Peterson, G.A. and Al-Laham, M.A. Journal of Chemical Physics, Vol. 94, pp. 6081 (1991).

Peterson, K.A. and Werner, H.-J. Journal of Chemical Physics, Vol. 99, pp. 302 (1993).

Peterson, K.A. and Werner, H.-J. Journal of Chemical Physics, Vol. 105, pp. 9823 (1996).

Peterson, K.A. Journal of Chemical Physics, Vol. 109, pp. 8864 (1998).

Petersson, G.A., Malick, D.K., Wilson, W.G., Ocliterski, J.W., Montgomery, J.A. Jr. and Frisch, M.J. Journal of Chemical Physics, Vol. 109, pp. 10570 (1998).

Peyerimhoff, S.D., in 'Computational Methods in Chemistry', edited by Bargon, J., Plenum, New York, (1980).

Pierce, L., DiCianni, N. and Jackson, R. Journal of Chemical Physics, Vol. 38, pp. 730 (1963).

Politzer, P. and Abu-Awwad, F. Molecular Physics, Vol. 95, pp. 681 (1998).

Pople, J.A., Head-Gordon, M., Fox, D.J., Raghavachari, K. and Curtiss, L.A. Journal of Chemical Physics, Vol. 90, pp. 5622 (1989).

Richardson, A.W., Redding, R.W. and Brand, J.C.D. Journal of Molecular Spectroscopy, Vol. 29, pp. 93 (1969).

Rockland, U., Baumgartel, H., Ruhl, E., Losking, O., Muller, H.P. and Willner, H. Physical Chemistry Chemical Physics, Vol. 99, pp. 969 (1995).

Roitberg, A., Gerber, B.R., Elber, R. and Ratner, M.A. Science, Vol. 268, pp. 1319 (1995).

Roothaan, C.C.J. Review Modern Physics, Vol. 23, pp. 69 (1951).

Rowland, F.S. Annual Review Physical Chemistry, Vol. 42, pp. 731 (1991).

Ruhl, E., Rockland, U., Baumgartel, H., Losking, O., Binnewies, M. and Willner, H. International Journal Of Mass Spectrometry, Vol. 187, pp. 545 (1999).

Saarinen, T., Kauppi, E. and Halonen, L. Journal of Molecular Spectroscopy, Vol. 142, pp. 175 (1990).

Sameith, D., Monch, J.P., Tiller, H.-J. and Schade, K. Chemical Physics Letters, Vol. 128, pp. 438 (1986).

Sander, S.P., Friedl, R.R. and Francisco, J.S. in "Progress and Problems in Atmospheric Chemistry", edited by Schaefer, A., Horn, H. and Ahlrichs, R. Journal of Chemical Physics, Vol. 97, pp. 2571 (1992).

Schmider, H.L. and Becke, A.D. Journal of Chemical Physics, Vol. 108, pp. 9624 (1998).

Searles, D. J. and von Nagy-Felsobuki, E. I. in "Vibrational spectra and structure", edited by Durig, J.R., Elsevier, Vol. 19, pp. 151-213 (1991).

Sekiya, H., Nishimura, Y. and Tsuji, M. Chemical Physics Letters, Vol. 176, pp. 477 (1991).

Sharp, T.E. and Rosenstock, H.M. Journal of Chemical Physics, Vol. 41, pp. 3453 (1964).

Shida, N., Almlöf, J.E. and Barbara, P.F. Theoretical Chimica Acta, Vol. 76, pp. 7 (1989).

Smith, W.L. and Warsop, P.A. Faraday Discussions Chemical Society, Vol. 64, pp. 1165 (1968).

Stock, G. and Domcke, W. Journal of Physical Chemistry, Vol. 97, pp. 12466 (1993).

Subbi, J. Chemical Physics, Vol. 122, pp. 157 (1988).

Suzuki, M., Washida, N. and Inoue, G. Chemical Physics Letters, Vol.131, pp. 24 (1986).

Takeshita, K. Journal of Chemical Physics, Vol. 86, pp. 329 (1987).

Takeshita, K. Journal of Chemical Physics, Vol. 101, pp. 2199 (1994).

Takeshita, K. and Shida, N. Chemical Physics, Vol. 210, pp. 461 (1996).

Tanimoto, M., Takeo, H., Matsumura, C., Fujitake, M. and Hirota, E. Journal of Chemical Physics, Vol. 91, pp. 2102 (1989).

Taubmann, G., Jones, H., Rudolph, H.D. and Takami, M. Journal of Molecular Spectroscopy, Vol. 120, pp. 90 (1986).

Taubmann, G. Z. Naturforsch. Vol. 42a, pp. 87 (1987).

Tennyson, J. and Sutcliffe, B.T. Journal of Chemical Physics, Vol. 77, pp. 4061 (1982).

Tennyson, J. and Sutcliffe, B.T. Journal of Chemical Physics, Vol. 79, pp. 43 (1983).

Tennyson, J. and Sutcliffe, B.T. Journal of Molecular Spectroscopy, Vol. 101, pp. 71 (1983).

Tevault, D., Walker, N., Smardzewski, R.R. and Fox, W.B. Journal of Physical Chemistry, Vol. 82, pp. 2733 (1978).

Thiel, W., Scuseria, G., Schaefer, H.F. III and Allen, W.D. Journal of Chemical Physics, Vol. 89, pp. 4965 (1988).

Thorn, R.P. Jr., Stief, L.J., Kuo, S.-C. and Klemm, R.B. Journal of Physical Chemistry, Vol. 100, pp. 14178 (1996).

Thorn, R.P.Jr., Monks, P.S., Stief, L.J., Kuo, S.-C., Zhang, Z. and Klemm, R.B. Journal of Physical Chemistry, Vol. 100, pp. 12199 (1996).

Truhlar, D.G. "A new version of a computer program for the calculation of the chemical reaction rates for polyatomics", University of Minnesota, Minneapolis, Minnesota 55455, the most recent version: 8.5, (2000).

Valenta, K.E., Vasudevan, K. and Grein, F. Journal of Chemical Physics, Vol. 72, pp. 2148 (1980).

Voorhis, T.V. and Scuseria, G.E. Journal of Chemical Physics, Vol. 109, pp. 400 (1998).

Wang, D.C., Lee, E.P.F., Chau, F.T., Mok, D.K.W. and Dyke, J.M. Journal of Physical Chemistry A, Vol. 104, pp. 4936 (2000).

Warshel, A. and Karplus, M. Chemical Physics Letters, Vol. 17, pp. 7 (1972).

Warshel, A. and Karplus, M. Journal of American Chemical Societry, Vol. 96, pp. 5677 (1974).

Warshel, A. Journal of Chemical Physics, Vol. 62, pp. 214 (1975).

Watson, J.K.G. Molecular Physics, Vol. 15, pp. 479 (1968).

Watson, J.K.G. Molecular Physics, Vol. 19, pp. 465 (1970).

Weaver, A. and Neumark, D.M. Faraday Discussions Chemical Society, Vol. 91, pp. 5 (1991).

Werner, H.-J., Knowles, P.J., Amos, R.D., Berning, A., Cooper, D.L., Deegan, M.J.O., Dobbyn, A.J., Eckert, F., Hampel, C., Leininger, T., Lindh, R., Lloyd, A.W., Meyer, W., Mura, M.E., Nicklaß, A., Palmieri, P., Peterson, K., Pitzer, R., Pulay, P., Rauhut, G., Schütz, M., Stoll, H., Stone, A.J. and Thorsteinsson, T. "MOLPRO version 98.1: A package of ab initio programs", University of Birmingham, UK, (1998).

Whitehead, R.J. and Handy, N.C. Journal of Molecular Spectroscopy, Vol. 59, pp. 459 (1976).

Wilson, Jr. E.B., Decius, J.C. and Cross, P.C. "Molecular Vibrations", McGraw-Hill, New York, (1955).

Woon, D.E. and Dunning, T.H.Jr. Journal of Chemical Physics, Vol. 98, pp. 1358 (1993).

Xie, D. and Guo, H. Chemical Physics Letters, Vol. 307, pp. 109 (1999).

Xu, C., Taylor, T.R., Burton, G.R. and Neumark, D.M. Journal of Chemical Physics, Vol. 108, pp. 1395 (1998).

Yamagouchi, M., Momose, T. and Shida, T. Journal of Chemical Physics, Vol. 93, pp. 4211 (1990).

Yang, D.S., Zgierski, M.Z., Rayner, D.M., Hackett, P.A., Martinez, A. Salahub, D.R., Roy, P.N. and Carrington, Jr.T. Journal of Chemical Physics, Vol. 103, pp. 5335 (1995).

Research Outputs of Mr. Wang Dechao

Journal Articles:

1. Chau, F.T., Wang, D.C., Lee, E.P.F., Dyke, J.M. and Mok, D.K.W. "The X^1A_1, a^3B_1 and A^1B_1 States of $SiCl_2$: Ab initio Calculations and Simulation of Emission Spectra". Journal of Physical Chemistry A, Vol.103, pp. 4925-4932 (1999).

2. Wang, D.C., Lee, E.P.F., Chau, F.T., Mok, D.K.W. and Dyke, J.M. "The X^2B_1, A^2B_2, B^2A_1 and C^2A_2 states of Cl_2O^+: Ab initio Calculations and Simulations of He I Photoelectron Spectrum". Journal of Physical Chemistry A, Vol.104, pp. 4936-4942 (2000).

3. Chau, F.T., Lee, E.P.F., Mok, D.K.W., Wang, D.C. and Dyke, J.M. "Simulation of Photoelectron and Electronic Spectra of Small Molecules". Journal of Electron spectroscopy and Related Phenomena, Vol.108, pp. 75-88 (2000).

4. Mok, D.K.W., Lee, E.P.F., Chau, F.T., Wang, D.C. and Dyke, J.M. "A new method of calculation of Franck-Condon factors which includes allowance for anharmonicity and the Duschinsky effect: Simulation of the He I photoelectron spectrum of ClO_2". Journal of Chemical Physics, Vol.113, pp. 5791-5803 (2000).

5. Wang, D.C., Chau, F.T., Mok, D.K.W., Lee, E.P.F., Beeching, L., Ogden, J.S. and Dyke, J.M. "The X^2B_1, $^2B_2$, $^2A_1$ and $^2A_2$ States of Oxygen Difluoride (F_2O^+): High-Level Ab initio Calculations and Simulation of the He I Photoelectron Spectrum of F_2O". Submitted to the Journal of Chemical Physics, (2001).

Conference and Symposium Presentations:

6. Mok, D.K.W., Lee, E.P.F., Wang, D.C. and Chau, F.T. "Photoelectron Spectrum Simulation with Anharmonic Effect Incorporated". Book of Abstracts of Sixth Symposium on Chemistry Postgraduate Research in Hong Kong, City University of Hong Kong, Hong Kong, 24 April 1999, Abstract No. pp.10.

7. Wang, D.C., Mok, D.K.W. and Chau, F.T. "Ab initio Studies of The Geometry, Ionization Potentials and Anharmonic Properties of Oxygen Difluoride (F_2O) and Spectral Simulation of Its He I Photoelectron Spectrum". The Seventh Symposium on Chemistry Postgraduate Research in Hong Kong, 29 April, 2000, Hong Kong, pp.6.

8. Chau, F.T., Wang, D.C., Mok, D.K.W. and Dyke, J.M. "$^2B_1$, $^2B_2$, $^2A_1$ and $^2A_2$ states of Cl_2O^+ Ab initio Calculations and Simulations of The He I Photoelectron Spectrum". The 219th American Chemical Society National Meeting, 26 - 30 Mar., 2000, San Franciso, CA, US, pp.385-PHYS.

9. Wang, D.C., Mok, D.K.W., Lee, E.P.F., Chau, F.T. and Dyke, J.M. "Simulation of the He I Photoelectron Spectrum of ClO_2 with the Inclusion of Anharmonicity and Duschinsky Effects". The 220th American Chemical Society National Meeting, 20 - 24 August, 2000, Washington, D.C. U.S.A., pp.394-PHYS.